

BIRZEIT UNIVERSITY
FACULTY OF GRADUATE STUDIES

**THE VACUUM BEAT-WAVE ELECTRON LASER
ACCELERATOR AND ASSOCIATED RADIATIVE
EFFECTS**

by

Ashraf Abdel-Haleem Khamis Titi

A THESIS SUBMITTED
IN PARTIAL FULFILLMENT OF THE
REQUIREMENTS FOR THE DEGREE
MASTER OF SCIENTIFIC COMPUTING

APPROVED, THESIS
COMMITTEE:

Dr. Yaqoub Anini

Dr. Aziz Shawabkeh

Dr. Jamal Sueiman

Dr. Wasel Ghanem

Birzeit, Palestine

August, 2004

ABSTRACT

In this work, we solve the relativistic equations of a single electron in beat wave laser beams, and we demonstrate three cases of interaction between laser field and electron which are capture, reflection, and transmission. When an electron is injected in a laser regime focused in a small dimensional area, the electron will absorb an amount of energy from the laser that depend on many factors related to the injection parameters of the electron and laser fields. In most cases the electron is captured by the laser and accelerated violently over a small spatial area, the last depend on how and when to inject the electron into the laser fields. Beat-wave laser configuration results by adding two propagated laser beams of the same amplitude but slightly different frequencies. Our aim is to investigate numerically the acceleration dynamics and radiative effects for such scheme for a single electron injected with an initial speed β (*speed scaled by the speed of light in vacuum c*) by using a famous numerical method which is adaptive Runge-Kutta. All theoretical parts of this work are based on the works and fields represented by Prof. Salamin. Laser fields will be modeled by Gaussian beam (i.e. tightly focused laser beam).

Acknowledgments

I would like to express my gratitude to my supervisors Prof.Y.I. Salamin and Dr.Yaqoub Anini for all their support, guidance, constructive criticism and ideas as well as encouragement to achieve success of this work. I would also like to thank Dr.Aziz Shawabkeh, Dr.Jamal Suleiman, Dr.Hassan Shebli, Dr.Wasel Ghanem and all physics department members at Birzeit University for their guidance, help, and support.

I also owe my gratitude to my parents for their encouragement and support, and to my brothers and sisters for making life so enjoyable.

Finally, I would like to thank my wife for his immense patience and support without which this work might never have been completed.

Contents

Abstract	ii
Acknowledgments	iii
List of Figures	vii
1 Conventional Accelerators	1
1.1 History, Prospects, and Practical Application	1
1.2 Problems And Limitation Of Particle Accelerators	8
2 Laser Accelerators	10
2.1 Historical Background	10
2.2 laser Acceleration Of Electron In Vacuum	15
2.3 Plasma Versus Vacuum Laser Acceleration	16
2.4 Acceleration By A Single Laser Beam	17
2.4.1 Plane wave model	17
2.4.2 Tightly focused laser beam (Gaussian beam)	20
2.4.3 Electron dynamics	23
2.4.4 The description of fields near the Gaussian beam fo- cus	28
2.4.5 Radiation and energy loss	32

3	Beat-Wave Laser Acceleration	35
3.1	Introduction	35
3.2	The Laser Plane Wave Model For The Beat-Wave Structure	37
3.3	The Laser Gaussian Beam Model For The Beat-Wave Structure	42
3.4	Objectives And Work Plan	44
4	Computing Techniques And Methodology	47
4.1	Algorithm And Code Structure	47
4.2	Program Input And Output Quantities	49
4.3	Code Stability And Verification Test	51
4.4	Manipulation Of Data And Results Generation	55
5	Discussion Of Results And Conclusion	57
5.1	Electron Acceleration With The Normal Laser Fields	59
5.2	Electron Acceleration With A Single Laser Gaussian Beam .	63
5.3	Electron Acceleration By Beat-Wave Laser And Associated Radiative Effects (Tightly Focused Laser Beams)	72
5.3.1	Injection On Both Sides Of The Focus	80
5.3.2	The Effect Of Waist Radius	82
5.3.3	The Effect Of Injection Energy	84

5.4	Optimum Conditions For Electron Acceleration In Beat-Wave Tightly Focused Laser Beam	86
5.5	Summary And Conclusion	95
A	Fields Near The Focus Of A Pulsed Gaussian Beam	99
B	C++ Code	104
	References	119

List of Figures

1.1	accelerators work by exerting an electric force on charged particle. The negative plate repels the bunch of electrons and a positive plate attracts them. The electrons thus gain energy in moving from the negative plate to the positive plate. By the time they reach the positive plate they are traveling so quickly that they pass through the hole in the plate and can be used for experiments	6
1.2	very high energies cannot be obtained by using just one pair of plates, in linear accelerator many pairs of plates are lined up and the particles being accelerated are given more and more energy as they pass through each pair of plates. In circular accelerator, only one pair of plates is used, but the particles are made to travel in a circle, thus passing through that pair of plates again and again. Each time they pass through the pair of plates they are given more energy.	7
2.1	a schematic diagram showing the configuration of electron injection into the electromagnetic field	19
2.2	The beam geometry.	20

2.3	Portions of trajectories illustrating reflection, capture and transmission, when the electron is injected into the focus. The dark lines mark the beam <i>boundaries</i> as defined in the text.	23
3.1	Construction of beat-wave	36
3.2	Schematic diagram of the electron interaction with the fields of the two component waves.	39
3.3	Schematic diagram represents the polarization of the two beams	43
4.1	Flow chart showing the flow of computation in the numerical integration	48
4.2	Electron energy gain versus the number of field cycles in the field of plane wave of wavelength $\lambda_1 = 1\mu m$ alone (dotted curves), in the field of a plane wave of wavelength $\lambda_2 = 1/3\mu m$ alone (chain curves), and in the field of beat-wave resulting from adding the two waves (full curves), see text for parameters	51
4.3	Scaled electron velocity y-component versus the number of field cycles in a beat field of two waves.	53

4.4	(a) Portions of trajectories illustrating reflection, capture and transmission, when the electron is injected into the focus. The dark lines mark the beam <i>boundaries</i> as defined through the text. (b) The transverse component, and (c) The longitudinal component of the electric field sensed by the electron along the transmission and capture trajectories displayed in (a).	54
5.1	X-component of the electron trajectory in the plane wave field of beat-wave laser	60
5.2	Z-component the electron trajectory in the plane wave field of beat-wave laser	61
5.3	Contour maps of the electric components of the laser field of a Gaussian beam over a square $30 \mu\text{m}$ on a side, centered at the beam focus and extending in the xy plane.	64
5.4	Contour maps of the magnetic component of a Gaussian beam over a square $30\mu\text{m}$ on a side, centered at the beam focus and extending in the xy plane, (see text for parameters)	65
5.5	The electron trajectories for various values of initial injection energy, for $\gamma_0 = 22$ (heavy curves), for $\gamma_0 = 15$ (light curves), for $\gamma_0 = 5$ (dotted curves).	67

5.6 The x-component of the electric field, for $\gamma_0 = 22$ (heavy curves), for $\gamma_0 = 15$ (light curves) , for $\gamma_0 = 5$ (dotted curves). 67

5.7 The z-component of the electric field , for $\gamma_0 = 15$ (light curves) , for $\gamma_0 = 5$ (dotted curves). 68

5.8 The y-component of the magnetic field, for $\gamma_0 = 15$ (light curves) , for $\gamma_0 = 5$ (dotted curves). 68

5.9 The electron energy gain for different values of initial injection energy, for $\gamma_0 = 15$ (light curves) , for $\gamma_0 = 5$ (dotted curves). 69

5.10 The electron energy loss for the case of initial injection energy $\gamma_0 = 5$ 69

5.11 The electron energy loss for the case of initial injection energy $\gamma_0 = 15$ 70

5.12 The electron energy loss for the case of initial injection energy $\gamma_0 = 22$ 70

- 5.13 Contour maps of the electric component of the laser of beat-wave Gaussian beams over a square $20\mu m$ on a side, centered at the beam focus and extending in the xy plane. The beams parameters are $w_0 = 5\mu m$ and $\lambda_1 = 1\mu m$, $\lambda_2 = 1.1\mu m$. in (a,c,e) the fields are given at $\omega t = 0$, and at (b,d,f) at $\omega t = \pi/2$. Note that the positive and negative values are distinguished by level of shading, dark means negative and bright positive 74
- 5.14 Contour maps of the magnetic component of the laser of beat-wave Gaussian beams over a square $30\mu m$ on a side, centered at the beam focus and extending in the xy plane. The beams parameters are $w_0 = 5\mu m$ and $\lambda_1 = 1\mu m$, $\lambda_2 = 1.1\mu m$. in the left figures the fields are given at $\omega t = 0$, and in the right at $\omega t = \pi/2$. Note that the positive and negative values are distinguished by level of shading, dark means negative and bright positive 75
- 5.15 The transverse component of the electric field sensed by the electron (for $w_0 = 5\mu m$ and $\lambda_1 = 1\mu m$, $\lambda_2 = 1.1\mu m$, $\psi_0 = 301$, $\gamma_0 = 6.5$, and $P = 10PW$.) 76

5.16	The longitudinal component of the electric field sensed by the electron (for $w_0 = 5\mu\text{m}$ and $\lambda_1 = 1\mu\text{m}$, $\lambda_2 = 1.1\mu\text{m}$, $\psi_0 = 301$, $\gamma_0 = 6.5$, and $P = 10\text{PW}$.)	77
5.17	The y-component of the magnetic field sensed by the electron (for $w_0 = 5\mu\text{m}$ and $\lambda_1 = 1\mu\text{m}$, $\lambda_2 = 1.1\mu\text{m}$, $\psi_0 = 301$, $\gamma_0 = 6.5$, and $P = 10\text{PW}$.)	77
5.18	The trajectories of electron in beat-wave fields for different injection energy, for $\gamma_0 = 4$ (dash curves), and for $\gamma_0 = 6.5$ (full curves), (other parameters the same for 5.15)	78
5.19	The Energy gain in beat-wave fields for different injection energy, for $\gamma_0 = 4$ (dash curves), and for $\gamma_0 = 6.5$ (full curves), (other parameters the same for 5.15)	79
5.20	The Energy losses in beat-wave fields for injection energy $\gamma_0 = 4$ (other parameters the same for 5.15)	79
5.21	The Energy losses in beat-wave fields for different injection energy, for $\gamma_0 = 6.5$ (other parameters the same for 5.15)	80
5.22	For electron with initial velocity vector pointing from $(x_0, 0, z_0 = -3\text{mm})$ to $(0, 0, s)$ the variation of energy gain with s is shown	81

5.23 For electron with initial velocity vector pointing from $(x_0, 0, z_0 = -3mm)$ to $(0, 0, s)$ the actual trajectories of four cases corresponding to different values of s is shown. The laser wavelength is $\lambda = 1\mu m$. Note that $x_0 = -(s - z_0) \tan \theta$. The interaction time in all cases is such that $\omega t = \pi \times 10^5$ The legends in 5.22 apply to 5.23 82

5.24 Energy gain vs the beam waist radius w_0 with wavelengths $\lambda_1 = 1\mu m, \lambda_2 = 1.1\mu m$ 84

5.25 Electron energy gain vs the scaled injection energy. In this case the electron is aimed at point on the beam axis a distance $s = -0.83 * zr_1$ to the left of focus. The laser wavelengths are $\lambda_1 = 1\mu m, \lambda_2 = 1.1\mu m$, and the laser output power is that $P=10PW, z_0 = -3mm, \psi_0 = 301, \theta = 10, W_0 = 5\mu m$ 85

5.26 Electron energy gain vs the scaled injection energy. In this case the electron is aimed at point on the beam axis a distance $s = 0$. The laser wavelengths are $\lambda_1 = 1\mu m, \lambda_2 = \lambda_1/1.1\mu m$, and the laser output power is that $P=10PW, z_0 = -5mm, \psi_0 = 0, \theta = 10, W_0 = 7\mu m$ 86

5.27	Plots of energy gain versus some parameters by mean of optimum parameters: (a)energy gain versus ψ_0 , (b)energy gain versus s , (c)energy gain versus γ_0 , (d) energy gain versus w_0 , (e) gain vs θ , and (f) gain vs z	89
5.28	Energy losses versus z . (for the optimum parameters)	91
5.29	x versus t , note that big deflection angle and high violent acceleration corresponds to much energy loss (for the optimum parameters)	92
5.30	z versus t . (for the optimum parameters)	92
5.31	velocity x-component(β_x) versus t (for the optimum parameters).	93
5.32	velocity z-component(β_z) versus t (for the optimum parameters).	94
5.33	x versus z (for the optimum parameters).	94

Chapter 1

Conventional Accelerators

1.1 History, Prospects, and Practical Application

In order to get an idea about the world, we must get an idea about the world of atom and nucleus; this needs a hard continuous investigation to be done by physicists to refine the knowledge about atoms and nuclei, the scheme of table of elements was developed first by Mendele'ef in the 1870's [4], and to understand the atomic processes, scientists first studied the hydrogen atom to know the distribution of matter within the atom.

Many models were introduced to capture the contents and construction of the atom by many physicists like Sir J.J. Thomson, Geiger-Mueller fame, and Lord Rutherford who, in 1911, bombarded a thin metallic foil target with alpha particles and observed the scattering of the alpha particles from the foil, which confirm the belief that most of the atom mass and positive charge is concentrated in the small core called the nucleus, and the electrons moves around the nucleus in orbits, until 1932 all research in nuclear physics was performed using alpha particles from naturally radioactive elements with high kinetic energies approximate to 8 MeV [5].

At that time namely in 1928 the Russian physicist George Gamow indicated that the use of less energetic ions could be useful [6], this led to

build accelerator that maintain a beam of particles useful for nuclear research. The first successful experiment depending on the previous idea was constructed at the University of Cambridge-England in early 1932 by John Douglas Cockcroft and Walton [1], they built electrostatic accelerator to produce potentials of about 800,000 volt, this system then had the ability to produce 800 KeV protons or 1600 KeV alpha particles, while modern types of Cockcroft-Walton devices are capable of accelerating protons up to about 3 MeV.

However, to investigate the interior of the nuclei, some probe or some other means of disturbing the nucleus was needed, through this a few problems arises when probing the nucleus including the need for high energy positive particles in order to penetrate the nucleus, (proton for example)[4], it needs kinetic energy above 1.5 MeV to enter aluminum nucleus, to achieve this energy the charged particle must be accelerated in a large potential difference, hence the need arises to develop a whole machine to provide this potential difference by mean of accelerators.

The first generation of accelerators is the cathode-ray tube that is used first by J.J. Thomson which produced (in modern language) electrons of a few tens of KeV. The first inventor of accelerators was the Norwegian engineer and physicist R. Wideroe [1] in early 1920s, who also proposed

the induction accelerator which later known as the Betatron, in addition to the linear RF accelerator. But the real accelerators that started to be used in nuclear research early in 1930s were the electrostatic accelerator known as Van-de-Graaff accelerator and the Lawrence cyclotron, a Van de Graaff generator can accelerate particles (usually protons, alpha particles or even heavier ions) through a potential to about 5-6 MeV.

Accelerator field of research started to grow through there use in process of nuclear weapon and nuclear energy development, it follows that in the 1940s and 1950s the concentration was on invention of outphasing and strong focusing, also in that time the long-awaited synchrotron radiation was used in electron accelerators.

The development of colliding beams open the way to new stage in high energy physics especially in 1956 when proton-proton collider based on special kind of ring that can store identical particles moving in opposite directions beside electron-electron collider that is based on storing and compression beams with the use of synchrotron radiation cooling were proposed.

Scientists succeed to carry out electron-electron experiment just in 1965, followed by the solution to problem of studying electron-positron annihilation at high energy in 1967. This led at that time to regard colliders as the leading tool in particle physics.

Since that time electron-positron colliders grew rapidly until culminating with operating of the 30 km circumference LEP that built in CERN, it results with 106 GeV per beam and 3 GeV energy loss per turn due to synchrotron radiation, and it was probably the limit to electron-positron collision due to the catastrophic rise of synchrotron radiation energy loss in this cyclic machine.

The researcher in Novosibirsk were electron-positron collision was studied understood that in order to reach hundreds of GeV for electron-positron collisions is to use linear accelerator, the use of linear accelerator minimize the catastrophic rise in energy loss. The completion of such research was presented in Novosibirsk at 1978, followed that the operation of first practical project a single-pass collider based on the Stanford Linear accelerator result in energy per beam 50 GeV. Many labs including CERN, SLAC and others now are developing technologies for higher than 500 GeV per beam.

A significant track in the accelerator field is the arranging of polarized beams in accelerators, storage rings and colliders. It is practical to inject polarized charged particle beams into accelerators directly from the polarized beam sources. Still to say it is easy in linear accelerators to prevent loss of the degree of polarization for any particles and for any direction of polarization (either transverse or longitudinal).

Another significant track in the accelerator field development is the effort to achieve high and higher accelerating gradients, if we consider the usual accelerator structure where the electromagnetic field is formed by metallic boundaries, the highest possible field for normal-conducting materials (in pulsed regime) is limited by the action of the electric field normal to the surface, which can produce cold emission and then discharge. This effect limits the accelerating gradient with a value of 100 MeV/m at a frequency of about 10 GHz even for perfectly machined surfaces, and to achieve much higher accelerating energy we need to use plasma formed electromagnetic field, the last is limited to few laser wavelengths.

The name accelerators comes from their role in accelerating charged particles to high kinetic energy, they are used for the purpose of obtaining the threshold and resonant energy that is needed for nuclear physics research in some nuclear reactions, in addition to obtain high momentum and small wave length to serve in small structures.

Accelerators are also used commercially for many applications including ion implantation, selective doping of semiconductors, alloying with minute quantities of rare metals, in surveying for hydrocarbons surrounding well shafts, as well as for the production of medical isotopes, changing the properties of plastics, and finally for radioactive dating.

The work of an accelerator can be described easily as bunch of charged particles pass through an electric field (figure 1.1) that yields voltage difference [7], and hence particles gain energy due to acceleration by the electric field. In principle, the charged particles in such accelerators move in a deep

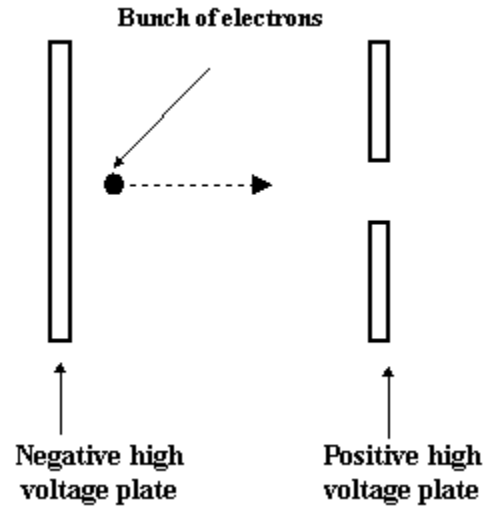


Figure 1.1 accelerators work by exerting an electric force on charged particle. The negative plate repels the bunch of electrons and a positive plate attracts them. The electrons thus gain energy in moving from the negative plate to the positive plate. By the time they reach the positive plate they are traveling so quickly that they pass through the hole in the plate and can be used for experiments

vacuum (i.e., 10^{-13} atmosphere) which is required to prevent the particles from losing energy [4], being scattered in various directions, or even being absorbed in collisions with gas molecules before reaching the target. The highest-energy accelerator in the world is the tevatron proton circular accelerator at Fermilab [4, 7] which is designed to produce 1 TeV with radius

of about 1 kilometer.

In general accelerators are either linear or circular (figure 1.2), in linear accelerator particles is propelled by strong electromagnetic field to gain all of its energy in one pass through the machine, whereas in the circular accelerator, the particles are magnetically constrained to move many times in circular closed path or orbit, and hence gain energy increasingly on each successive orbit by an accelerating electric field.

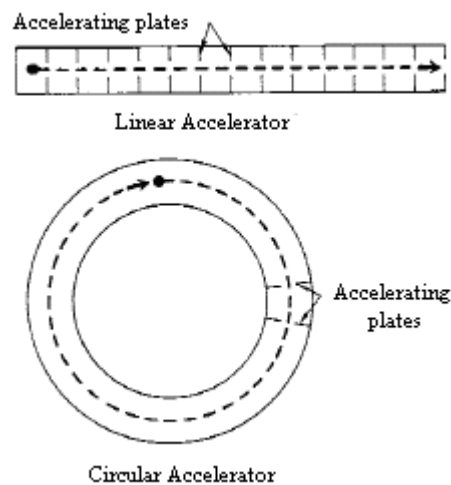


Figure 1.2 very high energies cannot be obtained by using just one pair of plates, in linear accelerator many pairs of plates are lined up and the particles being accelerated are given more and more energy as they pass through each pair of plates. In circular accelerator, only one pair of plates is used, but the particles are made to travel in a circle, thus passing through that pair of plates again and again. Each time they pas through the pair of plates they are given more energy.

1.2 Problems And Limitation Of Particle Accelerators

After we described how accelerators work, we now turn to the reasons for the variety of accelerators used in elementary particle physics: fixed-target accelerators and particle colliders, proton accelerators and electron accelerators, low energy accelerators and high-energy accelerators. The variety exists to serve the many different purposes of elementary-particle physics experiments.

Accelerators are machines that accelerate charged particles to high energies. They vary in shape and size and, hence, in building and running cost [17]. A linear machine can be quite long; the one at SLAC (Stanford Linear Accelerator Center in Palo Alto, California) is about two miles long. Circular machines can be quite big, too. A typical ring at CERN (European Center for Nuclear Research) has a one-kilometer long circumference. The need for ever higher particle energies continues to demand construction of ever bigger and more expensive machines. The same demand also fuels the imagination and talent of theoretical and experimental physicists to design smaller and cheaper accelerators.

Standard accelerators work by transferring microwave radiation energy to electrons, causing them to accelerate down a long, straight pipe [9]. But

reaching high energies can be difficult with this type of linear accelerator, or linac, because the electrons receive only small amount of energy at a time and are accelerated in several steps. As a result, high-energy linacs are usually several meters long and can be up to several kilometers in length in addition they are very expensive.

The acceleration effectiveness of the linear or circle accelerators is limited not only by geometrical size of them but also by the energy loss of accelerated particles which is caused by bremsstrahlung or braking radiation during the acceleration [3]. The amount of radiation, following from the Larmor formula (details below) emitted by accelerated charged particle in the linear accelerator the energy loss caused by radiation is smaller than in circular accelerator and it means that to obtain high energy particles in linear accelerator is more easy than in the circular accelerator.

Chapter 2

Laser Accelerators

2.1 Historical Background

The idea of laser acceleration follows historically the idea that light exerts pressure, the former idea was for the first time postulated by Johanness Kepler, the King astronomer in Prague, in 1619. He wrote that the pressure of Sun light is what causes the tails of comets to point away from the Sun. Newton gave explanation to that effect in his corpuscular theory of light.

The acceleration of charged particles by laser beam has been studied by many authors (Tajima and Dawson, 1979; Katsouleas and Dawson, 1983; Scully and Zubary, 1991; Baranova and Zel'dovich, 1994) [3].

More than fifty years ago, physicists have considered the mechanism of the interaction of charged particles with intense electromagnetic fields, and this was one of the first explanations put forward by early physicists (e.g. Fermi 1949) to explain the origin and energies of cosmic rays [8]. The idea behind interaction is that a charged particle say an electron is accelerated in intense electromagnetic field initially along the direction of the electric field. The ponderomotive force $\vec{v} \times \vec{B}$ causes the particle's path to bend into the direction of travel of the wave. The particle's velocity in large fields will reach rapidly the velocity of light and tends to travel with the

electromagnetic wave and hence accelerated due to the energy obtained from the wave.

Tajima and Dawson believed that generation of very high energies could be obtained by focusing intense laser light into plasma medium. Also they proposed the construction of a laser-electron accelerator which could be created when an intense laser pulse produced a wake of plasma oscillations (volumes of low and high densities of electrons). A bunch of high velocity electrons creates a wake of plasma waves as it passes through plasma. They used computer simulation demonstration on existing glass lasers of 10^{18} W/cm^2 , and they concluded that such glass laser could yield electron acceleration gradients of about 100 GeV/m while conventional accelerators are limited by electrical breakdown at fields of about 20 MV/m [8]; means that we can reach gradients up to 20 MeV/m, therefore we need to build very long conventional accelerator, and at these fields the electrons are torn from the atoms in the accelerator's support structure. Thus these plasma particle accelerators promise fields more than 1000 times stronger than those of the most powerful conventional accelerators.

Electron acceleration by intense laser fields in plasmas takes attention recently due to the advent of high power laser pulses and their potential application, Laser-plasma accelerators of particles, which have a potential to

become next-generation high-gradient accelerators [21], rely on laser excitation of large amplitude relativistic plasma waves (RPWs) for acceleration. Two main considerations drive a significant interest to this type of devices which are the availability of laser power sources producing multi GV/m electric fields and the fact that plasmas can sustain these very strong fields. And since the interaction length of a focused laser beam is limited fundamentally by diffraction, multistage acceleration is required to achieve the kinetic energy of interest for high-energy physics.

Different schemes of acceleration mechanisms have been proposed, including the plasma wave acceleration, the direct laser acceleration in vacuum, and the mixed acceleration from both transverse and longitudinal field [19]. Some of these are not sufficiently developed to be readily intelligible, others seem to be fallacious and others are unlikely to be relevant to ultra high energies. Some designs were developed only to observe pressure of laser light on microparticles in liquids and gas (Ashkin, 1970; Ashkin, 1972) [3].

From the time of beginning of laser science in early 1960s [8], hard works are made to increase laser intensities as well as power of lasers. Today laser systems are available with several Terawatts of power (e.g. Vulcan laser: located at Rutherford Appleton Laboratory, near Oxford in the UK, its power is 10^{15} watt), it is worth while to know that such laser can deliver

more than 100 joules of energy in a picosecond (10^{-12} s) pulse.

Up to now workers at the U.S. Department of Energy's Brookhaven National Laboratory have developed a compact linear accelerator that uses laser light to provide accelerated electrons with better efficiency and energy characteristics than ever before [9].

The experimental device, called Staged Electron Laser Acceleration, (STELLA), is a step forward in accelerator development, and may help electron accelerators become practical tools for applications in industry and medicine, such as radiation therapy for cancer patients.

In contrast to standard accelerators, over a distance of one-third of a meter, STELLA, which uses laser light rather than microwaves to accelerate electrons, shortened and improved the "step" method to achieve an energy gain that would have required a longer standard linac. The researchers were also able to overcome some of the challenges of using laser-driven linacs, such as making the electrons as monoenergetic (all have same energy), as possible, and keeping them tightly bunched together. These characteristics are vital to producing a high-quality, useful electron beam. While laser linacs still need substantial development, STELLA's success in performing these tasks suggests that linacs could be much smaller and more affordable in the future, making them appropriate for radiation treatment areas in

hospitals, for example.

In the experiment, the electrons entered STELLA with an initial energy of 45 million electron volts (MeV), having been previously accelerated with a standard linac, STELLA recorded an energy gain of 20 percent, accelerating the electrons from 45 MeV to more than 54 MeV [9].

It is important to say that Laser accelerators open the way for future compact, powerful accelerators, but we have a lot to learn until we can use them with the same dexterity as conventional machines.

With the appropriate focusing technology, a laser system is capable of making available to a charged particle [17], say an electron, huge amounts of energy to absorb from and get accelerated. However, it is now believed that the fields of such a laser system need to be made asymmetric over the space-time points of interaction with the particle, if the latter is to come out with any appreciable energy gain. This asymmetry may be brought about by superimposing two co-propagating laser beams that differ slightly in frequency, among other parameters. This leads to a beat structure which presents the electron with fields of much higher intensity than would otherwise be the case of a single beam. In this work we propose to investigate the problem of acceleration of a single particle, an electron, in such an environment using laser fields currently available to laboratory experiments.

2.2 laser Acceleration Of Electron In Vacuum

The development of high power laser continue to encourage creation of new concepts for accelerators [18], hence there are a challenges to create a new approaches with possible acceleration gradients larger than 100 MeV/m typical for proposed next-generation X-band Linacs.

Recent advances in laser technology especially the successful generation of subcycle pulses in microwave, far infrared, and femtosecond regimes [10], now promise to make possible the experimental testing of several ideas for laser acceleration of electrons. Lawson-Woodward theorem stated that an electron gains no net energy as a result of interaction in vacuum with a pulse containing a large number of field cycles, provided other conditions are met. However, a possible solution to the problem of net energy gain is to push the electron to interact with a fraction of a field cycle. This may be achieved possibly by extracting the electron at the right moment by means of suitable deflecting elements placed near the region of interaction with a multi-cycle pulse or, better yet, by employing a subcycle pulse, or as mentioned above to make the fields of such a laser system asymmetric by mean of superimposing co-propagating laser beams that differ slightly in frequency and among other parameters. The later idea led to many structures like the beat-wave structure, crossed beams structure, or an appropriately

applied extra DC electric field, among other methods.

All the laser accelerator schemes are considered to be successful if they can provide longitudinal component of the field, and remain in synchronization with the electron bunch [16], hence for a laser field regime this would imply structures of dimensions of $1 \mu\text{ m}$, which in turn, makes the tolerances on the electron beam size and position almost impossible.

One of the new approaches to particle acceleration is to make use of laser beams in vacuum in the far-field limit, i.e., in regions that are far (compared to the vacuum wavelength) from boundaries, thus mitigating material breakdown, plasma formation, and instability. Particle acceleration in vacuum by laser fields can be divided into two main categories: (1) Direct acceleration, in which the accelerating force is linearly proportional to the field, and (2) ponderomotive acceleration, in which the accelerating force is proportional to the square of the field.

2.3 Plasma Versus Vacuum Laser Acceleration

Laser-based plasma acceleration schemes face many of challenges to be overcome before considering any of these schemes to be practical [32], some of these challenges appeared because of the instability of plasma medium used to support the accelerating slow waves in addition to the probable scattering induction, other reason is in the case of positron acceleration,

which is necessary in lepton colliders, the rapid annihilation through plasma will be problematical.

Otherwise, the major difficulty in using the laser fields in vacuum to accelerate electrons is that the phase velocity of accelerated electrons electric field in vacuum faster than the speed of light when electrons travel over long distance three times comparable to the Rayleigh length [30].

2.4 Acceleration By A Single Laser Beam

2.4.1 Plane wave model

Many years ago physicists work on finding analytical solutions for the dynamics of electron in electromagnetic plane wave [32], but most of these solutions are limited for special cases where the electron is initially at rest or has a vanishing average velocity. The analytical solutions for the general situations of initially relativistic velocity and an arbitrary direction with respect to the propagation direction of the wave have just recently been given.

Addition of extra electric or magnetic fields make problem more complicated, for example, the case of addition a uniform magnetic field has been discussed in the past and has led to the introduction of the auto-resonance laser accelerator (ALA) scheme. Also the solution for this problem has been done lately [11, 12] with acceleration of the electron restricted to high

energies and the associated radiation aspects, where the case of a \sin^2 pulse and a uniform axial magnetic field has also been done more recently [13].

More recently the work of Salamin [32] added more one solution for such problem through finding the analytic solution for the dynamics of electron with more generality where an electron is injected in vacuum at some arbitrary angle to a) the direction of a uniform electric field of strength E_s , and (b) the propagation direction of a circularly-polarized plane-wave laser field of arbitrary intensity.

It is important to know that an exact analytic solution to the problem of electron acceleration by plane wave has not been done before. And the solution found by Salamin is important for the understanding of issues related to particle acceleration electron motion following ionization, and the scattering of radiation and, possibly, generation of harmonics in the presence of the added electric field [22, 14].

While the plane-wave-based analytic solution may approximately model a laboratory situation, Salamin in his work believes that it represents a good first step towards the analysis of a realistic scheme. It leads to better insights into the problem at hand, and it may help one to benchmark the numerical codes that need ultimately be used to simulate schemes of similar nature.

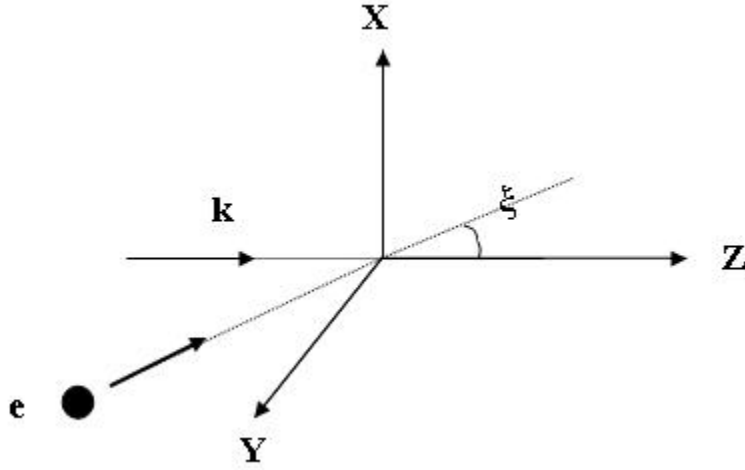


Figure 2.1 a schematic diagram showing the configuration of electron injection into the electromagnetic field

As mentioned above we are restricted to use the fields of Salamin. Hence, in our computations we are starting up with a test case using plane wave model for the laser beam. If a single relativistic electron, injected initially at some arbitrary angle ξ to the propagation direction $+Z$ of linearly polarized laser plane-wave polarized in $+X$ (means that $\hat{k} \times \vec{E} = \vec{B}$) and has arbitrary intensity. (See figure 2.1 for schematic diagram) [22].

The electric field \vec{E} and magnetic field \vec{B} for such laser wave are given as the following:

$$\vec{E} = \hat{i}E_0 \sin(\omega t - kz) \quad (2.1)$$

$$\vec{B} = \hat{j}E_0 \sin(\omega t - kz) \quad (2.2)$$

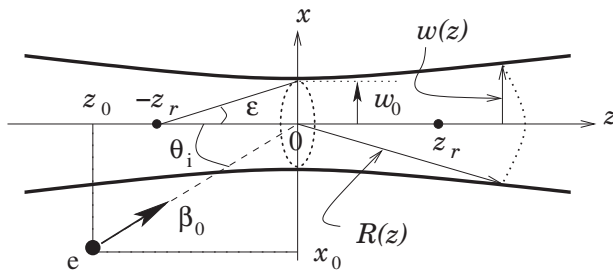


Figure 2.2 The beam geometry.

Where E_0 is the maximum value for electric field, ω is the angular frequency of laser wave, z is the direction of propagation of laser.

It is well known in the above case as followed from Lawson-Woodward theorem that the electron gains virtually no net energy as a result of interaction with an integer number of laser field cycles, but it is gained energy in a subcycle of the laser wave.

2.4.2 Tightly focused laser beam (Gaussian beam)

Now, in the tightly focused laser beam, state-of-the-art petawatt laser beams can be focused down to few-micron spot sizes five times of wavelength [35]. In this case, the Rayleigh length can be comparable to or even shorter than the laser and electron interaction region. This configuration can produce violent electron acceleration as a result of extremely intense and asymmetric fields. For studying the electron and laser interaction better, we must consider the variety of laser beam waist. Here, we considered the acceleration of an electron using the following simple interaction model,

by selecting the proper initial position of both the electron and the laser pulse, the electron is accelerated near the focus where the laser beam waist is smaller but the power is bigger and decelerated far away the focus where the laser beam waist is bigger but the power is weaker.

The acceleration and deceleration can't be canceled because of the variety of laser beam waist and intensity. As a result, For intensities above $10^{19}W/cm^2$, when the electron is apart from the laser pulse, energy gain in the range of GeV can be realized. We also find the dependence of energy gain on the electron's initial position and the scattering angle of electrons distributed in different coordinates in the focus plane.

Classical fifth order calculations in the diffraction angle show that electron, injected sideways into the tightly focused laser beam, get captured and gain energy in the GeV regime.

Figure (2.2) shows the polarization plane of laser beam which is the xz -plane (plane of the page), also the injection of electron is in this plane, without any loss of generality, the electron, in all the examples to be considered through this work, will be fired from the point whose Cartesian coordinates are $(x_0, 0, z_0)$ towards a point on the beam axis a distance s from the focus. Hence, motion outside the plane of polarization turns out to be negligibly small, in addition we will consider only projection of the

trajectories onto this plane .

It is also shown in figure (2.2) that the boundaries of the beam is the curves in the xz -plane defined by $x = \pm w(z)$, after the interaction between the injected electron and the laser fields, the electron will be considered as one of three possibilities, it is considered to be *transmitted* if its trajectory crosses the line $x = w(z)$, it will be considered *reflected* if the trajectory crosses the line $x = -w(z)$ twice, or not crossing at all. Otherwise, it will be considered *captured* by the beam.

Strictly speaking, the field intensity on the curves $x = \pm w(z)$ falls down to $1/e^2$ of its maximum value on axis. Thus a transmitted or reflected electron will be weakly affected by the laser fields beyond the beam boundaries.

Figure (2.3) illustrates the three distinct cases of electron motion following injection towards the focus of the beam. Note in particular that the capture and transmission cases exhibit features similar to those of the stretched-out familiar from the plane-wave discussion. This is not surprising because close to the beam focus the wavefronts are also planar. We recall that the asymmetry in the tightly-focused regime is essential, because, according to the Lawson-Woodward theorem, in a symmetric plane-wave where every *accelerating* half cycle is followed by an equally *decelerating*

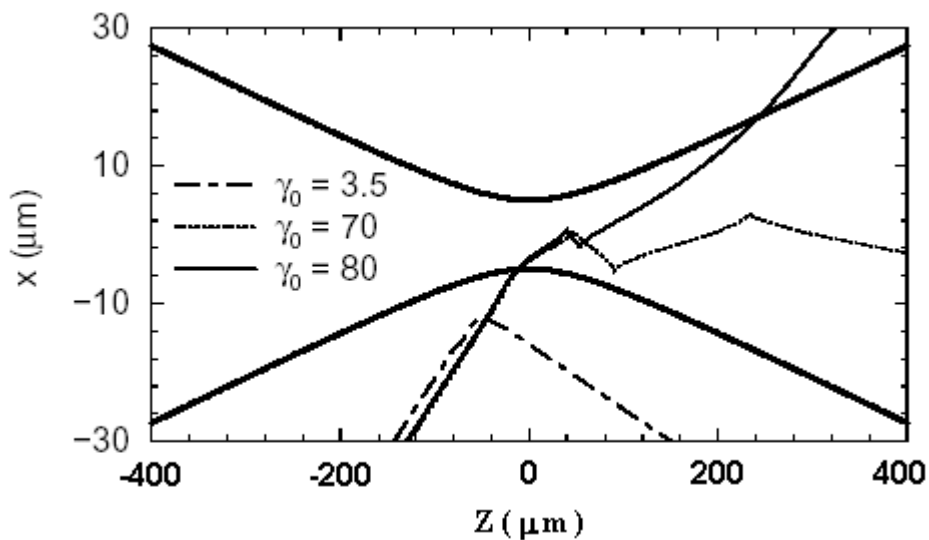


Figure 2.3 Portions of trajectories illustrating reflection, capture and transmission, when the electron is injected into the focus. The dark lines mark the beam *boundaries* as defined in the text.

one, no net gain is to be expected.

2.4.3 Electron dynamics

In this section we focus our attention to describe the motion of electron in the while interacting with tightly focused laser beam (full description of fields will be in the next section). The dynamics of such electron of mass m , and charge $-e$ injected with initial speed β_0 at an arbitrary angle θ with the direction of propagation of laser beam as shown in figure (2.2), will be investigated by numerically solving the following set of coupled equations:

$$\frac{d\vec{p}}{dt} = -e[\vec{E} + \vec{\beta} \times \vec{B}] \quad (2.3)$$

$$\frac{d\mathcal{E}}{dt} = -ec\vec{\beta} \cdot \vec{E} \quad (2.4)$$

Equation (2.3) is nothing but Newton's second law of motion for the electron, the other equation (2.4), on the other hand, gives the rate at which energy is gained or lost by the electron during the course of interaction with the same set of fields.

The outcome of solving the above set of equations, analytically or numerically, will basically be a detailed knowledge of the actual electron trajectory; in other words, a parametric representation of the electron's coordinates x, y , and z as functions of the time t , or some other parameter like $\eta = \omega t - kz$.

In Eqs.(2.3, 2.4) the quantities have their usual definitions: \vec{E} is the electric field of laser, where \vec{B} stands for the laser magnetic field. Furthermore the relativistic momentum and energy of the electron are given respectively as:

$$\vec{p} = \gamma mc\vec{\beta}, \quad \mathcal{E} = \gamma mc^2 \quad (2.5)$$

The Lorentz factor $\gamma = (1 - \beta^2)^{-1/2}$, and the velocity, normalized by the speed of light c in vacuum, is $\vec{\beta}$. The peak field intensity I_0 will be expressed in terms of $q = eE_0/mc\omega$, where $I_0\lambda^2 \approx 1.375 \times 10^{18} q^2 \text{ (W/cm}^2\text{)}(\mu\text{m})^2$. The scaled velocity vector is :

$$\vec{\beta} = \beta_x \hat{i} + \beta_y \hat{j} + \beta_z \hat{k} \quad (2.6)$$

Where

$$\beta_x = \frac{v_x}{c}, \quad \beta_y = \frac{v_y}{c}, \quad \beta_z = \frac{v_z}{c} \quad (2.7)$$

The electric and magnetic vector components is given by:

$$\begin{aligned} \vec{E} &= E_x \hat{i} + E_y \hat{j} + E_z \hat{k} \\ \vec{B} &= B_x \hat{i} + B_y \hat{j} + B_z \hat{k} \end{aligned} \quad (2.8)$$

The vectors $\hat{i}, \hat{j}, \hat{k}$ are the usual unit vectors in the Cartesian coordinate system. By substituting the quantities of equation (2.3) with their values from equation (2.5) we will get:

$$\frac{d(\gamma\vec{\beta})}{dt} = -\frac{e}{mc}[\vec{E} + \vec{\beta} \times \vec{B}] \quad (2.9)$$

Taking into account that for our purpose in this work we consider the x component of magnetic field to be zero(i.e. $B_x = 0$), hence the second term in the right hand side of equation (2.9) will be simplified by means of expansion, and after multiplications we get:

$$\vec{\beta} \times \vec{B} = \hat{i}(\beta_y B_z - \beta_z B_y) - \hat{j}(\beta_x B_z) + \hat{k}(\beta_x B_y) \quad (2.10)$$

By substituting result from equation (2.10) together with the expansion of

\vec{E} from equation (2.8) into equation (2.9) we get:

$$\frac{d(\gamma\vec{\beta})}{dt} = -\frac{e}{mc} [\hat{i}(E_x + \beta_y B_z - \beta_z B_y) + \hat{j}(E_y - \beta_x B_z) + \hat{k}(E_z + \beta_x B_y)] \quad (2.11)$$

The result in equation (2.11) is a vector form derivative equation, so it can be divided into three equations, one component along each direction (i.e. x, y, z):

$$\frac{d(\gamma\beta_x)}{dt} = -\frac{e}{mc} [E_x + \beta_y B_z - \beta_z B_y] \quad (2.12)$$

$$\frac{d(\gamma\beta_y)}{dt} = -\frac{e}{mc} [E_y - \beta_x B_z] \quad (2.13)$$

$$\frac{d(\gamma\beta_z)}{dt} = -\frac{e}{mc} [E_z + \beta_x B_y] \quad (2.14)$$

Recall that from the definition of relativistic energy is $\mathcal{E} = \gamma mc^2$, so using this relation together with expansions of both the relativistic velocity and electric field to simplify the energy rate equation (2.4), after rearrangement of terms we get:

$$\frac{d\gamma}{dt} = -\frac{ec}{mc^2} [\beta_x E_x + \beta_y E_y + \beta_z E_z] \quad (2.15)$$

If we expand the left hand side of Eqs.(2.12-2.14), this leads to the following three equations respectively:

$$\beta_x \frac{d\gamma}{dt} + \gamma \frac{d\beta_x}{dt} = -\frac{e}{mc} [E_x + \beta_y B_z - \beta_z B_y]$$

$$\begin{aligned}\beta_y \frac{d\gamma}{dt} + \gamma \frac{d\beta_y}{dt} &= -\frac{e}{mc} [E_y - \beta_x B_z] \\ \beta_z \frac{d\gamma}{dt} + \gamma \frac{d\beta_z}{dt} &= -\frac{e}{mc} [E_z + \beta_x B_y]\end{aligned}$$

Substitution of the result $(d\gamma/dt)$ from equation (2.15) in the above equations and rearrange terms yields three equations, in each one, the left side is a derivative in one direction for the relativistic velocity β with respect to the time t .

$$\frac{d\beta_x}{dt} = -\frac{e}{\gamma mc} [E_x + \beta_y B_z - \beta_z B_y - \beta_x \beta_x E_x - \beta_x \beta_y E_y - \beta_x \beta_z E_z] \quad (2.16)$$

$$\frac{d\beta_y}{dt} = -\frac{e}{\gamma mc} [E_y - \beta_x B_z - \beta_y \beta_x E_x - \beta_y \beta_y E_y - \beta_y \beta_z E_z] \quad (2.17)$$

$$\frac{d\beta_z}{dt} = -\frac{e}{\gamma mc} [E_z + \beta_x B_y - \beta_z \beta_x E_x - \beta_z \beta_y E_y - \beta_z \beta_z E_z] \quad (2.18)$$

Remember that $(\vec{\beta} = \vec{v}/c)$, therefor we get another first order differential equations for trajectories:

$$\frac{dx}{dt} = c\beta_x \quad (2.19)$$

$$\frac{dy}{dt} = c\beta_y \quad (2.20)$$

$$\frac{dz}{dt} = c\beta_z \quad (2.21)$$

The six equations (2.16- 2.21) are first order coupled differential equations, represent the state model for the dynamics of electron, to be solve numerically by means of system of nonlinear equations. Solving these equations

by using numerical integration method called the Adaptive Runge-Kutta Method, will lead to the trajectories and relativistic velocities of the injected electron. Many physical quantities will be calculated depending on the results such as the momentum, energy gain, radiation losses, and others.

2.4.4 The description of fields near the Gaussian beam focus

Most theoretical treatments of electron laser acceleration employ low-order Gaussian or Bessel beams[46], the aim is to reach GeV or even TeV energies, the last demand use of extreme high intensity laser fields. The laboratory production of this intensity is done by focusing over a small spatial dimensions of order of microns, this needs detailed knowledge of the fields near the beam focus.

Recall that from Salamin work [35], the beam shown in figure(2.2) may be modeled by a vector potential linearly polarized along the $+x$, the beam axis is taken along the z direction with propagation along the $+z$.

According to this scheme, the cross section through the beam focus is circular and has a radius w_0 ; a cross section through an arbitrary point z on axis is also circular with radius given by:

$$w(z) = w_0 \sqrt{1 + (z/z_r)^2}$$

With $k = 2\pi/\lambda$, the Rayleigh length is $z_r = kw_0^2/2$ and the diffraction angle is $\epsilon = w_0/z_r$, typically, much less than one and can serve as expansion parameter.

Now, let us define some dimensionless parameters: $\xi = x/w_0$, $v = y/w_0$, and $\zeta = z/z_r$. Furthermore, $k = \omega/c$, and $\rho = r/w_0$.

$$r^2 = x^2 + y^2 \implies (\text{change with previous values}) \implies \rho^2 = \xi^2 + v^2.$$

Since we seek fields that propagate in the $+z$, in this case, the vector potential \vec{A} has only x component.

The fields will be derived from the trial linearly-polarized vector potential given as:

$$\vec{A} = \hat{i}A_0g(\eta)\psi(\vec{r})e^{i\eta} \quad (2.22)$$

Where,

$$\vec{E} = -\frac{1}{c}\frac{\partial\vec{A}}{\partial t} \quad (2.23)$$

$$\vec{B} = \nabla \times \vec{A} \quad (2.24)$$

For simplicity, let us define some variables as they are used through the

definitions of both the electric and magnetic fields components,

$$E = E_0 \frac{w_0}{w} \exp \left[-\frac{r^2}{w^2} \right]; \quad E_0 = kA_0, \quad (2.25)$$

$$S_n = \left(\frac{w_0}{w} \right)^n \sin(\psi + n\psi_G); \quad n = 0, 1, 2, \dots \quad (2.26)$$

$$C_n = \left(\frac{w_0}{w} \right)^n \cos(\psi + n\psi_G). \quad (2.27)$$

The functions ψ and g are varying slowly, where

$$\psi = \psi_0 + \psi_P - \psi_R + \psi_G \quad (2.28)$$

ψ_0 is a constant phase, and

$$\psi_P = \eta = \omega t - kz \quad (2.29)$$

is the plane wave phase. The Guoy phase associated with the fact that a Gaussian beam undergoes a total phase change of π as z changes from $-\infty$ to $+\infty$ is:

$$\psi_G = \tan^{-1}(z/z_r) \quad (2.30)$$

And,

$$\psi_R = kr^2/(2R) \quad (2.31)$$

is the phase associated with the curvature of the wave fronts, and

$$R(z) = z + z_r^2/z \quad (2.32)$$

is the radius of curvature of a wave-front intersecting the beam axis at the coordinate z .

The final fields near the focus of the beam resulting from derivation upon the above introduced variables and parameters are given as the following (full derivation in appendix 1).

The electric field components are:

$$E_x = E \left\{ S_0 + \epsilon^2 \left[\xi^2 S_2 - \frac{\rho^4 S_3}{4} \right] + \epsilon^4 \left[\frac{S_2}{8} - \frac{\rho^2 S_3}{4} - \frac{\rho^2(\rho^2 - 16\xi^2)S_4}{16} - \frac{\rho^4(\rho^2 + 2\xi^2)S_5}{8} + \frac{\rho^8 S_6}{32} \right] \right\}, \quad (2.33)$$

$$E_y = E\xi v \left\{ \epsilon^2 S_2 + \epsilon^4 \left[\rho^2 S_4 - \frac{\rho^4 S_5}{4} \right] \right\}, \quad (2.34)$$

$$E_z = E\xi \left\{ \epsilon C_1 + \epsilon^3 \left[-\frac{C_2}{2} + \rho^2 C_3 - \frac{\rho^4 C_4}{4} \right] + \epsilon^5 \left[-\frac{3C_3}{8} - \frac{3\rho^2 C_4}{8} + \frac{17\rho^4 C_5}{16} - \frac{3\rho^6 C_6}{8} + \frac{\rho^8 C_7}{32} \right] \right\}. \quad (2.35)$$

Similarly, the magnetic field components are given by:

$$B_x = 0, \quad (2.36)$$

$$B_y = E \left\{ S_0 + \epsilon^2 \left[\frac{\rho^2 S_2}{2} - \frac{\rho^4 S_3}{4} \right] + \epsilon^4 \left[-\frac{S_2}{8} + \frac{\rho^2 S_3}{4} + \frac{5\rho^4 S_4}{16} - \frac{\rho^6 S_5}{4} + \frac{\rho^8 S_6}{32} \right] \right\}, \quad (2.37)$$

$$B_z = E v \left\{ \epsilon C_1 + \epsilon^3 \left[\frac{C_2}{2} + \frac{\rho^2 C_3}{2} - \frac{\rho^4 C_4}{4} \right] + \epsilon^5 \left[\frac{3C_3}{8} + \frac{3\rho^2 C_4}{8} + \frac{3\rho^4 C_5}{16} - \frac{\rho^6 C_6}{4} + \frac{\rho^8 C_7}{32} \right] \right\}. \quad (2.38)$$

These equations were derived from a vector potential with an amplitude A_0 and frequency ω . The fields given above satisfy Maxwell's equations $\nabla \cdot \vec{E} = 0 = \nabla \cdot \vec{B}$, plus terms of order ϵ^6 .

2.4.5 Radiation and energy loss

As the electron undergoes acceleration it radiates and therefore loses energy [10, 22]. Energy loss through radiation can severely limit the performance of an accelerator design. To discuss this issue in connection with the VBWA we report to the relativistic generalization of Larmor's formula for instantaneous power [37]

$$P(t) = \frac{2}{3} \frac{e^2}{c} \gamma^6 \left\{ \left[\frac{d\beta}{dt} \right]^2 - \left[\beta \times \frac{d\beta}{dt} \right]^2 \right\}. \quad (2.39)$$

The above result equation(2.39) is called the Liénard result. One area of application of the relativistic expression for radiated power is that charged-particle accelerators. For a given applied force (i.e. a given rate of change of momentum) the radiated power (2.39) depends inversely on the square of the mass of the particle involved. Consequently these radiative effects are the largest for electrons.

In linear accelerator, for example, the motion is one dimensional. In

this case, it is evident that the radiated power is

$$P = \frac{2}{3} \frac{e^2}{m^2 c^3} \left(\frac{dp}{dt} \right)^2 \quad (2.40)$$

The rate of change of momentum is equal to the change in energy of the particle per unit distance, consequently

$$P = \frac{2}{3} \frac{e^2}{m^2 c^3} \left(\frac{dE}{dx} \right)^2 \quad (2.41)$$

showing that for linear motion the power radiated depends only on the external forces which determine the rate of change of the particle energy with distance, not on the actual energy or momentum of the particle. Equation (2.41) shows that the radiated loss in an electron linear accelerator will be unimportant unless the gain energy is of order of $mc^2 = 0.511$ MeV in distance of $e^2/mc^2 = 2.82 \times 10^{-13}$ cm, or of the order of 2×10^{14} MeV/meter. Typical energy gains are less than 10 MeV/meter. Hence, radiation losses are completely negligible in linear accelerators, whether for electrons or heavier particles.

Part of the energy absorbed by the electron is inescapably re-emitted (scattered) and may show up as radiation at frequencies that are integer multiples of the laser field frequency. This process is termed *Harmonic Generation* (HG). In this work, HG will be reported in terms of the doubly-differential scattering cross-section or the energy per unit time per unit

frequency that is scattered into a unit solid angle $d\Omega$ [37]

$$\frac{d^2I}{d\omega d\Omega} = \frac{e^2}{4\pi^2c} \left| \left\{ \frac{\hat{n} \times [\hat{n} - \vec{\beta}] \times \dot{\vec{\beta}}}{(1 - \hat{n} \cdot \vec{\beta})^3} \right\}_{ret} \right|^2, \quad (2.42)$$

where *ret* implies the quantity is to be calculated at the retarded time or the time of the emitter $t' = t - R(t)/c$, with $R(t)$ the instantaneous emitter-to-detector separation.

Furthermore, \hat{n} is a unit vector pointing instantaneously from the emitter to the detector. One of the approximate, easier-to-handle, *versions* of this equation [37] may ultimately be used, due to the fact that the emission takes place over very small spatial dimensions, by comparison to the distance $R(t)$.

Chapter 3

Beat-Wave Laser Acceleration

3.1 Introduction

A vacuum beat wave acceleration as denoted by (VBWA), is an acceleration configuration in which two laser beams of differing wavelengths and arbitrary intensities generate a beat wave that can impart a net acceleration to particle [10, 18]. The mechanism relies on the ponderomotive force ($\vec{v} \times \vec{B}$) in such a way to circumvent the so-called Lawson-Woodward theorem (an electron gain no net energy as a result of interaction in vacuum with a pulse containing a large number of field cycles). However, a net energy gain is possible if the electron is made to interact with a fraction of a field cycle or, better yet, employing the beat-wave structure in which the fields need not to be symmetric.

Through this work, we propose to investigate the problem of acceleration of a single particle, an electron, in such an environment in this work, using laser fields currently available to laboratory experiments. Those fields are mentioned in the previous chapter and applying the tightly focused laser beam (Gaussian beam).

Figure (3.1) shows a schematic diagram of the interaction of the electron with the electromagnetic field configuration. The upper part is a diagram

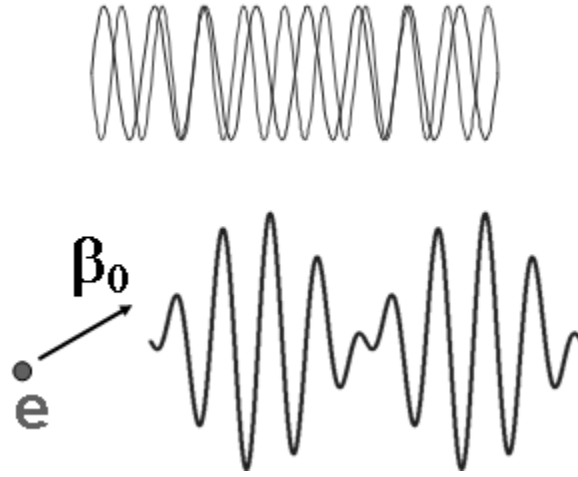


Figure 3.1 Construction of beat-wave

showing two co-propagated beams of the same amplitude but slightly different frequencies. The bottom part of the figure shows the resulting beat-wave structure and the way the electron is injected for acceleration by it. The electron is injected with an initial speed $\vec{\beta}_0$ (speed scaled by c , the speed of light in vacuum). Injection is at some angle θ (not shown) to the direction of propagation of the laser field, the latter coinciding with the coordinate z -axis and pointing left to right in the figure. Without any loss of generality, the initial injection direction is confined to the xz -plane (plane of the page) with the x -axis pointing in the direction of the laser field polarization (of at least one of the beams, should they differ in polarization). Optimum conditions that will lead to a maximum of energy gain will be sought in our calculations.

The configuration shown in figure (3.1) has recently been thoroughly investigated analytically, employing a plane-wave representation of the laser fields [10, 5]. What is new about the present work is to employ the most realistic model of a tightly focused laser beam in terms of the highly accurate Gaussian-beam description, which has been advanced recently [47, 48]. Analytic solutions of the motion equations, using the idealistic plane-wave representation of the laser fields, have yielded some valuable insight that may guide us in attacking the realistic version of the situation at hand. The numerical simulations we propose to carry out will open to us the door on a wide range of other related configurations which we will study and try to optimize for the purposes of particle acceleration and harmonic generation.

3.2 The Laser Plane Wave Model For The Beat-Wave Structure

Recent developments in laser technology, especially the successful generation of subcycle pulses in various laser regimes, makes it possible for the experimental testing of several ideas for the laser electron acceleration [10].

Salamin in his work [10] analyzed analytically the electron dynamics in the presence of the fields of two linearly polarized interfering co-propagating laser beams of different frequencies and arbitrary intensity. In one trial, the laser fields are modeled by plane waves, and in other, the fields are

allowed to have one-dimensional \sin^2 pulse shapes which model focusing in the propagation direction. It is found that an electron may be accelerated, even from rest, to GeV energies over short distances using present-day laser field intensities. This leads, in principle, to energy gradients in the TeV/m range.

In the above work the electron is considered to be injected sideways into the laser beam as shown in figure(3.2). In this section, we investigate the vacuum beat wave accelerator (VBWA) scheme using a one-dimensional model of the laser fields which involves the use of a pulse-shape function that governs the variations in the field amplitude in the forward propagation dimension.

The proposed model of laser pulse-shape is only approximate, but has the theoretical advantage of leading to analytic solutions, as well as, it enhance our understanding of the underlying physics and may be used to create codes for handling numerically the real situations when precise numbers are sought. We solve the relativistic equations of motion Eqs.(2.3, 2.4) of the electron in the fields of the two waves and obtain exact (within the limitations of our model) analytic expressions for its energy, momentum and trajectory, all in terms of the phase of one of the waves as a variable.

Injection at an angle results in the electron suffering more Compton en-

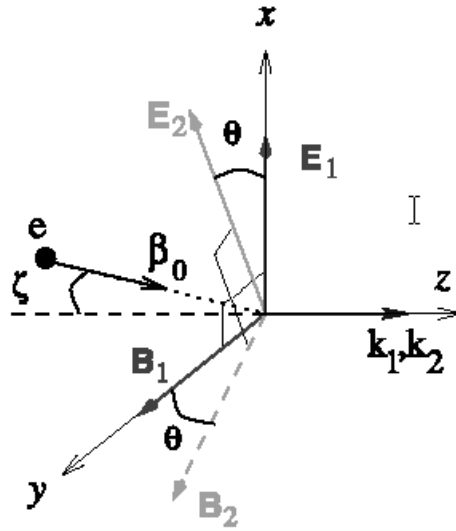


Figure 3.2 Schematic diagram of the electron interaction with the fields of the two component waves.

counters than when initially injected parallel to the direction of propagation of the wave as proposed by Esarey et al [45]. It is found that the net energy gain in the sideways injection much more than the case in parallel injection, other preference to the sideways injection over the parallel is, for example, in the parallel injection the constructive interference of two equal-intensity waves leads the electron to absorb a little more than four times the maximum amount of energy it would, otherwise gain from interacting with only one of the component waves.

Now let us study the motion of a single relativistic electron of mass m and charge $-e$ in the presence of electromagnetic fields of two waves co-

propagating along the z -axis and polarized linearly, one of the beams is polarized in the $+x$ direction while the other makes an arbitrary angle θ with the axis of the first one figure (3.2).

In such scheme, the electron is initially injected sideways with arbitrary angle ζ and initial linear velocity vector given as:

$$\vec{v}_0 = v_0(\hat{k} \cos \zeta + \hat{j} \sin \zeta) \quad (3.1)$$

If the two waves have amplitude E_j , angular frequencies ω_j and phase $\eta_j = \omega_j(t - z/c)$, where j is the label of the two wave either 1 or 2, t is time, z is the electron coordinate along the propagation direction, and c as usual the speed of light in vacuum. Then axial variation of the fields for both waves are modeled by a pulse -shape function $g(\eta_j)$, and the amplitudes variation of the fields are given as :

$$\begin{aligned} \vec{E} = & \hat{i}[E_1 g(\eta_1) \sin \eta_1 + E_2 \cos \theta g(\eta_2) \sin \eta_2] \\ & + \hat{j} E_2 \sin \theta g(\eta_2) \sin \eta_2 \end{aligned} \quad (3.2)$$

$$\begin{aligned} \vec{B} = & \hat{j}[E_1 g(\eta_1) \sin \eta_1 + E_2 \cos \theta g(\eta_2) \sin \eta_2] \\ & - \hat{i} E_2 \sin \theta g(\eta_2) \sin \eta_2 \end{aligned} \quad (3.3)$$

In the beat-wave scheme the phase of one wave is proportional to the other, this proportionality is represented by setting $\eta_1 = \eta$, and $\eta_2 = \alpha\eta$,

where α is the proportionality constant for which the frequency of the second wave is a multiple of the first by a factor α , hence $\alpha = \omega_2/\omega_1$.

Analogous to the derivation of the state model for electron motion Eqs.(2.16- 2.21), we can apply the usual equations of motion Eqs.(2.3,2.4) along with the same definitions for parameters listed in section (2.4.3) , but this time using fields from beat-wave structure Eqs.(3.2, 3.3), to find out a new set of equations governing the motion of injection of electron sideways in the presence of beat-wave lase fields, the equations are given as the following:

$$\begin{aligned} \frac{d\beta_x}{dt} &= \frac{1}{\gamma} \{ -(q_1\omega_1 g(\eta) \sin \eta + q_2\omega_2 \cos(\theta)g(\eta) \sin(\alpha\eta))(1 - \beta_z) \\ &\quad + \beta_x((q_1\omega_1 g(\eta) \sin \eta + q_2\omega_2 \cos(\theta)g(\alpha\eta) \sin(\alpha\eta))\beta_x \\ &\quad + q_2\omega_2 \sin(\theta)g(\alpha\eta) \sin(\alpha\eta)\beta_y) \} \end{aligned} \quad (3.4)$$

$$\begin{aligned} \frac{d\beta_y}{dt} &= \frac{1}{\gamma} \{ -q_2\omega_2 \sin(\theta)g(\alpha\eta) \sin(\alpha\eta)(1 - \beta_z) \\ &\quad + \beta_y((q_1\omega_1 g(\eta) \sin \eta + q_2\omega_2 \cos(\theta)g(\alpha\eta) \sin(\alpha\eta))\beta_x \\ &\quad + q_2\omega_2 \sin(\theta)g(\alpha\eta) \sin(\alpha\eta)\beta_y) \} \end{aligned} \quad (3.5)$$

$$\begin{aligned} \frac{d\beta_z}{dt} &= \frac{1}{\gamma} \{ -(q_1\omega_1 g(\eta) \sin \eta + q_2\omega_2 \cos(\theta)g(\alpha\eta) \sin(\alpha\eta))\beta_x \\ &\quad - q_2\omega_2 \sin \theta g(\alpha\eta) \sin(\alpha\eta) + \beta_z((q_1\omega_1 g(\eta) \sin \eta \\ &\quad + q_2\omega_2 \cos(\theta)g(\alpha\eta) \sin(\alpha\eta))\beta_x \end{aligned}$$

$$+q_2\omega_2 \sin(\theta)g(\alpha\eta) \sin(\alpha\eta)\beta_y)\} \quad (3.6)$$

And $dx/dt, dy/dt, dz/dt$ remains the same as in Eqs.(2.19-2.21). And in the above equations we have introduced the dimensionless intensity parameter:

$$q_j = \frac{eE_j}{mc\omega_j} \quad (3.7)$$

Where $q_j^2 = 1$ is equivalent to a field intensity of $10^{18}Wcm^{-2}$.

We will investigate the motion of a single electron in the presence of fields for beat-wave laser applying the plane wave structure numerically in the next chapter, for verification purpose, all results will be compared to the obtained analytical results of Salamin [10] as test cases for the validity of the code.

3.3 The Laser Gaussian Beam Model For The Beat-Wave Structure

In this section, we will consider the motion of electron of mass m and charge $-e$ described in section (2.4), but what is new for this section is, the injection of the electron sideways in the focus of two tightly focused laser beams of slightly different frequencies. Still to know that all definitions of quantities will be used the same through this section.

The fields for a single tightly focused laser beam are described in section (2.4.4). The fields components resulted from using two parallel beams with

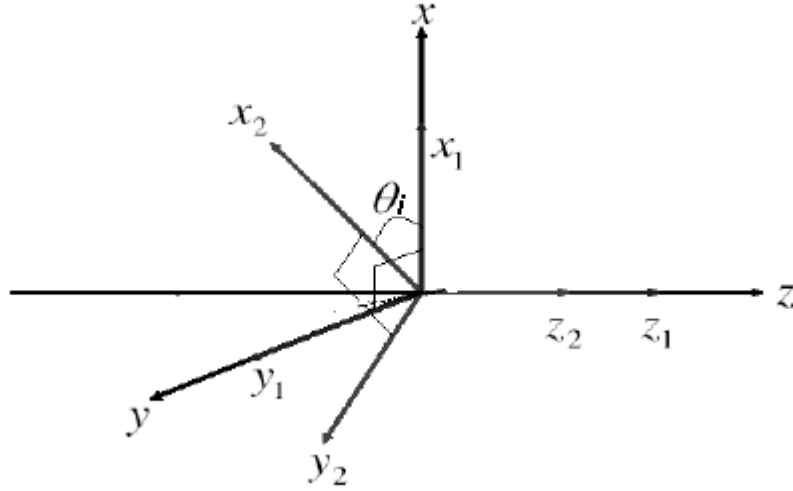


Figure 3.3 Schematic diagram represents the polarization of the two beams means of beat-wave will be obtained from vector sum of the fields for a single beam. In figure (3.2), two beams are used, upon close inspection with the help of figure (3.3), one finds that (with E_{1x} standing for the electric field component of beam 1 along x_1 , B_{2z} representing the magnetic field component of beam 2 along z_2 , and so forth):

$$E_x = E_{1x} + E_{2x} \cos \theta_i - E_{2y} \sin \theta_i \quad (3.8)$$

$$E_y = E_{1y} + E_{2y} \cos \theta_i + E_{2x} \sin \theta_i \quad (3.9)$$

$$E_z = E_{1z} + E_{2z} \quad (3.10)$$

$$B_x = 0 - B_{2y} \sin \theta_i \quad (3.11)$$

$$B_y = B_{1y} + B_{2y} \cos \theta_i \quad (3.12)$$

$$B_z = B_{1z} + B_{2z} \quad (3.13)$$

The three sets of coordinates, on the other hand, transform amongst each other through

$$x_1 = x \quad (3.14)$$

$$y_1 = y \quad (3.15)$$

$$z_1 = z \quad (3.16)$$

$$x_2 = x \cos \theta_i + y \sin \theta_i \quad (3.17)$$

$$y_2 = y \cos \theta_i - x \sin \theta_i \quad (3.18)$$

$$z_2 = z \quad (3.19)$$

Note that (θ_i) is the angle between the polarization of the two beams, where (x, y, z) is the beam coordinates as seen in the frame of reference.

3.4 Objectives And Work Plan

The main objectives of the present work may be succinctly put in the following:

1. Working out optimal conditions for the acceleration of (or energy gain by) a single particle (an electron) in the beat-wave laser scheme described above.

2. Calculation of the single-particle emission spectra associated with the acceleration process.
3. Provided time and space allow it, points (1) and (2) will be tried for an electron bunch (many electrons distributed in space according to some function).

The work plan:

We wish to solve the equations numerically using adaptive fourth-order Runge-Kutta routines. Following is a rough outline of the steps we anticipate the work will follow:

1. The starting point will be to write the code(s) for the complete solution of the equations
2. Next, the code(s) will be tested using a plane-wave description of the radiation (laser) fields. Results from the tests will be compared with the analytic work of Salamin et al.[10]. This process will be repeated for various configurations and parameters, etc. until stable and highly efficient codes are well developed.
3. Then, the radiation fields will be modeled most realistically. For this purpose the Gaussian beam description, advanced recently by Salamin et al, [34, 36, 37]. will ultimately be adopted

As the work progresses, we will look for some features of the electron dynamics and emitted radiation, these features will be listed at the first of chapter 5 which discuss the results.

Chapter 4

Computing Techniques And Methodology

This chapter will focus on computations. Various items will be discussed such as describing the numerical methods used through computations as an important part of this work, as well as the algorithm used and code structure, another thing will be the description of code outputs beside the verification of results.

4.1 Algorithm And Code Structure

In this work a famous numerical methods called the *Runge-Kutta-Fehlberg Method* [38] is used, it is adaptive method, means that this method is capable for changing the integration step size at moments it is not suitable. In other words, the step size is bigger when the value of integrated function is small, on the other hand, the step size is small when the integrated function value is big.

The algorithm for the later method is not ready to be used to solve a system of the form like the one here, it is ready for solving a single first order initial value differential equation, so a new algorithm is developed with help of [39] in order to solve a system of six coupled first order initial value problems, mean the equations of motion (3.4-3.6, and 2.19-2.21)of

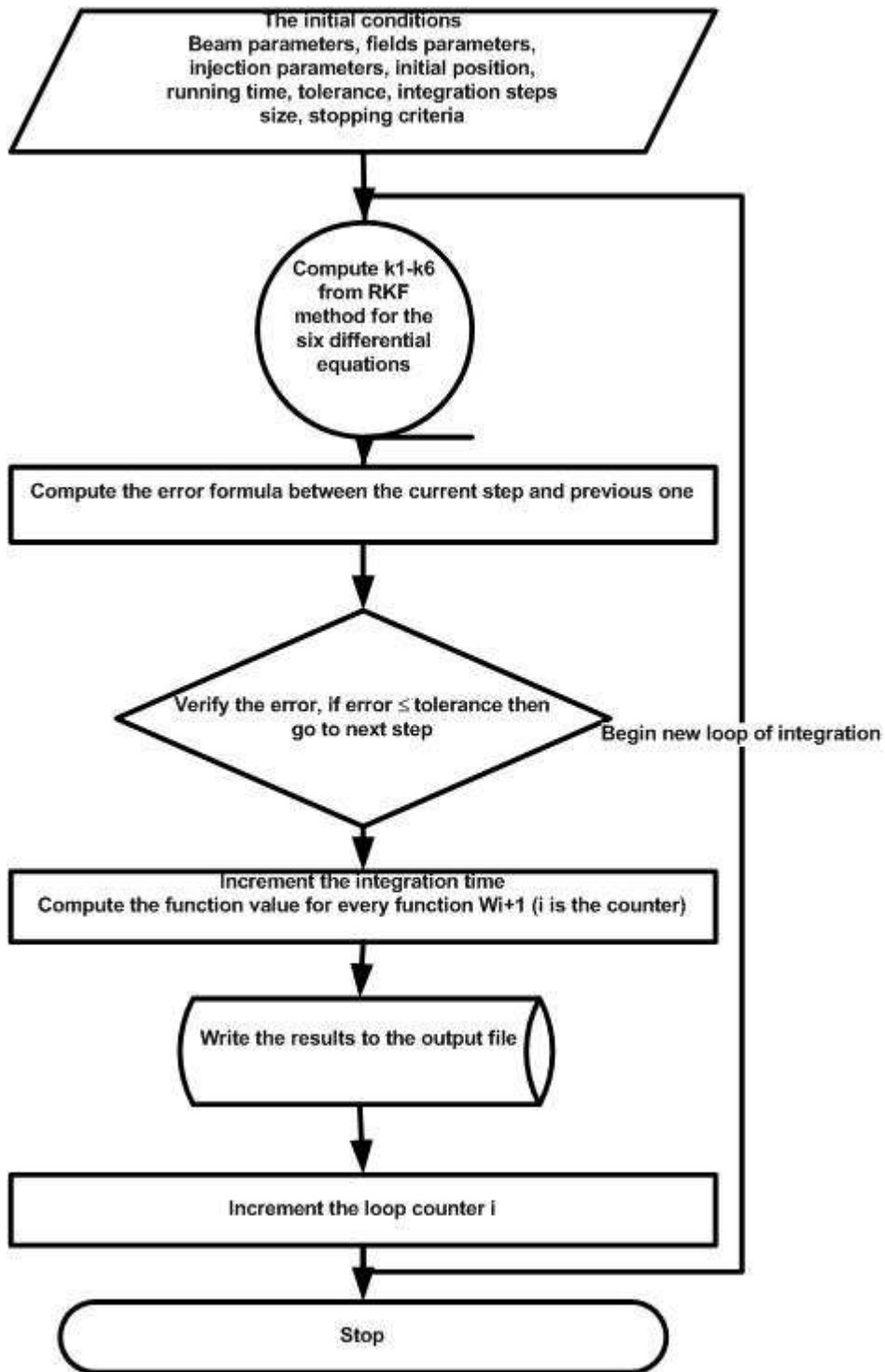


Figure 4.1 Flow chart showing the flow of computation in the numerical integration

electron described later in section(3.2).

The algorithm is interpreted to C++ programming language code [40], C++ is used because it is a powerful language in addition to its capability to execute huge programs faster than others. The algorithm and code will be listed in appendix 2 "for whom it may be concern". Note that the code is built to be fixed for each purpose, hence, many versions of the code are written each for one case only of the acceleration scheme. In this section, the final code used in work problem is only described, which is the laser beat-wave acceleration and its radiative effects.

Figure (4.1) shows the flowchart for the computation program, it shows the flow of data starting from initial conditions and ending with the best electron trajectories and velocities, the program is self contained as much as possible (i.e. minimize the input parameters).

4.2 Program Input And Output Quantities

Our aim is to compute many quantities for the electron acceleration in this work depending on our program, hence, the program is built into three stages. The first stage was using two plane waves beam model to accelerate the electron, as a result, a first sample of the code is built distinct for dealing with plane wave , then the code is developed to deal with Tightly focused laser beam as the second stage, at the last the code is developed to deal

with two tightly focused laser beams by means of beat-wave as the third stage.

There are few inputs as well as outputs will be shared for all cases, and others will be distinct for each case . At this moment , the shared input parameters are [10]: electron mass (m), electron charge ($-e$), speed of light (c),the beam wavelength λ , in addition to the injection initial conditions $(x_0, y_0, z_0, t_0, \beta_{x0}, \beta_{y0}, \beta_{z0})$. Whereas for the plane wave case the additional inputs are: the dimensionless intensity parameter (q_1, q_2) , the beams angular frequency (ω_1, ω_2) for the first and second beam respectively.

In the second stage, at the begging of the program the intensity parameter (q) is computed in terms of the laser power equation (5.3),and entering, the waist radius w_0 , the constant phase ψ_0 , the parameter s that determines the injection distance from the focus, the dimensionless Lorentz factor γ_0 that represents the initial energy of the electron, and the angels (θ, θ_i) for the injection angle and polarization angle respectively, whereas the remaining inputs still the same as previous case.

In the third stage, the additional parameters are, α which determines the difference between the beams angular frequency, the dimensionless Lorentz factor γ_0 , and the other parameters still the same as in stage two.

According to the outputs for each stage, we will list some of them

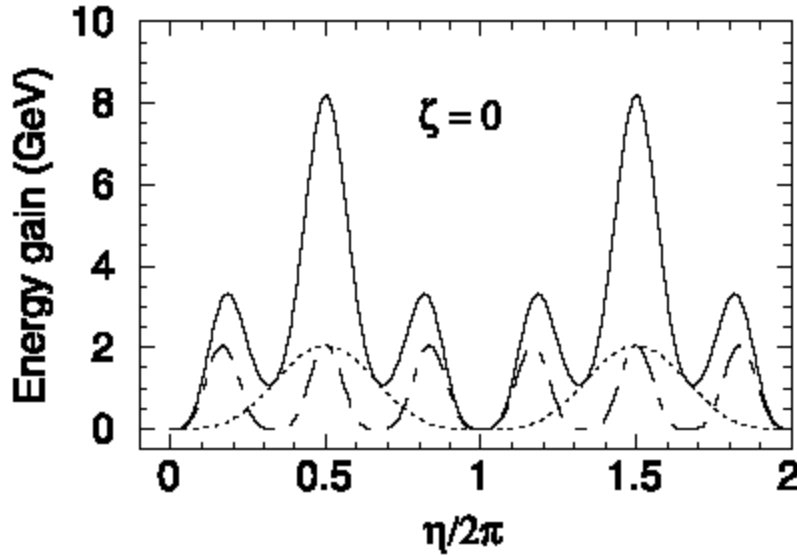


Figure 4.2 Electron energy gain versus the number of field cycles in the field of plane wave of wavelength $\lambda_1 = 1\mu m$ alone (dotted curves), in the field of a plane wave of wavelength $\lambda_2 = 1/3\mu m$ alone (chain curves), and in the field of beat-wave resulting from adding the two waves (full curves), see text for parameters

, in all cases the program can compute the trajectories of the electron $(x, y, z, \beta_x, \beta_y, \beta_z)$ as functions of the time t , the energy gain ($Gain = mc^2(\gamma - \gamma_0)$), some other parameters like $\eta = \omega t - kz$, and the radiation losses.

4.3 Code Stability And Verification Test

This work will be published as a scientific research, hence, the results and all computations done must be exact. By way it is cleared that we are constrained to compare most of the results with that obtained analytically

by Salamin. As a test case, the case of beat-wave using the normal laser fields will be checked and to be compared with results in [10].

Figure (4.2) is result of solving the coupled equations (3.4-3.6 and 2.19-2.21) for the case of beat-wave in which the laser is modeled by plane-wave, and shows the energy gain versus the number of field cycles in the field of a plane wave of wavelength $\lambda_1 = 1\mu m$ alone (dotted curves), in the fields of a plane wave of wavelength $\lambda_2 = 1/3\mu m$ alone (chain curves), and in the field of the beat wave resulting from addition of the two previous waves (full curves). In all cases, the intensity is approximately $10^{20}W/cm^2$ corresponding to ($q_1 = q_2 = 10$) and the initial injection kinetic energy is approximately 4.5 MeV corresponding to ($\gamma_0 = 10$). Note that $q_1 = q_2$ does not imply that the two amplitudes are equal, but rather that $E_1/\omega_1 = E_2/\omega_2$. Also note that the beat field is composed of $N_1 = 2$ field cycles of the wavelength λ_1 and $N_2 = 6$ of the field cycles of the wave of wavelength λ_2 .

Other case of interest, is to see the velocities change versus the number of field cycles. Figure (4.3) shows the Scaled electron velocity y-component versus the number of field cycles in a beat field of two waves of equal intensity ($q_1 = q_2 = 10$). The initial injection kinetic energy is approximately 0.511 MeV corresponding to ($\gamma_0 = 2$), the beam polarization angle $\theta = \pi/2$

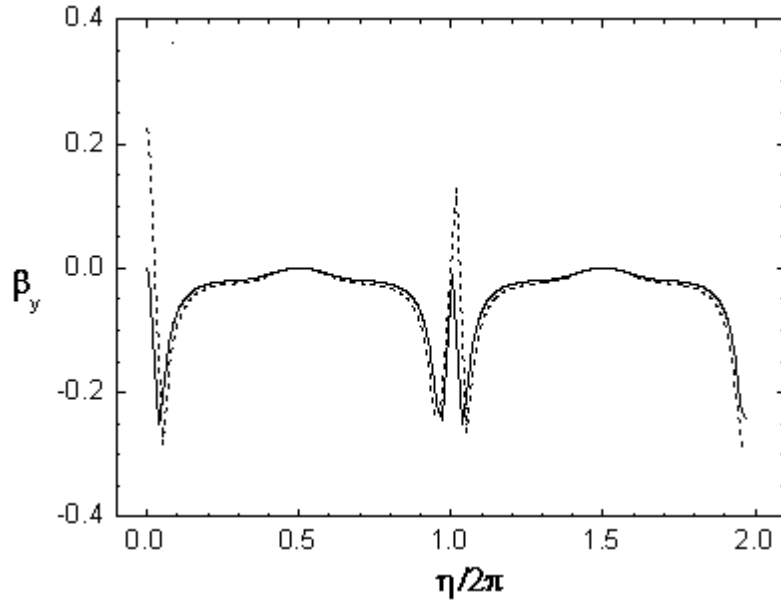


Figure 4.3 Scaled electron velocity y-component versus the number of field cycles in a beat field of two waves.

and the wavelengths differs by a factor $\alpha = 2$. The figure contains two plot lines, the first for parallel injection $\zeta = 0^\circ$ (full curves), and injection at angle $\zeta = 15^\circ$ (dotted curves), other parameters are the same for figure(4.2).

It is clearly shown that our results in figures(4.2,4.3) are identical to that published by Salamin [10] as (fig3.a, fig4.b) respectively.

Finally, for more test cases, figure 4.3.(a) illustrates the three distinct cases of electron motion following injection towards the focus of the beam shown in figure(2.2). Figures 4.3.(b) and 4.3.(c) show the variation of E_x, E_z respectively, along the electron trajectories.

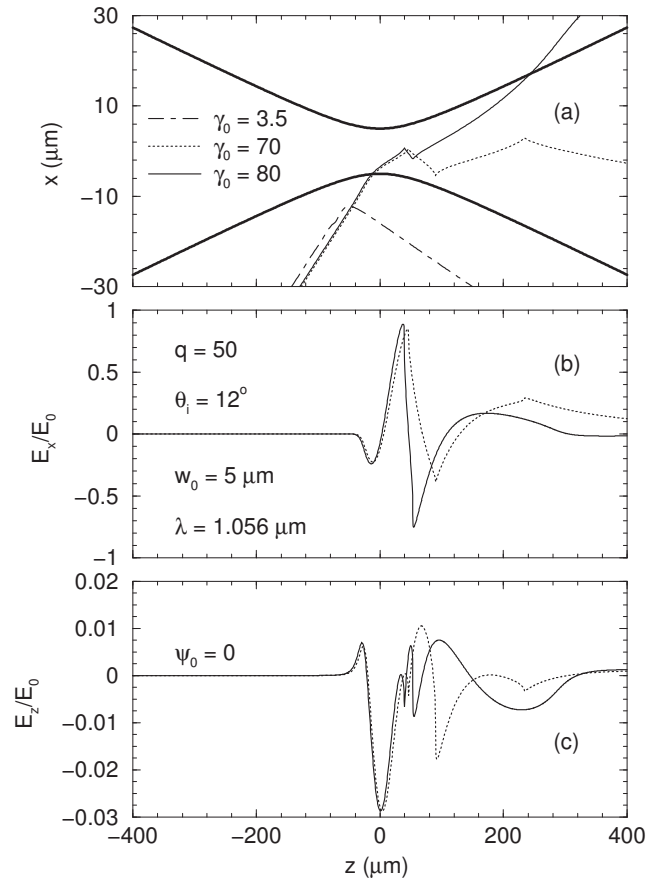


Figure 4.4 (a) Portions of trajectories illustrating reflection, capture and transmission, when the electron is injected into the focus. The dark lines mark the beam *boundaries* as defined through the text. (b) The transverse component, and (c) The longitudinal component of the electric field sensed by the electron along the transmission and capture trajectories displayed in (a).

For all cases, $z_0 = -3$ mm, and peak intensity $I_0 \approx 3.08 \times 10^{21}$ W/cm². The *full* interaction time is such that $\omega t = \pi \times 10^5$, at the end of which the gains are ≈ 207 MeV (capture), ≈ 40 MeV (transmission) and ≈ 25 MeV (reflection). The legends in (a) apply to (b) and (c). The later is similar to that obtained by Salamin in [35].

One can see that these examples and others (not listed here), that our results are the same for results given in [10, 34, 35, 36]. So we are now confident that our code and computations as well as results are true. Hence, we can depend on our program to be used for new case that are not discussed yet. Now, we will use the program to solve the equations of motion for electron injection in the fields of beat-wave laser applying the tightly focused laser beam model.

4.4 Manipulation Of Data And Results Generation

In this section we will talk about the manipulation of the data in order to get the results. One of the most important thing in our work is to get the energy gain, and then looking for the radiation losses. These items are dependent directly on the electron trajectories (*i.e.*, x, y, z) as well as scaled velocities (*i.e.*, $\beta_x, \beta_y, \beta_z$) in addition to the total time of interaction t (a sample data file will be listed in appendix 3).

To compute the energy gain we first compute the square of the scaled

velocity vector given as $(\beta^2 = \beta_x^2 + \beta_y^2 + \beta_z^2)$, and then we can compute the Lorentz factor $\gamma = 1/\sqrt{1 - \beta^2}$, and the energy gain is calculated by the following formula:

$$Gain = mc^2(\gamma - \gamma_0) \quad (4.1)$$

where γ_0 is the injection energy scaled by the electron's rest energy mc^2 .

Chapter 5

Discussion Of Results And Conclusion

As mentioned in chapter 3, this chapter will discuss the obtained results according to our view of the problem. At this moment, the following features of the electron dynamics and emitted radiation will be looked at:

1. The spatial electron trajectories will be studied and its motion in real space-time will be described. This may involve the use of appropriate visualization techniques and/or animation.
2. The electron velocity components will be looked at as functions of the time and/or the forward distance of travel. These will help us work out optimum conditions for efficient acceleration over small spatial dimensions.
3. Overall energy gain plots (versus time and/or a spatial dimension) will be produced and the parameters will be adjusted so as to lead to the best energy gradients (gain per unit forward distance of travel).
4. Accumulated data (mainly for the trajectories and velocities) will then be used to calculate the emission spectra.
5. Energy loss by the particle to the radiation field will be compared

somehow to the energy gain in order to better assess the efficiency of the configuration at hand as a mechanism of acceleration.

6. Other features will also be investigated as we see fit. As an example, some radiation patterns will be produced and reported if they turn out to be both useful and interesting.
7. Issues that may play a role in highlighting and elucidating of certain, and perhaps hitherto unanticipated, aspects of the acceleration process will be investigated.

Let us first specify some concluding remarks on this work that are related to the system of units used here. The Gaussian systems of units, followed by reference [37], will be adopted throughout this work unless specifically stated otherwise. Within the context of this cgs (centimeter-gram-second) system, one has:

- electron charge is $e = 4.8 \times 10^{-10} esu$
- electron mass is $m = 9.11 \times 10^{-28} g$
- speed of light in vacuum is $c = 3 \times 10^{10} cm/s$

As a starting point we demonstrated the electron acceleration in the presence of beat-wave laser beams treating the normal plane wave described

in section (3.2). And then treating the acceleration of electron by applying a single laser beam modeled by Lowest-order Gaussian beams ,fields for the later are described in section (2.4.4). Then finally, we demonstrated the electron acceleration in the present of beat-wave laser beams treating the tightly focused laser beams (Gaussian beams) described in section (3.3). We have presented an investigation based on representation of the fields for the Gaussian beam in which up to and including the fifth order in the diffraction angle ε to correct the electric and magnetic laser fields. The complexity of such fields, however, rends an impossible analytical solution to the electron's equations of motion. Hence, we solve the equations of motion numerically.

5.1 Electron Acceleration With The Normal Laser Fields

Following our discussion for beat-wave acceleration using plane wave representation for the laser that mentioned previously in section 3.2, for an electron of mass m and charge $-e$, we consider here the injection at an angle ζ relative to the propagation direction \hat{k} of two linearly polarized laser beams, the first along the x direction, and the second polarized at an angle θ with the other one. Without any loss of generality, the initial direction of motion of the electron will be considered here in the xz -plane. In other

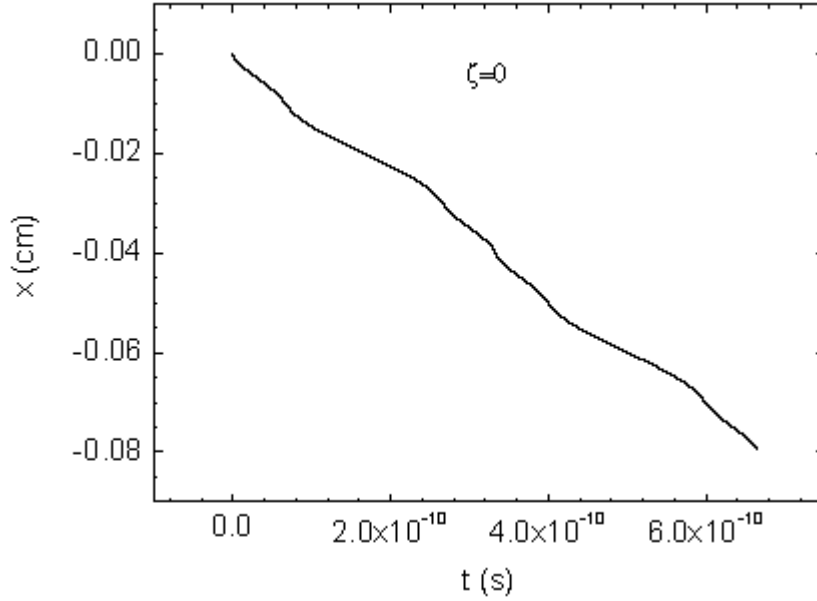


Figure 5.1 X-component of the electron trajectory in the plane wave field of beat-wave laser

words, the initial velocity will be

$$\vec{\beta}_0 = \beta_0(\hat{i} \sin \zeta + \hat{k} \cos \zeta) \quad (5.1)$$

In general, the electron relativistic dynamics will be discussed in terms of energy-momentum 4-vector (equations 2.5), the electron trajectories will be given as a function of the the plane-wave phase $\eta = \omega t - kz$ or the interaction time t .

Figure (5.1) shows the x-component of the electron trajectory as a function of time t result from solving the dynamic equations (3.4 – 3.6 and

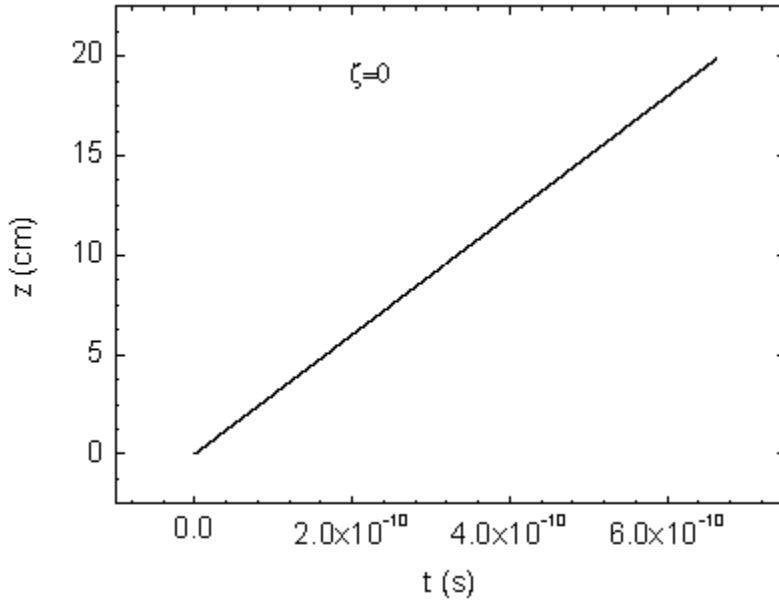


Figure 5.2 Z-component the electron trajectory in the plane wave field of beat-wave laser

2.19 – 2.21). Note that the electron interact with beat-wave composed of $N_1 = 2$ field cycles of the wave of wavelength $\lambda_1 = 1\mu m$ and $N_2 = 6$ field cycles of the wave of wavelength $\lambda_2 = 1/3\mu m$, and is injected from the point with coordinates $(0, 0, 0)$ with initial injection kinetic energy approximately 4.5 MeV ($\gamma_0 = 10$), the intensity is approximately $10^{20}W/cm$ ($q_1 = q_2 = 10$), the injection angle is ($\zeta = 0$), and the polarization angle ($\theta = 0$).

The corresponding Z-component of the electron trajectory for the above case is shown in figure(5.2). And the corresponding energy gain versus the

propagation direction z is shown in figure(4.2), the maximum energy gain result when the electron interact with one cycle of the first beam and two cycles from the second one, and in the other field cycles the electron retains a small part of energy gain.

It is shown in figure (4.2) that the electron energy oscillates with the phase of the laser fields. The electron interaction with the field cycles satisfies the Lawson-Woodward theorem [10] since it is gained energy in one part and deposit its energy in the other part. The underlying physics behind this theorem is, that the phase velocity of the laser fields near the interaction region is grater than the speed of light. Thus, it is argued that inevitable phase slippage would lead the electron to experience alternately acceleration and deceleration phase regions as it traverse the laser fields, which would result in the cancelation of the energy gain for unlimited interaction length.

So, we conclude in this section, while it is analytically tractable,that the plane wave treatment allows to build a clear intuitive picture, and the plane wave treatment is only approximate. Among its virtues also the fact that it help us to design suitable numerical codes that is needed ultimately for calculations that models the fields more realistically.

5.2 Electron Acceleration With A Single Laser Gaussian Beam

Since we intend to investigate the electron acceleration in relativistic regime of laser intensities, and because the required high intensity-laser fields can be realized by focusing over small dimensions, a detailed knowledge of the laser electric and magnetic fields near the focus of Gaussian is essential[35-36,40]. According to the discussion for Gaussian beam in sections(2.4.3, 2.4.4), figures(5.3, 5.4) show contours map of the electric and magnetic fields in the plane perpendicular to the beam axis and crossing it at the focus, the above maps are for the case of Gaussian beam with waist radius $w_0 = 5\mu m$ and wavelength $\lambda = 1.056\mu m$. In figures(5.3(a - c)) the fields are given at $\omega t = 0$, where in figures(5.3(d - f)) the fields are given at $\omega t = \pi/2$. Note that the positive and negative values are distinguished by the level of shading, dark for negative values and bright for positive values. The description of figure 5.3 is also applied to figure 5.4.

It is clear from the above figures that the fields are rapidly changing functions of the time. Moreover, the electron position at any time depends upon the initial injection parameters (i.g. initial position $(x_0, 0, z_0)$, injection energy γ_0 , injection angle ζ) and among other parameters that play a role in determining the ensuing dynamics include w_0 , q , and ψ_0 .

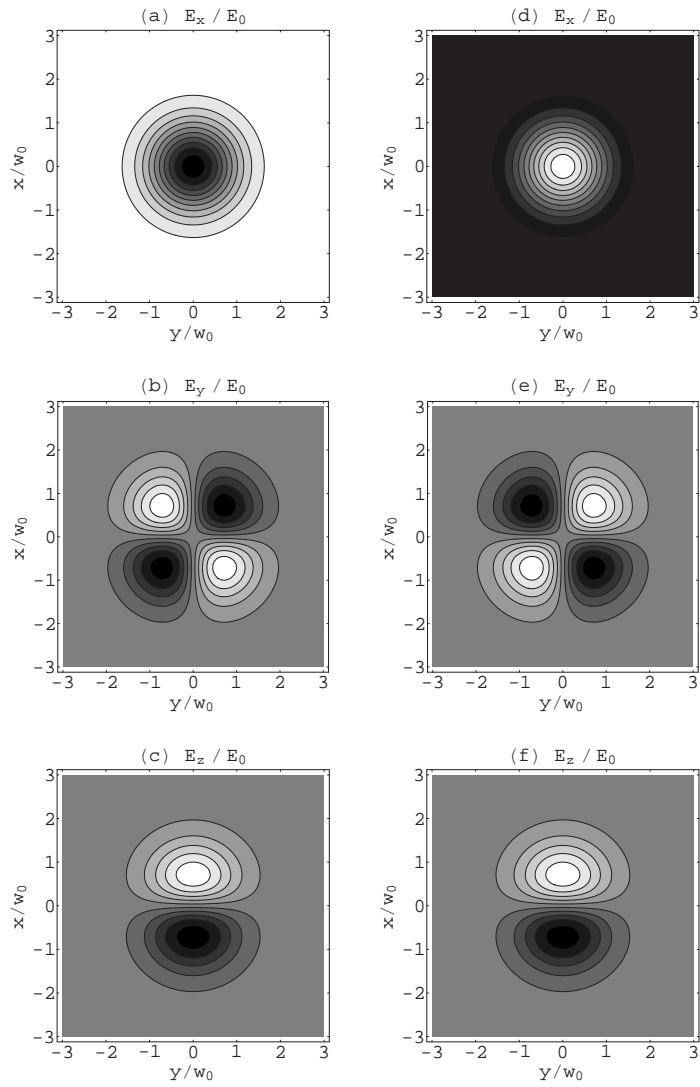


Figure 5.3 Contour maps of the electric components of the laser field of a Gaussian beam over a square $30 \mu\text{m}$ on a side, centered at the beam focus and extending in the xy plane.

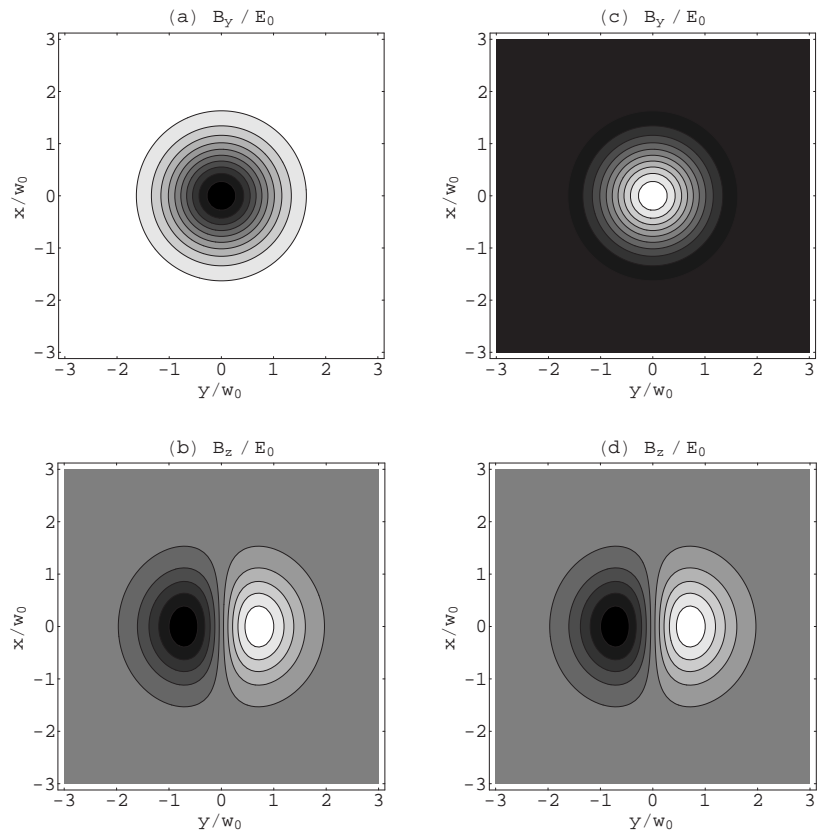


Figure 5.4 Contour maps of the magnetic component of a Gaussian beam over a square $30\mu\text{m}$ on a side, centered at the beam focus and extending in the xy plane, (see text for parameters)

In this level any energy gain or loss takes place at a time rate governed by equation (2.4). We illustrate the general procedure and give preliminary comments on some of the results, via the examples shown in figures (5.5 – 5.9). In these figures trajectories, some field components, and energy gains are shown for three sets of parameters for the initial injection energy (i.e. $\gamma_0 = 22, \gamma_0 = 15, \gamma_0 = 5$), and in all cases considered $z_0 = -5\text{mm}, \theta_i = 10^\circ, q = 10, w_0 = 5\mu\text{m}$, and $\lambda = 1\mu\text{m}$.

In figure(5.5) parts of the actual trajectories in the full fields are given, along with the spatial extension of the *beam boundaries* as background. Strictly speaking, it is not accurate to talk about a *boundary* for a laser beam, but for definiteness, we will adopt the curves in the (\hat{k}, \vec{E}) plane of the functions $x = \pm w(z)$ as giving the loci of points of intersection of a *beam surface* with that plane. On those lines the field intensity falls to e^{-2} of its maximum value on the beam axis. Typically, an electron trajectory starts from the injection point with coordinates $(z_0, x_0) = (-5, -5\tan\theta_i)$ mm, heads towards the focus, interacts with the beam and gets *reflected, captured, or transmitted*.

Figures (5.6 – 5.9) show plots of the field components E_x, E_z , and B_y sensed by the electron along its trajectory for the examples considered above. Note first that E_z is typically some two orders of magnitude smaller

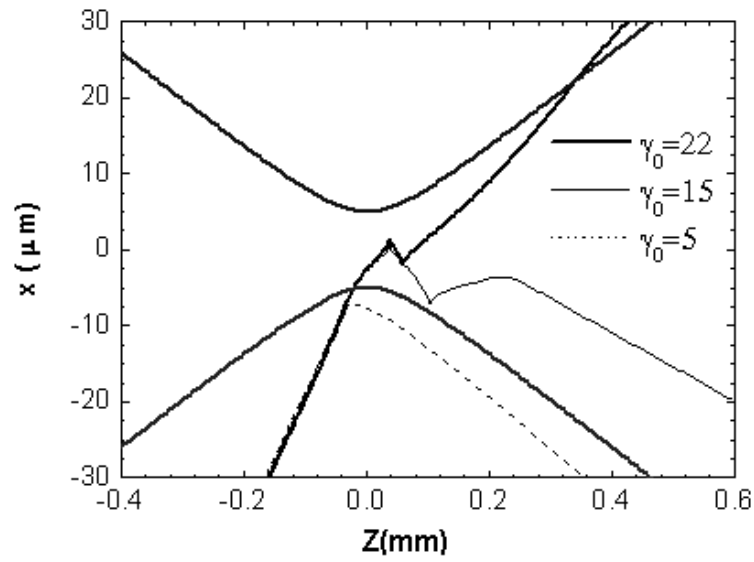


Figure 5.5 The electron trajectories for various values of initial injection energy, for $\gamma_0 = 22$ (heavy curves), for $\gamma_0 = 15$ (light curves), for $\gamma_0 = 5$ (dotted curves).

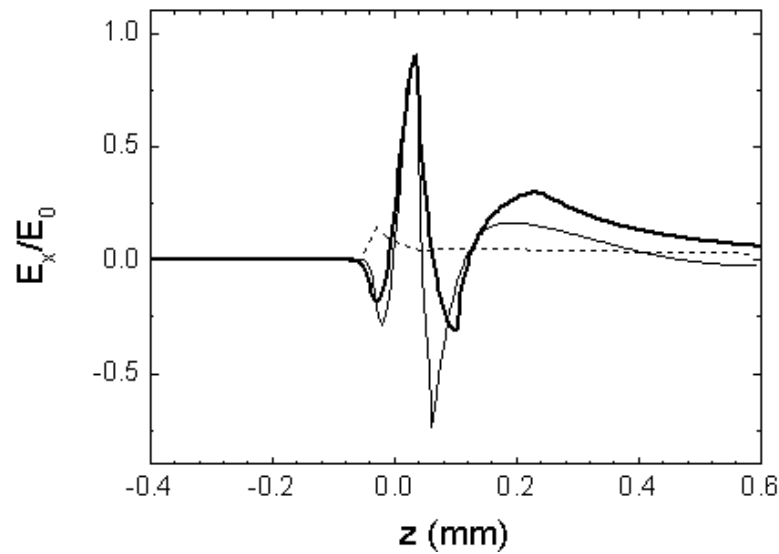


Figure 5.6 The x-component of the electric field, for $\gamma_0 = 22$ (heavy curves), for $\gamma_0 = 15$ (light curves), for $\gamma_0 = 5$ (dotted curves).

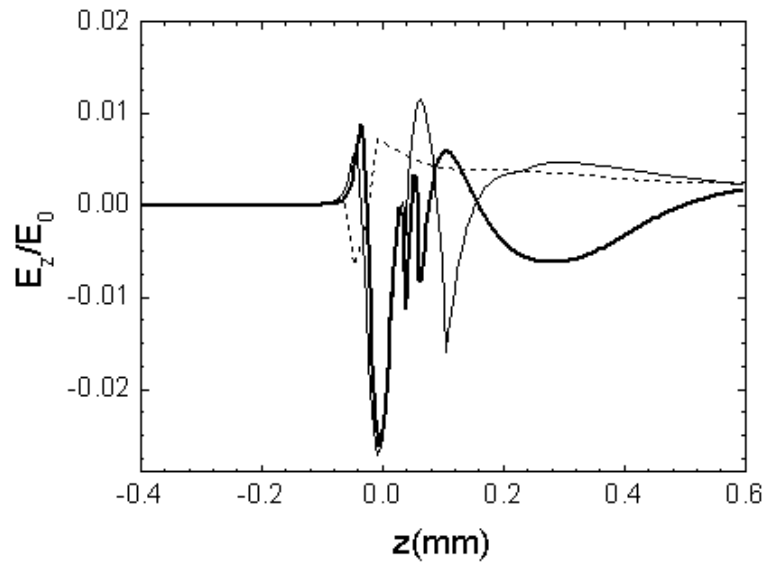


Figure 5.7 The z-component of the electric field , for $\gamma_0 = 15$ (light curves) , for $\gamma_0 = 5$ (dotted curves).

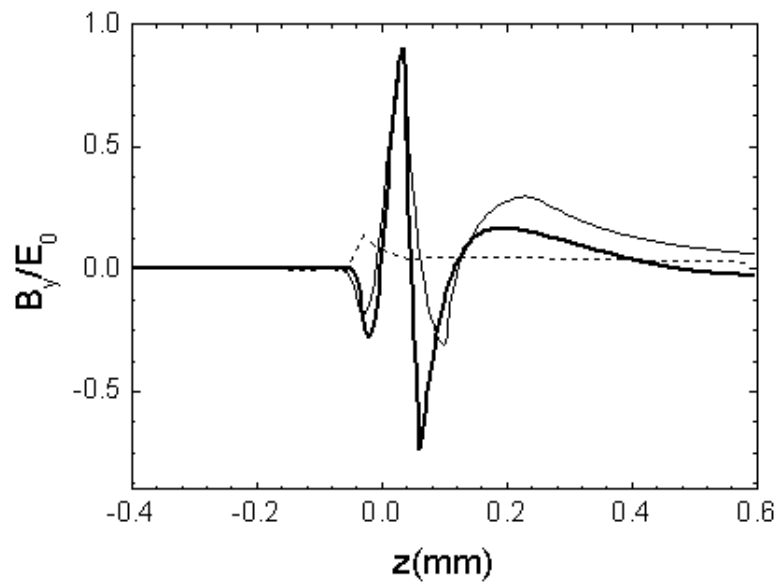


Figure 5.8 The y-component of the magnetic field, for $\gamma_0 = 15$ (light curves) , for $\gamma_0 = 5$ (dotted curves).

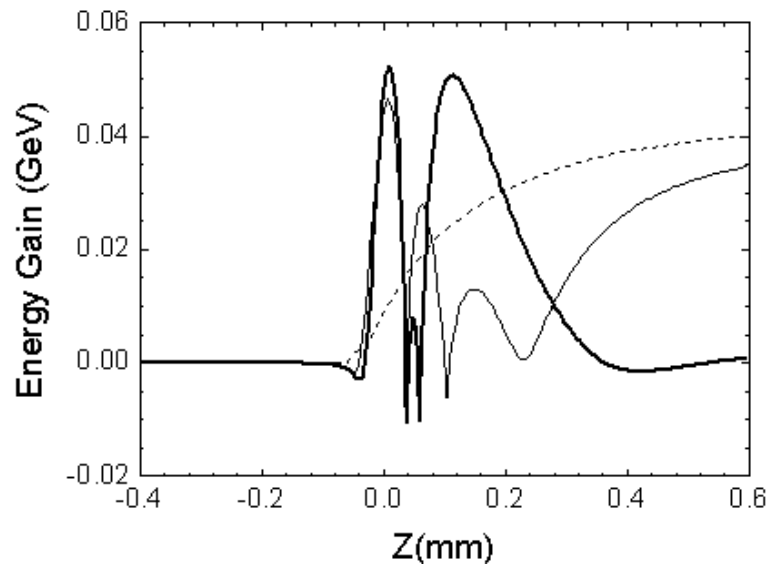


Figure 5.9 The electron energy gain for different values of initial injection energy, for $\gamma_0 = 15$ (light curves) , for $\gamma_0 = 5$ (dotted curves).

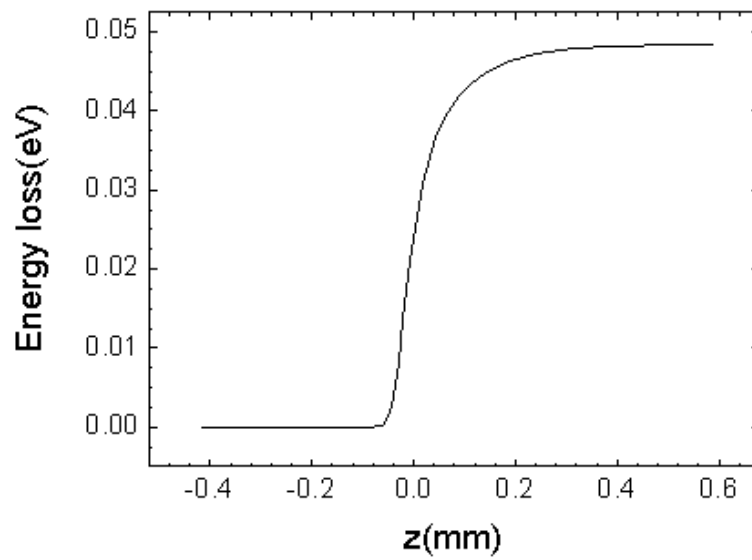


Figure 5.10 The electron energy loss for the case of initial injection energy $\gamma_0 = 5$.

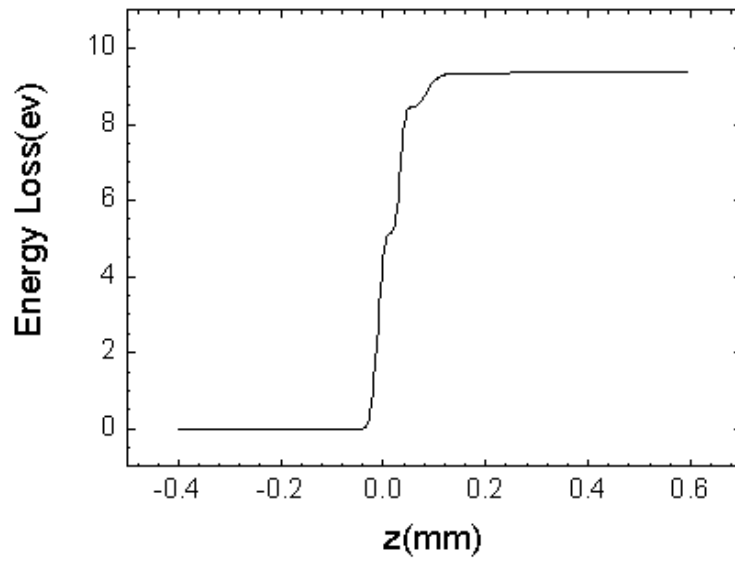


Figure 5.11 The electron energy loss for the case of initial injection energy $\gamma_0 = 15$.

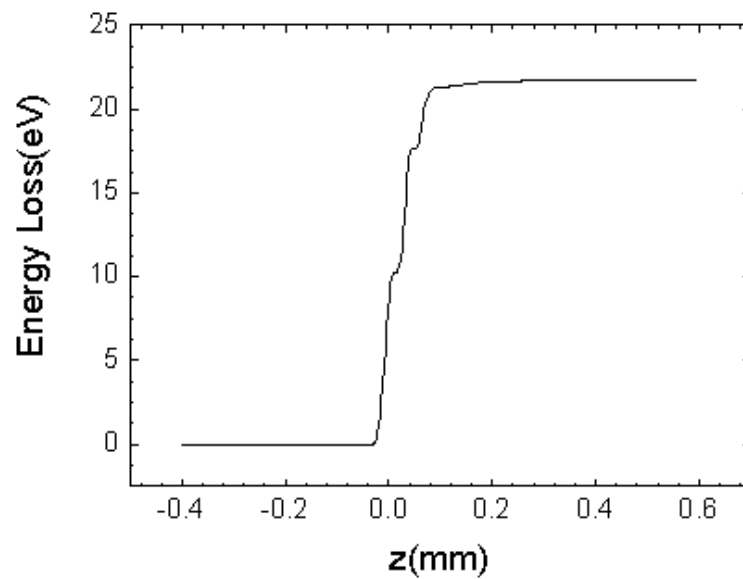


Figure 5.12 The electron energy loss for the case of initial injection energy $\gamma_0 = 22$.

than E_x and that $E_x \sim B_y$, in the gaussian system of units we are using. It is not hard to notice the lack of symmetry in the field oscillations (not to be confused with the field cycles). Thus interaction of the electron with a negative portion of, say E_x , results in energy gain. Subsequent interaction with the following positive portion does not result in total loss of the gained energy, and so on. This may be seen by studying figures (5.6) and (5.9) together.

Furthermore, by studying a typical trajectory portion given in figure 5.5) together with the corresponding fields in (5.6 – 5.8) one can easily understand the correlation between, say the turning points on a typical trajectory, and the points at which, say E_x , ceases to increase (or decrease), and so on.

In figure (5.9) the electron energy gain, defined by equation (4.1) and calculated numerically here, is shown.

The radiation losses for the above sets of parameters are also shown here in figures(5.10 – 5.12) which are computed using equation(2.39).

5.3 Electron Acceleration By Beat-Wave Laser And Associated Radiative Effects (Tightly Focused Laser Beams)

In this section we will show our work through investigation of the dynamics of an electron interacting with the fields of beat-wave laser beam resulting from adding two gaussian beams of slightly different frequencies.

We must point out that for a particular set of parameters here, the results will be different, for example when we test any factor like the injection on both sides of the focus, then the results will be unique for the set of parameters taken for the beam and the electron initial conditions.

Since we intend to investigate the electron dynamics in such relativistic regime of laser intensities, a detailed knowledge of the laser electric and magnetic fields near the focus of gaussian beat-wave is essential.

Following the discussion about tightly focused laser fields in section 2.4.4, and the beat-wave construction in section 3.3, we consider here the injection of an electron with initial scaled speed β_0 sideways at an angle θ to the direction of propagation of beat-wave resulting from adding two Gaussian beams of slightly different frequencies. The first beam is polarized in the x direction, where the other is polarized at an angle θ_i relative to the first one. Schematic diagrams that describe the process are shown in figures (2.2, 3.3), but instead, the fields are for beat-wave.

In figures (5.13, 5.14) we show contour maps of the electric and magnetic fields in plane perpendicular to the beams axes and crossing them at the focus. The maps are snapshot taken at $t = 0$ and, later, at $t = \pi/(2\omega)$, bright spots correspond to positive values and dark areas represent negative ones. So an, otherwise free, electron will feel a force of attraction and, hence, be accelerated in dark regions and vice versa.

Needless to say that the fields are rapidly changing functions of the time and so are the field strength and sign at any one point. Moreover, where the electron will be at any point in time depends also upon its injection parameters, namely, the initial position $(x_0, 0, z_0)$, the initial injection energy γ_0 , and the initial injection angle θ . Other parameters that play a role in determining the ensuing dynamics include w_0, q , and ψ_0 .

Roughly speaking, since E_x and B_y are the largest field components, the ensuing electron motion will most strongly be influenced by them. For the high field intensities of interest to us in this work, $q \gg 1$, motion out of the (\mathbf{k}, E) plane turns out to be small. So, projection of the electron trajectory onto this plane will be considered only. On the other hand, E_x and E_z will play the biggest part in producing the energy gain.

Figures (5.15, 5.16) show the transverse and longitudinal variation of

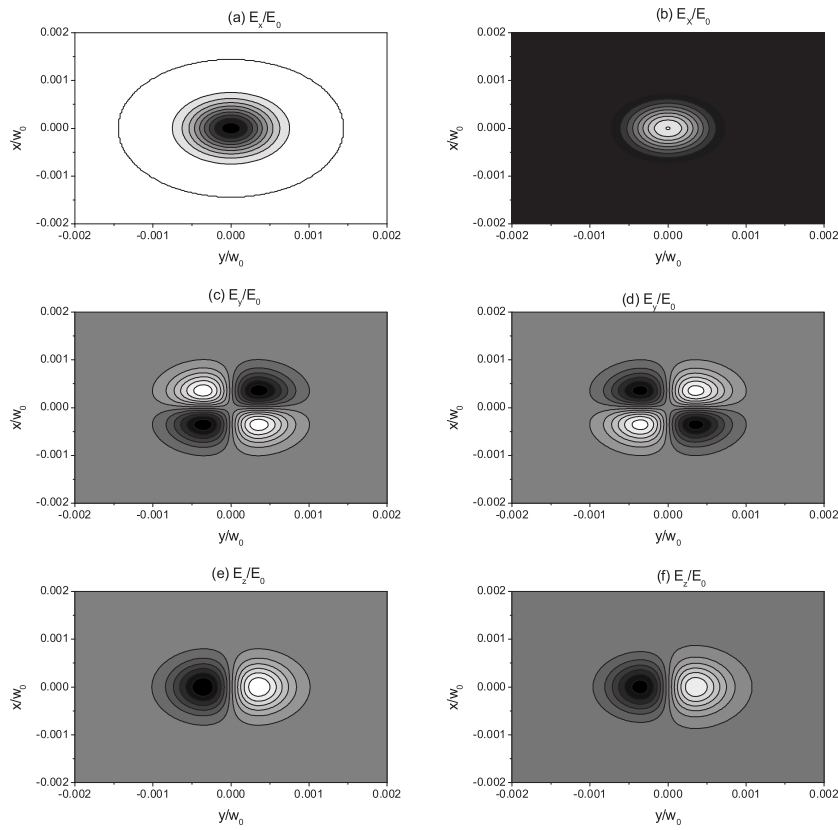


Figure 5.13 Contour maps of the electric component of the laser of beat-wave Gaussian beams over a square $20\mu m$ on a side, centered at the beam focus and extending in the xy plane. The beams parameters are $w_0 = 5\mu m$ and $\lambda_1 = 1\mu m$, $\lambda_2 = 1.1\mu m$. in (a,c,e) the fields are given at $\omega t = 0$, and at (b,d,f) at $\omega t = \pi/2$. Note that the positive and negative values are distinguished by level of shading, dark means negative and bright positive

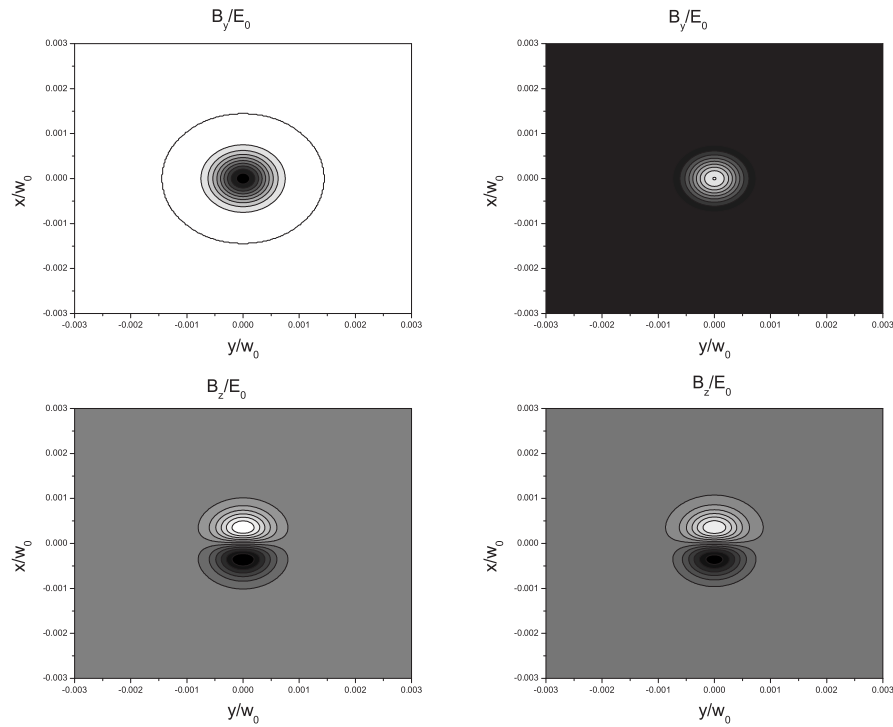


Figure 5.14 Contour maps of the magnetic component of the laser of beat-wave Gaussian beams over a square $30\mu m$ on a side, centered at the beam focus and extending in the xy plane. The beams parameters are $w_0 = 5\mu m$ and $\lambda_1 = 1\mu m$, $\lambda_2 = 1.1\mu m$. in the left figures the fields are given at $\omega t = 0$, and in the right at $\omega t = \pi/2$. Note that the positive and negative values are distinguished by level of shading, dark means negative and bright positive

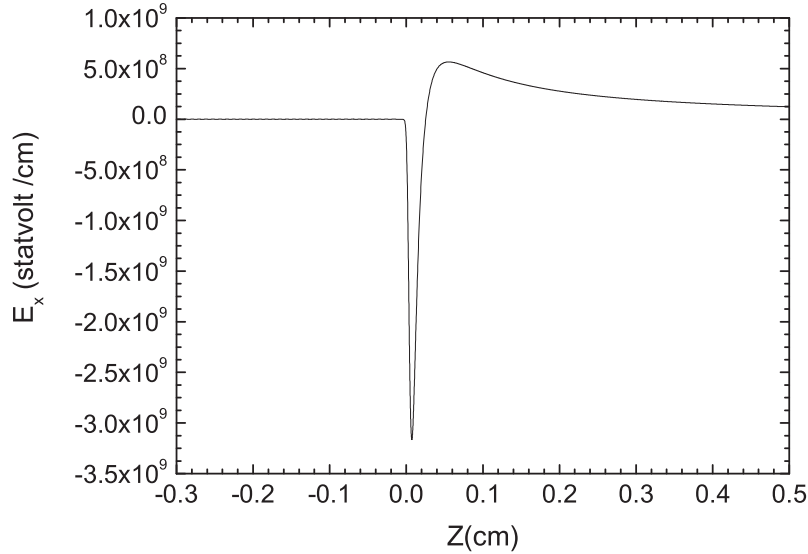


Figure 5.15 The transverse component of the electric field sensed by the electron (for $w_0 = 5\mu m$ and $\lambda_1 = 1\mu m$, $\lambda_2 = 1.1\mu m$, $\psi_0 = 301$, $\gamma_0 = 6.5$, and $P = 10PW$).

the electric field respectively along the electron trajectories, the fields are taken at initial energy $\gamma_0 = 6.5$, waist radius $w_0 = 5\mu m$, wavelengths $\lambda_1 = 1\mu m$, $\lambda_2 = 1.1\mu m$, laser power $P = 10PW$, and injection angle $\theta = 10^\circ$. The full interaction time is such that $\omega t = \pi \times 10^5$. Note that E_z is typically some 1 order of magnitude smaller than E_x . The maximum value for the fields here is of order of 10^9 , this means that the quantum effect is negligible.

Figure(5.17) shows the variation of the y-component with the forward distance of travel z , note that $B_y \sim E_x$. In all cases considered in this work, the electron sense the effect of both electric and magnetic fields since it is injected in high relativistic velocity. The electric field plays a role in accelerating the electron while the magnetic field play the role as a steering

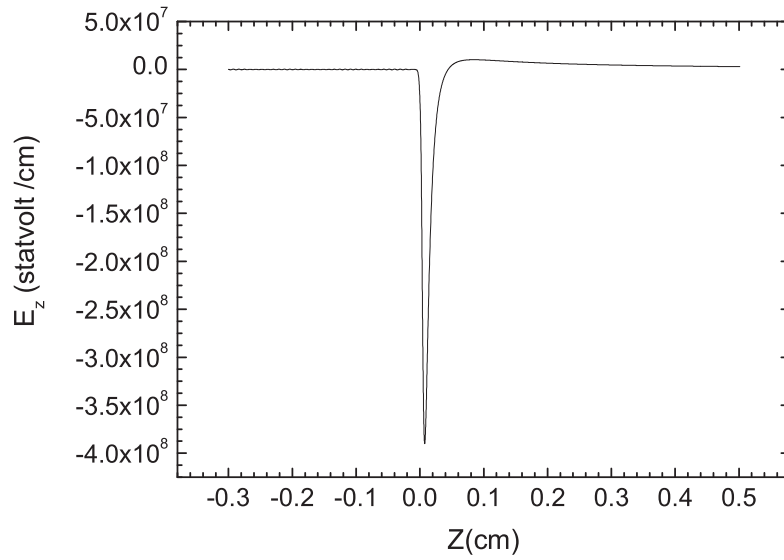


Figure 5.16 The longitudinal component of the electric field sensed by the electron (for $w_0 = 5\mu\text{m}$ and $\lambda_1 = 1\mu\text{m}$, $\lambda_2 = 1.1\mu\text{m}$, $\psi_0 = 301$, $\gamma_0 = 6.5$, and $P = 10\text{PW}$.)

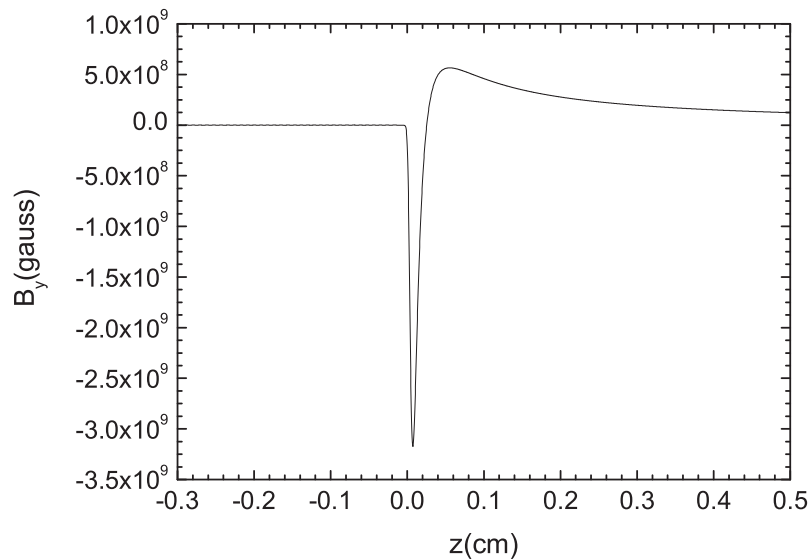


Figure 5.17 The y-component of the magnetic field sensed by the electron (for $w_0 = 5\mu\text{m}$ and $\lambda_1 = 1\mu\text{m}$, $\lambda_2 = 1.1\mu\text{m}$, $\psi_0 = 301$, $\gamma_0 = 6.5$, and $P = 10\text{PW}$.)

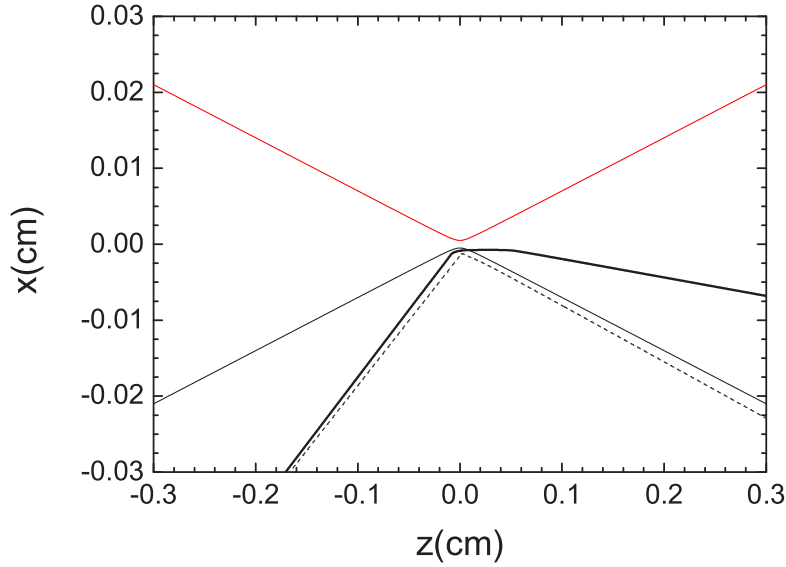


Figure 5.18 The trajectories of electron in beat-wave fields for different injection energy, for $\gamma_0 = 4$ (dash curves), and for $\gamma_0 = 6.5$ (full curves), (other parameters the same for 5.15)

force on the electron, hence, the trajectory of the electron is affected by the magnetic field.

The trajectories of electron corresponding to the above fields are shown in figure (5.18), the reflection is shown at initial injection energy with $\gamma_0 = 4$, and the capture is shown for $\gamma_0 = 6.5$, the other parameters is the same in figures (5.15, 5.16).

The corresponding energy gain and energy loss are shown in figures (5.19 – 5.21). It is clear from the figures that in the case of capture the energy gain and also the energy losses are much bigger than for the case of reflection, and this happens because the electron spends more time in phase with the laser fields as well as its path change and hence violently

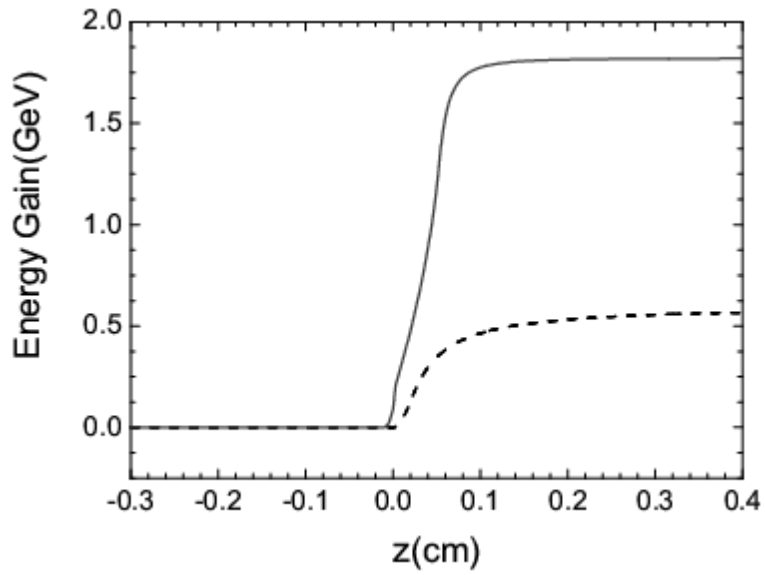


Figure 5.19 The Energy gain in beat-wave fields for different injection energy, for $\gamma_0 = 4$ (dash curves), and for $\gamma_0 = 6.5$ (full curves), (other parameters the same for 5.15)

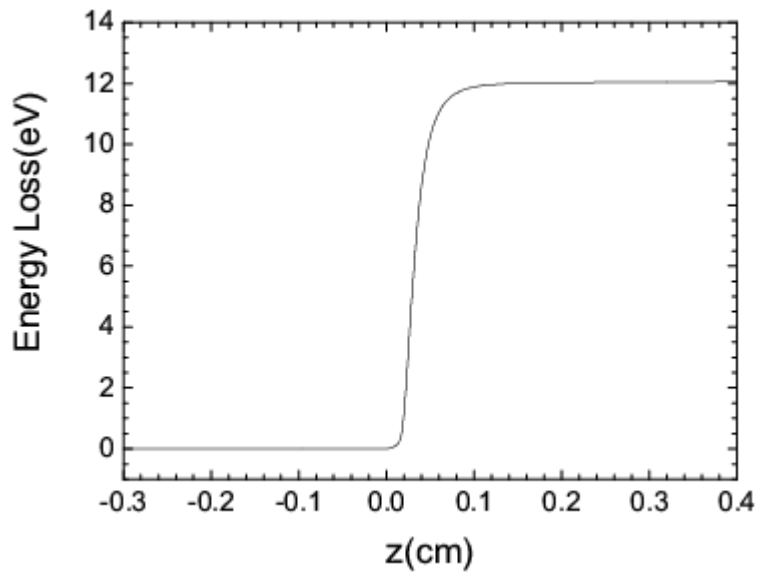


Figure 5.20 The Energy losses in beat-wave fields for injection energy $\gamma_0 = 4$ (other parameters the same for 5.15)

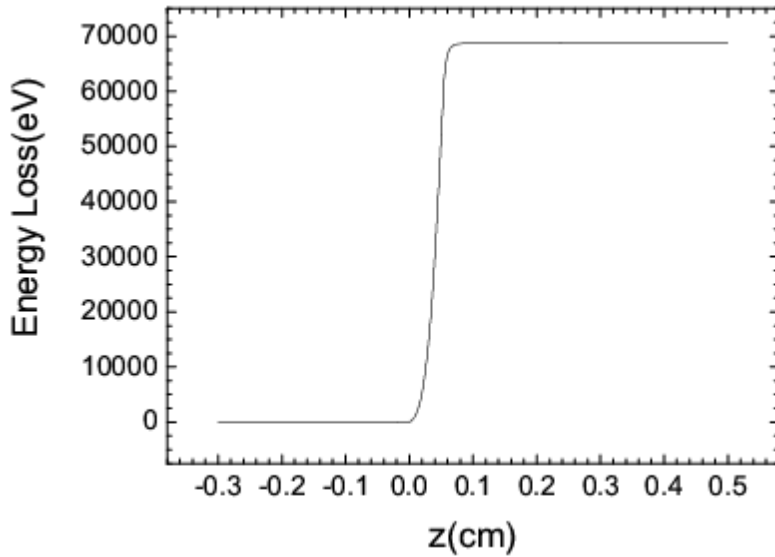


Figure 5.21 The Energy losses in beat-wave fields for different injection energy, for $\gamma_0 = 6.5$ (other parameters the same for 5.15)

accelerated. According to Larmor's formula for instantaneous power loss equation (2.39), the electron lose more energy as its relativistic velocity and acceleration components become larger.

5.3.1 Injection On Both Sides Of The Focus

In all cases considered so far, the electron was aimed directly at the beam focus (0,0,0). This has been done to let the electron sample the regions of highest field intensity, but this does not always lead to the best gain. The focus like other parameters may present the electron with strong accelerating fields, but sometimes these fields are symmetric, and according to Lawson-Woodward theorem no net energy gain will result as the electron interact with symmetric fields. On the other hand, on both sides of the

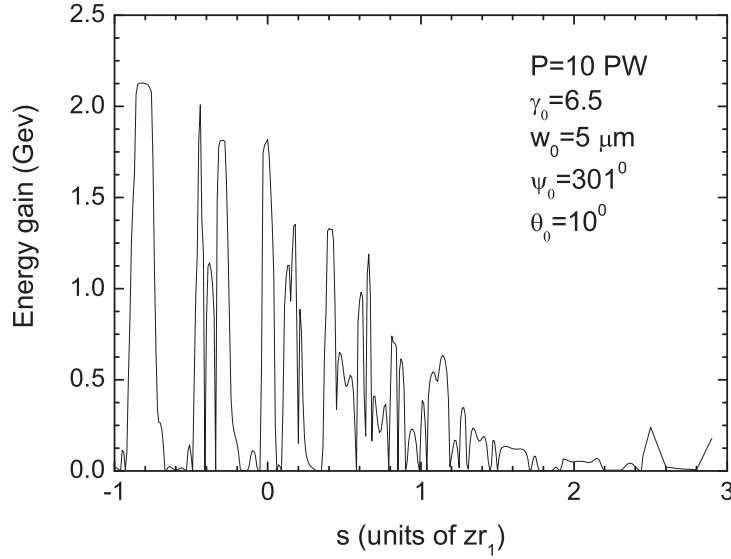


Figure 5.22 For electron with initial velocity vector pointing from $(x_0, 0, z_0 = -3mm)$ to $(0, 0, s)$ the variation of energy gain with s is shown

focus, the fields occupy a much larger volume and hence the interaction time is longer. Figure (5.22) shows the variation of the energy gain versus the coordinate z value, denoted by s , of the point on the axis towards which the electron is initially aimed. In all cases here the injection angle is $\theta = 10^\circ$ and the initial injection point z -coordinate is $z_0 = -3mm$.

The highest energy gain found for the chosen set of parameters in the above configuration is $2.25GeV$. Looking on figure (5.22) we found that the gain goes down as we move the target point away from the focus, since the intensity drops markedly in the downstream regions of the beam, and the

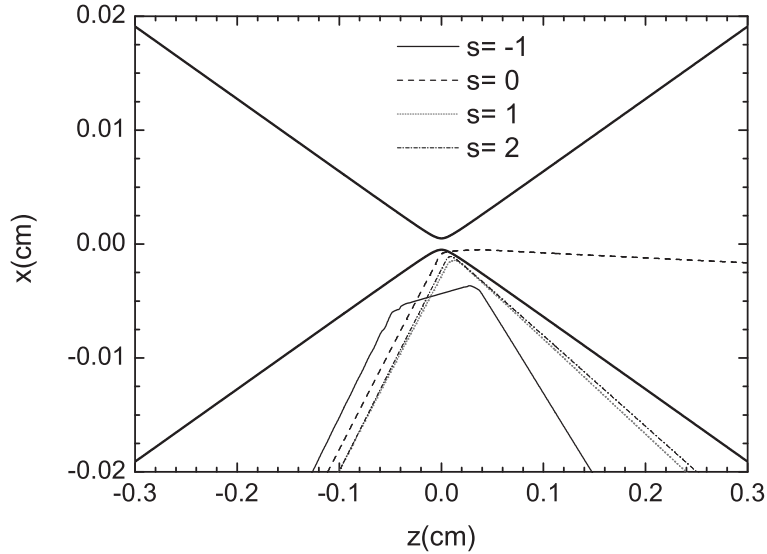


Figure 5.23 For electron with initial velocity vector pointing from $(x_0, 0, z_0 = -3mm)$ to $(0, 0, s)$ the actual trajectories of four cases corresponding to different values of s is shown. The laser wavelength is $\lambda = 1\mu m$. Note that $x_0 = -(s - z_0) \tan \theta$. The interaction time in all cases is such that $\omega t = \pi \times 10^5$. The legends in 5.22 apply to 5.23

gain is maximum if we inject the electron a slight distance to the left of the focus since the fields strength is higher than in the focus.

The view become more clear when we try different values of parameter s and looking on the trajectory (figure 5.23), most of the cases where no gain is obtained, come from the reflection of the electron, where in the capture case, we found that a weak, or, high gain is available.

5.3.2 The Effect Of Waist Radius

A laser system is often characterized by its output power P [28]. For the fields given below by Eqs(2.33-2.38), the power may be calculated by integrating the time-averaged poynting vector (equation 5.2: the poynting

vector represents the energy flow, and has dimensions of [*energy/area* \times *time*]) over a plane through the beam focus and perpendicular to its axis.

$$\vec{S} = \frac{c\vec{E} \times \vec{B}}{4\pi} \quad (5.2)$$

Dropping terms of order ϵ^5 and higher in the result [30], one gets

$$\begin{aligned} P[TW] &= \frac{\pi w_0^2}{2} I_0 \left[1 + \frac{\epsilon^2}{4} + \frac{\epsilon^4}{8} \right], \\ &\approx 0.0216 \left(\frac{q w_0}{\lambda} \right)^2 \left[1 + \frac{\epsilon^2}{4} + \frac{\epsilon^4}{8} \right], \end{aligned} \quad (5.3)$$

where $I_0 = I(0, 0, 0) = cE_0^2/8\pi$ is the peak intensity (at the focus). Equation (5.3) clearly shows that, for a fixed laser output, the peak intensity is inversely proportional to the square of the beam waist radius w_0 or, equivalently, the dimensionless intensity parameter $q = eE_0/(mc\omega)$ is inversely proportional to w_0 . Note that the Gaussian cgs unit of system is used through this work. In figure (5.24) we show the energy gain as a function of the beam waist radius w_0 . For the given set of parameters one can distinguish between three regions. In the first region R_1 for which $w_0 < 4\mu\text{m}$, the fields is highly symmetric and corresponds to low orders of ϵ , yields no energy gain as the fields sensed by the electron in this regime become highly symmetrical. In R_2 , or $4 < w_0 < 8\mu\text{m}$, corresponds to high orders of ϵ namely ϵ^5 there is energy gain, and in R_3 , or $w_0 > 8\mu\text{m}$, corresponds

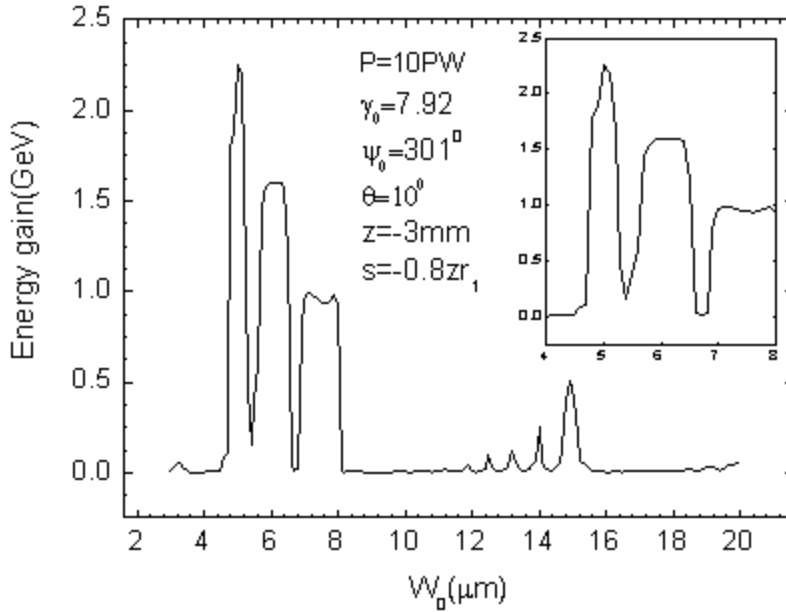


Figure 5.24 Energy gain vs the beam waist radius w_0 with wavelengths $\lambda_1 = 1\mu\text{m}$, $\lambda_2 = 1.1\mu\text{m}$

to moderate orders of ε namely ε^3 , yields a little gain.

We conclude that the need to focus the beam over a small spatial dimensions raises question about the modeling of the tightly focused beam in ascending power of ε .

5.3.3 The Effect Of Injection Energy

In this section we investigate the role of injection energy in the electron acceleration, it is known that an initially slow electron will not be able to penetrate the high intensity regions of the beam and hence reflected with little or no energy gain. on the other hand, an initially fast electron may pass through undeviated and gain energy or lose a small amount of energy.

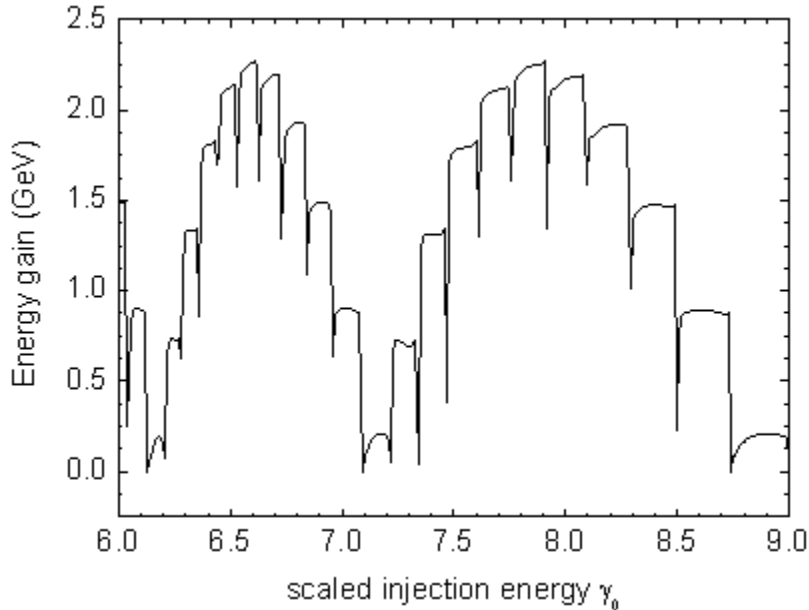


Figure 5.25 Electron energy gain vs the scaled injection energy. In this case the electron is aimed at point on the beam axis a distance $s = -0.83 * zr_1$ to the left of focus. The laser wavelengths are $\lambda_1 = 1\mu m, \lambda_2 = 1.1\mu m$, and the laser output power is that $P=10PW, z_0 = -3mm, \psi_0 = 301, \theta = 10, W_0 = 5\mu m$

For an initially very fast electron, it may penetrate the beam boundaries and transmit through the intense regions, for this case the electron may initially be accelerated and then be decelerated due to energy loss.

More specifically, figure 5.25 show a plot for the energy gain versus the scaled injection energy, the situation here is similar to the shape of beat-wave, this is due to the fact that if the electron reach the focus at the time where constructive interference between the two child waves, it will be highly accelerated, and at this moment the electron senses a maximally asymmetric set of fields. When it reach at the time where destructive interference present, then it will not gain energy.

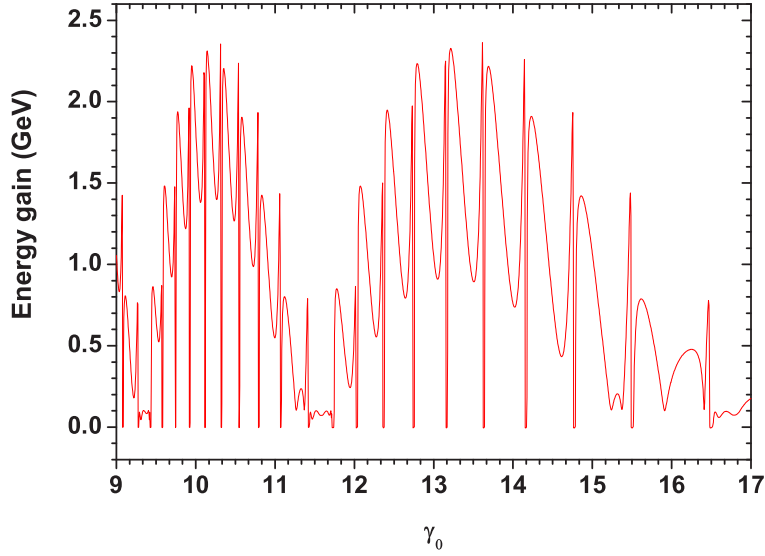


Figure 5.26 Electron energy gain vs the scaled injection energy. In this case the electron is aimed at point on the beam axis a distance $s = 0$. The laser wavelengths are $\lambda_1 = 1\mu m, \lambda_2 = \lambda_1/1.1\mu m$, and the laser output power is that $P=10PW, z_0 = -5mm, \psi_0 = 0, \theta = 10, W_0 = 7\mu m$

Other case of interest is, when the initial injection z component is $z_0 = -5mm$, then the initial scaled energy parameter γ_0 range will be shifted to higher values as shown in figure 5.26, this phenomena appears because broad electrons must have more energy than in case of $z_0 = -3mm$ in order to reach the fields intense region.

5.4 Optimum Conditions For Electron Acceleration In Beat-Wave Tightly Focused Laser Beam

In this section we investigate the optimum conditions for achieving maximum energy gain when the electron is accelerated by beat-wave tightly focused laser beam. We search for optimal set of parameters which are

not unique, changing one parameter will yield a different set of optimum conditions.

We search for such set of optimum parameters through the following procedure:

- We plot the gain versus ψ_0 for particular values of the remaining parameters($0 < \psi_0 < 360$).
- For $\psi_0 = \psi_{max}$ from the previous step, we plot the gain versus s ($-zr_1 < s < 3zr_1$).
- For s_{max} from previous step we plot the gain versus γ_0 ($3 < \gamma_0 < 15$).
- we plot gain versus the waist radius w_0 for some γ_0 from previous step ($4 < w_0 < 20\mu\text{m}$).
- We plot gain versus the injection angle θ for some w_0 from previous step ($0 < \theta < 20$).
- Finally we plot gain versus the waves polarization angle θ_i for some θ from previous step ($0 < \theta_i < 90$).

At the moment the above procedure is finished, we will have a set of parameters that satisfy the maximum gain, we then use these parameters

in the main program to plot the gain versus the electron forward distance of travel (z -coordinate).

Figure (5.27) show plots for the energy gain versus some parameters related to the electron injection and laser field, these figures are found depending on the above procedure. At the end we use the accumulate parameters to find the maximum energy gain for this configuration as well as the energy losses, in addition to the spatial electron trajectories and velocity components.

Figure (5.27(a)) shows energy gain versus ψ_0 in units of degrees for arbitrary parameters: $s=-0.2zr_1$, $\gamma_0 = 6.5$, $\lambda_1 = 1.1\mu m$, $\lambda_2 = 1.0\mu m$, output power=10 PW, $w_0 = 10\mu m$, $z_0 = -3mm$, $x_0 = -(s - z_0) \tan \theta$, $\theta = 10^\circ$ and the maximum gain is found at $\psi_0 = 222^\circ$. Figure (5.27(b)) shows energy gain versus s in units of zr_1 , and the used parameters are: $\psi_0 = 222^\circ$, $\gamma_0 = 6.5$, $\lambda_1 = 1.1\mu m$, $\lambda_2 = 1.0\mu m$, output power=10 PW, $w_0 = 10.0\mu m$, $z_0 = -3mm$, $x_0 = -(s - z_0) \tan \theta$, $\theta = 10^\circ$, and the maximum gain is found at $s=-0.06zr_1$.

Figure (5.27(c)) shows energy gain versus γ_0 , the used parameters are: $s=-0.06zr_1$, $\psi_0 = 222^\circ$, $\lambda_1 = 1.1\mu m$, $\lambda_2 = 1.0\mu m$, output power=10 PW, $w_0 = 10.0\mu m$, $z_0 = -3mm$, $x_0 = -(s - z_0) \tan \theta$, $\theta = 10^\circ$, and the maximum gain is found at $\gamma_0 = 6.39$. Figure (5.27(d)) shows energy gain versus w_0

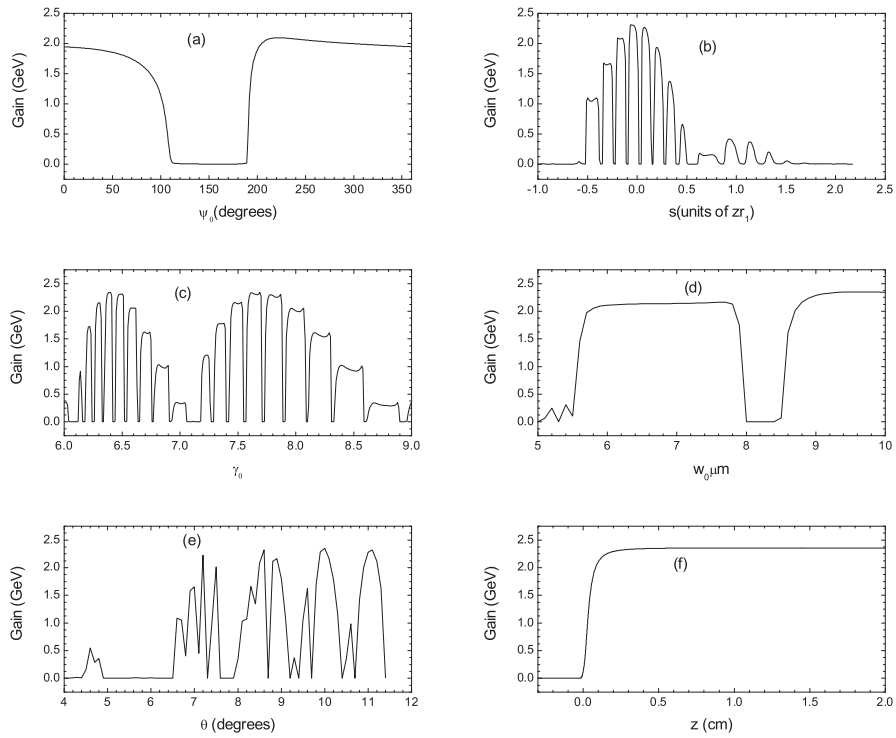


Figure 5.27 Plots of energy gain versus some parameters by mean of optimum parameters: (a) energy gain versus ψ_0 , (b) energy gain versus s , (c) energy gain versus γ_0 , (d) energy gain versus w_0 , (e) gain vs θ , and (f) gain vs z .

in units of (μm), the used parameters are: $s=-0.06zr_1$, $\psi_0 = 222^\circ$, $\gamma_0 = 6.39$, $\lambda_1 = 1.1\mu m$, $\lambda_2 = 1.0\mu m$, output power=10 PW, $z_0 = -3mm$, $x_0 = -(s - z_0) \tan \theta$, $\theta = 10^\circ$, and maximum gain is found at $w_0 = 9.6\mu m$.

Figure (5.27(e)) shows energy gain versus θ in units of degrees, the used parameters are: $s=-0.06zr_1$, $\psi_0 = 222^\circ$, $\gamma_0 = 6.39$, $\lambda_1 = 1.1\mu m$, $\lambda_2 = 1.0\mu m$, output power=10 PW, $w_0 = 9.6\mu m$, $z_0 = -3mm$, $x_0 = -(s - z_0) \tan \theta$, and the maximum gain is found at $\theta = 9.6^\circ$. Finally Figure (5.27(f)) shows energy gain versus z for all the previous optimum parameters.

The optimum parameters for this configuration is schemed in the following table:

Parameter	Optimum value
ψ_0	222°
s	$-0.06zr_1$
γ_0	6.39
w_0	$9.6\mu m$
θ	10°
Laser output power	10 PW
z_0	-3 cm

The corresponding energy gain and energy loss plots for beat-wave accel-

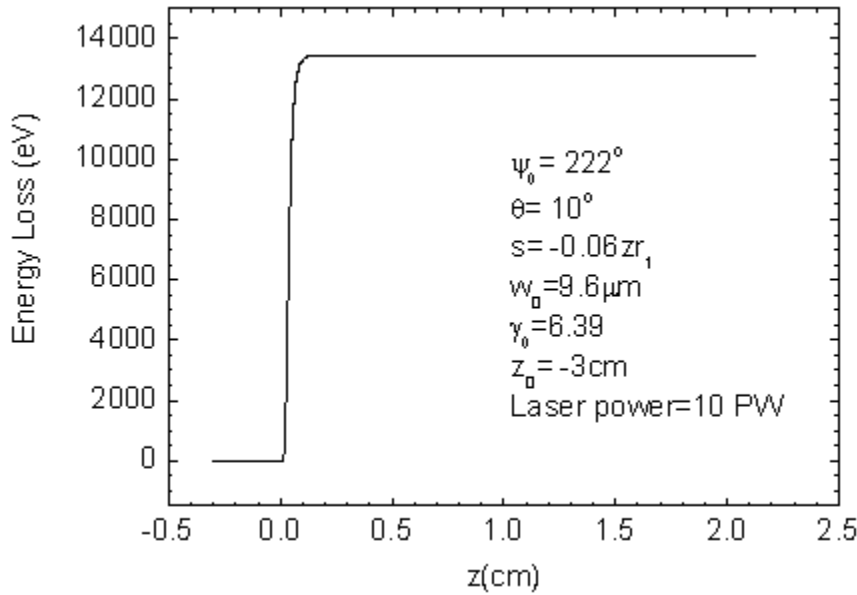


Figure 5.28 Energy losses versus z . (for the optimum parameters)

eration scheme with the optimum parameters shown in figures (5.27(f), 5.28) respectively . The maximum energy gain scored for this configuration at ($z=2.0\text{cm}$) is (2.35774 GeV), and the maximum energy loss is (13454.3 eV). This corresponds to energy gradient about (117.981 GeV/m).

On the other hand, for more focusing on the problem, we can show the trajectories and velocity components as a function of time or the forward distance of travel z for the same parameters above.

Figure (5.30) shows the variation of forward distance of travel z with time, it shows a linear relation between z and t , and from figures (5.31, 5.32) we see some oscillations at the begging of interaction between the electron and the fields, suddenly the velocities become stable and reach the ve-

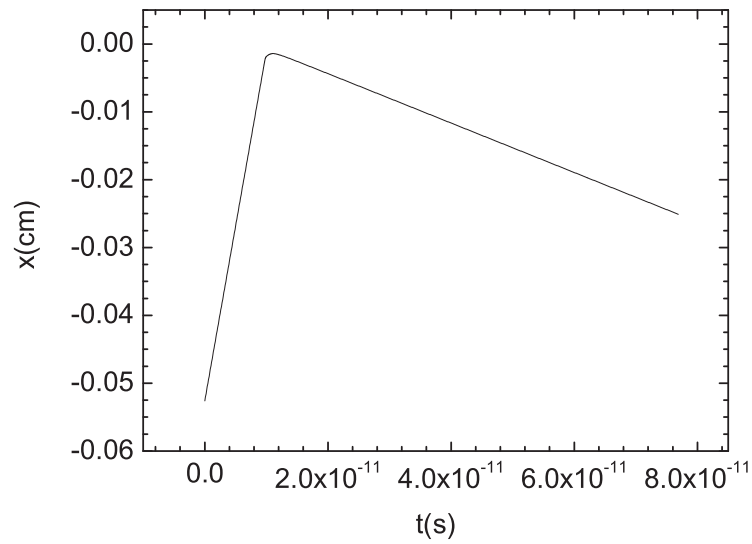


Figure 5.29 x versus t , note that big deflection angle and high violent acceleration corresponds to much energy loss (for the optimum parameters)

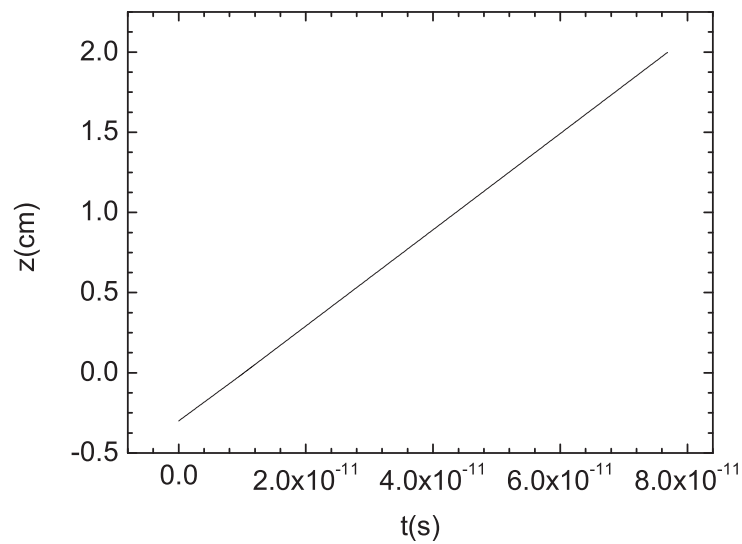


Figure 5.30 z versus t . (for the optimum parameters)

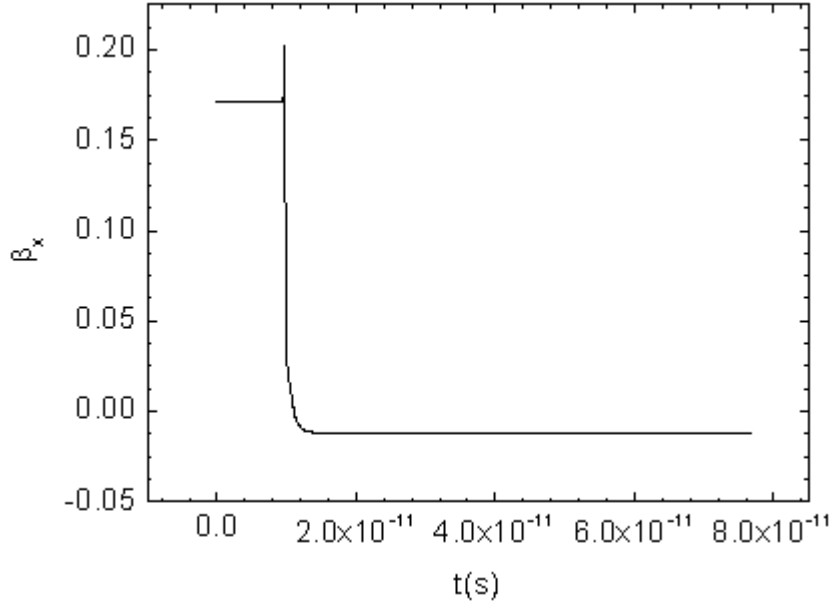


Figure 5.31 velocity x-component(β_x) versus t (for the optimum parameters).

locity of light as for β_z , the small value for β_x results from the effect of y-component of magnetic field as mentioned later, which is a secondary acceleration agent.

A close look on the figures (5.27(f)–5.33) give us an overview about the acceleration of beat-wave laser in vacuum. Figure 5.27(f) show the variation of energy gain with the forward distance of travel within the optimum parameters found later, the electron is captured and violently accelerated to GeV energies within a small distance approximate to 0.3 cm, after that the gain is stable. Also we found that the electron loses more energy as its

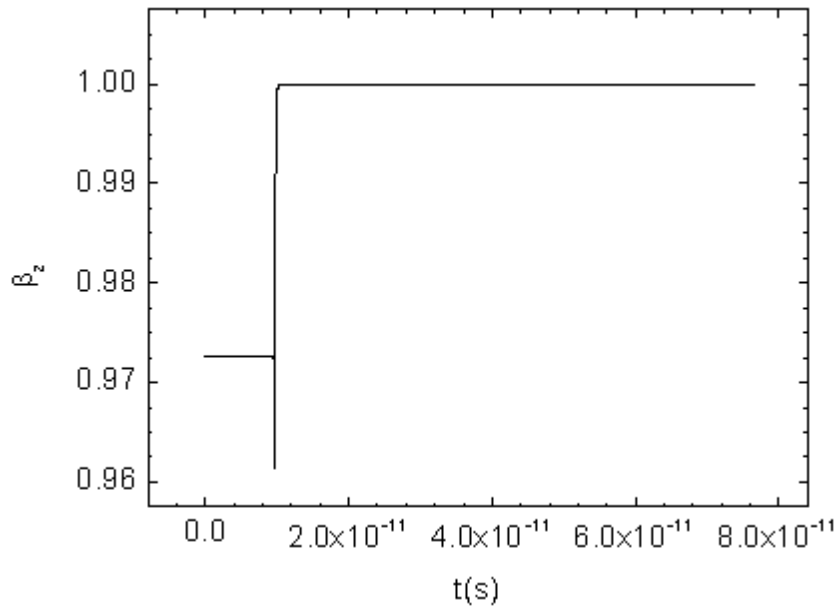


Figure 5.32 velocity z-component(β_z) versus t (for the optimum parameters).

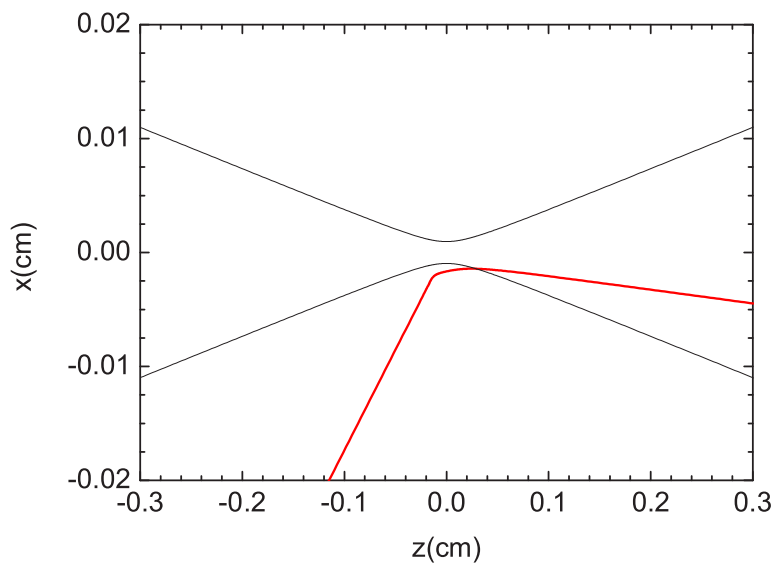


Figure 5.33 x versus z (for the optimum parameters).

acceleration gradient become larger.

If we compare the obtained results for beat-wave with that of a single beam, with maximum gain approximate to 1.5 GeV, we found that we raise the energy gain about 36%, which is better for this configuration.

5.5 Summary And Conclusion

The aim of this research is to study the acceleration of single electron in the fields of beat-wave laser in vacuum using the tightly focused laser(Gaussian beam) to model the laser. In comparison with the conventional acceleration of particles, in the sample calculations presented, present-day laser intensities have been considered and the obtained results demonstrate that the electrons may be accelerated, even from rest, to GeV energies over small distances (in our work acceleration distance ~ 1.32 cm). Future higher intensities require focusing over smaller dimensions, and lead to acceleration to TeV energies but over much longer distances, of order of meters. Our simulation predict that it may be possible in a real design to employ focusing mechanisms as means of maintaining the high field intensities over longer distances.

Most treatments of laser-electron acceleration that model the radiation field in terms of plane waves, help to demonstrate acceleration only in principle. Lowest-order Gaussian beams model the intense fields, that may

lead to sizeable electron acceleration, much better, but also ignore corrections that may otherwise alter the electron dynamics quite appreciably. We have presented an investigation based on a representation of the fields of a Gaussian beam in which up to and including fifth-order corrections to the various electric and magnetic laser fields have been retained. The complexity of such fields, however, renders an analytic solution to the electron's equations of motion almost impossible.

We have solved the equations numerically, employing corrections to the fields of up to order 5 in the diffraction angle. Using our solutions, we have investigated a number of issues concerning the injection, and acceleration of a single electron in the fields of the linearly polarized Gaussian beam.

One conclusion may be summarized as follows. It is relatively easy for an energetic electron to pierce through the small beam focus. When an electron is injected at an angle to the beam axis, it mainly passes through with little deviation from the initial direction of motion and with very little gain or loss of energy. In some cases, especially when the injection energy is not great enough, the electron may be captured or reflected, again with some energy gain. However, if aimed at a point slightly to the left of the focus, the electron is captured and accelerated to high energy almost always. It is much less probable for such an electron to be reflected or transmitted.

We have also shown that the radiation losses during acceleration are smaller compared with the rate at which electrons gain energy from the laser fields. Still the radiative losses are large when compared with what typically is the case in conventional linear accelerator [38].

Conditions to maximize the gain have been investigated that correspond to a predetermined arbitrary subset of laser parameters and initial conditions on the electron injection. These conditions include the initial position and velocities of the electron, as well as, the waist radius, injection energy, the aimed point around the focus, the laser wavelength, the injection angle, the polarization angle, and finally the output power of the laser. It is important to note that aiming the electron slightly to the left of the common focus result in better energy gain than directly in the focus.

The configuration employing two interfering laser beams with slightly different frequencies was studied using most of the single-beam parameters and initial conditions. The gain found in this case did not match the maximum obtained for single beam case due to the interference effects (which were apparently destructive or constructive in the examples we looked at). More energy gain could be obtained if the electron samples regions around the common beams focus where constructive interference takes place.

In general, specially in the present work case, the type of calculations

made, is quite time-consuming. We have found that the injection energy needs to be large enough to allow the electron to penetrate to the high-intensity points near the common focus of the two beams. Otherwise, multiple reflections would occur and slow the electron down instead of accelerating it.

Finally, the maximum attainable energy gain for beat-wave configuration in the present optimum parameters in a distance of (2 cm) is about (2.35774 GeV), and the maximum energy loss in the same distance is about (13454.3 eV). We think that these results are better in the present of today laboratory intensities, and we predict by simulation that as the intensity of laser increase we will get higher energy gain.

Appendix A

Fields Near The Focus Of A Pulsed Gaussian Beam

We briefly outline here the derivation of the electric and magnetic fields near the focus of a pulsed Gaussian beam following the procedure given by McDonald [41], which in turn proceeds along lines similar to those of Davis [42] and Barton and Alexander [43]. The beam axis will be taken along z and its focus at $z = 0$.

The fields will be assumed to have harmonic time-dependence that goes like $e^{i\omega t}$. On the other hand, we follow McDonald in employing a pulse-shape function $g(\eta)$, where $\eta = \omega t - kz$, subject to a restriction to be encountered below. The fields will be derived from the linearly-polarized vector potential

$$A = \hat{x}A_0g(\eta)\Psi(\mathbf{r})e^{i\eta}, \quad (\text{A.1})$$

where A_0 is a constant amplitude. The vector potential satisfies the following wave equation

$$\nabla^2 A - \frac{1}{c^2} \frac{\partial^2 A}{\partial t^2} = 0, \quad (\text{A.2})$$

provided the Lorentz gauge condition

$$\frac{1}{c} \frac{\partial \phi}{\partial t} + \nabla \cdot A = 0, \quad (\text{A.3})$$

is simultaneously satisfied. Direct substitution, followed by some algebra,

leads to

$$\nabla^2 \Psi - 2ik \frac{\partial \Psi}{\partial z} \left(1 - i \frac{g'}{g} \right) = 0, \quad (\text{A.4})$$

where g' stands for a single differentiation with respect to η . As suggested by McDonald [41], we will look for a pulse-shape function that satisfies the condition

$$g' \ll g. \quad (\text{A.5})$$

This condition will be used repeatedly in the derivations to be carried out below. Next, we introduce a rescaling of the coordinates by letting

$$\xi = \frac{x}{w_0}, \quad v = \frac{y}{w_0}, \quad \zeta = \frac{z}{z_r}; \quad z_r = \frac{kw_0^2}{2}, \quad (\text{A.6})$$

where w_0 is the radius of the beam waist at focus and z_r is the Rayleigh length. With these transformations Eq. (A.4) becomes

$$\nabla_{\perp}^2 \Psi - 4i \frac{\partial \Psi}{\partial \zeta} + \epsilon^2 \frac{\partial^2 \Psi}{\partial \zeta^2} = 0, \quad (\text{A.7})$$

where

$$\nabla_{\perp}^2 = \frac{\partial^2}{\partial \xi^2} + \frac{\partial^2}{\partial v^2}; \quad \epsilon = \frac{w_0}{z_r} = \frac{\lambda}{\pi w_0}. \quad (\text{A.8})$$

ϵ is the diffraction angle. Note that ϵ^2 is small and may thus be used as an expansion parameter for a form of $\Psi(\xi, v, \zeta)$. Hence, we try

$$\Psi = \Psi_0 + \epsilon^2 \Psi_2 + \epsilon^4 \Psi_4 + \dots. \quad (\text{A.9})$$

With this substitution, Eq. (A.7) splits into

$$\nabla_{\perp}^2 \Psi_0 - 4i \frac{\partial \Psi_0}{\partial \zeta} = 0, \quad (\text{A.10})$$

$$\nabla_{\perp}^2 \Psi_2 - 4i \frac{\partial \Psi_2}{\partial \zeta} + \frac{\partial^2 \Psi_0}{\partial \zeta^2} = 0, \quad (\text{A.11})$$

$$\nabla_{\perp}^2 \Psi_4 - 4i \frac{\partial \Psi_4}{\partial \zeta} + \frac{\partial^2 \Psi_2}{\partial \zeta^2} = 0, \quad (\text{A.12})$$

$$\vdots$$

These equations have exact solutions. It can be shown, by direct substitution, that

$$\Psi_0 = f e^{-f \rho^2}, \quad (\text{A.13})$$

$$\Psi_2 = \left(\frac{f}{2} - \frac{f^3 \rho^4}{4} \right) \Psi_0, \quad (\text{A.14})$$

$$\Psi_4 = \left(\frac{3f^2}{8} - \frac{3f^4 \rho^4}{16} - \frac{f^5 \rho^6}{8} + \frac{f^6 \rho^8}{32} \right) \Psi_0, \quad (\text{A.15})$$

where

$$f = \frac{i}{\zeta + i} = \frac{e^{i \tan^{-1} \zeta}}{\sqrt{1 + \zeta^2}}; \quad \rho^2 = \xi^2 + v^2. \quad (\text{A.16})$$

Ψ_0 leads to the lowest order Gaussian beam solution of the fields, Ψ_2 is the correction to order ϵ^2 , and so on. Assuming that the scalar potential has the same general structure as that of the vector potential, i.e.,

$$\phi \sim g(\eta) \Phi(\mathbf{r}) e^{i\eta}, \quad (\text{A.17})$$

then the Lorentz gauge (A.3) yields

$$\frac{\partial \phi}{\partial t} = i\omega \phi \left(1 - i \frac{g'}{g} \right) \approx i\omega \phi. \quad (\text{A.18})$$

Hence,

$$\phi = \frac{i}{k} \nabla \cdot A. \quad (\text{A.19})$$

Finally, the fields may be derived from

$$E = -ikA - \frac{i}{k}\nabla(\nabla \cdot A), \quad (\text{A.20})$$

$$B = \nabla \times A. \quad (\text{A.21})$$

Dropping all terms of order ϵ^6 and higher from Eq. (A.9), we now write

$$A \approx \hat{x}A \left\{ 1 + \epsilon^2 \left[\frac{f}{2} - \frac{f^3\rho^4}{4} \right] + \epsilon^4 \left[\frac{3f^2}{8} - \frac{3f^4\rho^4}{16} - \frac{f^5\rho^6}{8} + \frac{f^6\rho^8}{32} \right] \right\}, \quad (\text{A.22})$$

$$A = A_0g(\eta)\Psi_0e^{i\eta}. \quad (\text{A.23})$$

This permits us to write the *complex* electric field components as

$$E_x = -ikA \left\{ 1 + \epsilon^2 \left[f^2\xi^2 - \frac{f^3\rho^4}{4} \right] + \epsilon^4 \left[\frac{f^2}{8} - \frac{f^3\rho^2}{4} - \frac{f^4}{16}(\rho^4 - 16\xi^2\rho^2) - \frac{f^5}{8}(\rho^6 + 2\xi^2\rho^4) + \frac{f^6\rho^8}{32} \right] + \dots \right\}, \quad (\text{A.24})$$

$$E_y = -ikA \left\{ \epsilon^2 [f^2] \xi v + \epsilon^4 \left[f^4\rho^2 - \frac{f^5\rho^4}{4} \right] \xi v + \dots \right\}, \quad (\text{A.25})$$

$$E_z = kA \left\{ \epsilon [f] \xi + \epsilon^3 \left[-\frac{f^2}{2} + f^3\rho^2 - \frac{f^4\rho^4}{4} \right] \xi + \epsilon^5 \left[-\frac{3f^3}{8} - \frac{3f^4\rho^2}{8} + \frac{17f^5\rho^4}{16} - \frac{3f^6\rho^6}{8} + \frac{f^7\rho^8}{32} \right] + \dots \right\}. \quad (\text{A.26})$$

On the other hand, the *complex* magnetic field components are

$$B_x = 0, \quad (\text{A.27})$$

$$\begin{aligned}
B_y = & -ikA \left\{ 1 + \epsilon^2 \left[\frac{f^2 \rho^2}{2} - \frac{f^3 \rho^4}{4} \right] \right. \\
& + \epsilon^4 \left[-\frac{f^2}{8} + \frac{f^3 \rho^2}{4} \right. \\
& \left. \left. + \frac{5f^4 \rho^4}{16} - \frac{f^5 \rho^6}{4} + \frac{f^6 \rho^8}{32} \right] + \dots \right\}, \tag{A.28}
\end{aligned}$$

$$\begin{aligned}
B_z = & kA \left\{ \epsilon [f] v + \epsilon^3 \left[\frac{f^2}{2} + \frac{f^3 \rho^2}{2} - \frac{f^4 \rho^4}{4} \right] v \right. \\
& \left. + \epsilon^5 \left[\frac{3f^3}{8} + \frac{3f^4 \rho^2}{8} + \frac{3f^5 \rho^4}{16} - \frac{f^6 \rho^6}{4} + \frac{f^7 \rho^8}{32} \right] v + \dots \right\}. \tag{A.29}
\end{aligned}$$

The real parts of these expressions give rise to the physical fields, Eqs.

(2.33)-(2.38), that enter into the calculations.

Appendix B

C++ Code

References

1. Skrinsky, A. "Accelerators: Their Role, History, Status, Prospects, and Practical Applications", Budker Institute of Nuclear Physics, Novosibirsk, 630090 Russia.
2. J.L.Hsu, *Laser Acceleration In Vacuum*, Proc. PAC's97, (7 March 2003), pp.684-686,
(URL:<http://www.triumf.ca/pac97/papers/pdf/7V021.pdf>)
3. Miroslav, Pardy, "Quantum Field Theory of the Laser Acceleration, Why laser acceleration," Department of Theoretical Physics and Astrophysics, Masaryk University, Faculty of Science, Kotlarska 2, 611 37 Brno, Czech Republic,
(e-mail:pamir@physics.muni.cz)
4. FDA 82-8181, *A Primer on Theory and Operation of Linear Accelerators in Radiation Therapy*, US Department of Health and Human Services, Rockville, MD, 1981 Goble, A. T., Baker, D. K., *Elements of Modern Physics*, 2d ed, The Ronald Press Co, (1971).
5. Y.I. Salamin, et al, *Phys. Rev. ST-AB* 3, No. 59001, (2000), pp. 1-3.
6. J. Humphries, *Principle Of Charged Particles Acceleration*, USA: John Wiley And Sons, (1999).
7. "Accelerators For Elementary-Particle Physics." In "*Elementary Particle Physics*", The National Academy Of Science, (2000).
(URL:<http://www.nap.edu/openbook/030903567/html/98.html>)
8. K.W.D. Ledingham, et al, "Laser-Induced Nuclear Physics And Applications:Historical Perspective." *Europhysics News* , (2002), Vol.33, No.4,
(URL:<http://www.europhysicsnews.com/full/16/article3/article3.html>)
9. DOE/Brookhaven National Laboratory, " ScientistsAt Brookhaven Contribute To The Development Of A Better Electron Accelerator",
(URL:http://www.eurekalert.org/pub_releases/2004_01/dnl_sab030304.php)

10. Y.I. Salamin, et al, "Analysis Of Electron Acceleration In A Vacuum Beat Wave," *J. Phys. B: At. Mol. Opt. Phys.* 33, No 8, (2000), PP. 5057-5076.
11. Y.I. Salamin, F.H.M. Faisal, *Phys. Rev. A* 58, No. 3221, (1998).
12. F.H.M. Faisal, Y.I. Salamin, *Phys. Rev. A* 60, No. 2505, (1999).
13. Y.I. Salamin, F.H.M. Faisal, *Phys. Rev. A* 61, No. 043801, (2000).
14. K.Z. Hatsagortsian, C.H. Keitel, *Phys. Rev. Lett*, in press.
15. C. D. Barnes, et al, *Laser Acceleration Of Electrons In Vacuum*, SLAC Proposal E-163, Stanford Linear Accelerator Center, Stanford University. August 24,(2003).
16. R. Tikhoplav, A. Melissinos, N. Barov, J. Santucci, "Laser Acceleration Of Electrons." *EPAC*, Paris, France, (2002), pp. 984–985.
17. D.H.Perkins, *Introduction To High Energy Physics*, 2nd ed, Addison-Wesley, Oxford, (1982).
18. B. Hafizi, et al, " Vacuum Beat Wave Acceleration," *Phys. Rev. E* 55, No 5, (May 1997), PP. 5924-5932.
19. Z.-M. Sheng, et al, "Stochastic Heating and Acceleration of Electrons in Colliding Laser Fields in Plasma." *Phys. Rev. Lett* 88, No 5 (4 Feb 2002), PP. 1-4.
20. R.L. Byer, et al, *Progress Of The Laser Electron Accelerator Project At Stanford University* , SLAC-PUB-9411, Stanford Linear Accelerator Center, Stanford University, August (2002).
21. S. Ya. Tochitsky, R. Narang, C.V. Filip. "Acceleration Of Injected Electrons In A Laser Beatwave Experiment, " Department of Electrical Engineering, Department of Physics, UCLA, 405 Hilgard avenue, Los Angeles, CA, 90095, USA,
(URL:http://pbpl.physics.ucla.edu/Literature/_library/tochitsky_2003_0515.pdf)
22. Y.I. Salamin, et al, "Electron Acceleration In Combined Laser And Uniform Electric Field ," *J. Phys. A: Math. Gen.* 34, (2001), PP. 2819–2837.

23. C. D. Barnes, et al, "An Electron Source For A Laser Accelerator," SLAC, 2575 Sand Hill Road, Mail Stop 07, Menlo Park, CA 94025, USA,
(URL:www.slac.stanford.edu/grp/arb/tn/arbvol14/ARDB345.pdf)
24. X. Feng, S. Lee, "The beat-wave accelerator in a relativistic electron oscillation plasma," *J. Phys. B: At. Mol. Opt. Phys.* 29, No 3 (1996), PP. L373-L380.
25. Y.I. Salamin, "Classical Relativistic Dynamics Of A Free Electron In An Intense Laser Field," *J. Phys. A: Math. Gen.* 30, (1997), PP. 4399-4412.
26. Y.I. Salamin, et al, "Subcycle High Electron Acceleration By Crossed Laser Beams," *App. Phys. Lett* 77, No 8, (21 Aug 2000), PP. 1082-1884.
27. P. X. Wang,, et al, "Vacuum Electron Acceleration By An Intense Laser," *App. Phys. Lett* 78 , no 15, (9 Apr 2001), PP. 2552-2555.
(URL:<http://ojps.aip.org/aplo/aplcr.jsp>)
28. R.L. Byer, et al, "Status Of The Laser Electron Accelerator Project," National Tsinghua University, Hsinchu, Taiwan 30043.
(URL:www.slac.stanford.edu/grp/arb/tn/arbvol13/ARDB227.pdf)
29. E. R. COLBY, " Critical Issues For Vacuum Laser Acceleration," Stanford Linear Accelerator Center 2575 Sand Hill Road MS 07 Menlo Park, CA 94025 USA.
30. V. Yakimenko, et al, "Parameter Optimizations For Vacuum Laser Acceleration At Atf/Bnl," Particle Accelerator Conference, Chicago, (2001).
31. P.X. Wang, et al, "The Output Properties Of Laser-Driven GeV Electron Bunches," *Nuclear Instruments and Methods in Physics Research A* 482, (2002), PP. 581-586.
32. Y.I. Salamin, "Electron Dynamics In Circularly-Polarized Laser And Uniform Electric Fields: Acceleration In Vacuum ," *Physics Letters A* 283, (7 May 2001), PP. 37-43.
33. Ph. Mine, " Accelerator Schemes Based On Lasers And Plasmas," LPNHE Ecole Polytechnique, IN2P3 And CNRS, 91128 Palaiseau, France, PP. 103-107.

34. Y.I. Salamin, et al, "Electron Scattering And Acceleration By A Tightly Focused Laser Beam, " *Phys. Rev. ST-AB*. 5, No 101301, (2002).
35. Y.I. Salamin, et al, "Electron Acceleration By A Tightly Focused Laser Beam, " *PhysRevLett*.
36. R.L. Burden, J.D. Faires, *Numerical Analysis*, 6thed, USA: Brooks/Cole Publishing Company, (1997).
37. Y.I. Salamin, et al, " Optimum Conditions for Electron Acceleration Using Tightly Focused Laser Beams, " *Laser Physics* 13, No. 4, (2003), pp. 407-413.
38. J.D. Jackson, *Classical Electrodynamics*, 2nded, USA: John Wiley And Sons, (1975).
39. A. Kazmierczak, "Trajectories of Skiers in Nordic Jumping", PP. 42–55,(1999).
40. Deitel and Deitel, *C++ How to Program* , 2nd.ed, USA: Prentice Hall International, Inc.
41. K.T. McDonald, "Gaussian Laser Beams and Particle Acceleration", (26 May 1995),
(URL:
<http://www.hep.princeton.edu/mcdonald/accel/gaussian.ps>)
42. L. W. Davis, "Gaussian Laser Beams and Particle Acceleration", *Phys. Rev. A* 19, No 1177 (1979),
(URL:www.hep.princeton.edu/mcdonald/accel/gaussian2.ps)
43. J. P. Barton, D. R. Alexander, "Fifth-order corrected electromagnetic field components for a fundamental Gaussian beam", *J. Appl. Phys.* 66, PP. 2800-2802 (1989).
44. M. O. Scully, M. S. Zubairy, *Phys. Rev. A* 44, 2656 (1991).
45. E. Esary, *Phys. Rev. E* 52, No. 5443, (1995).
46. B. Hafizi, A. Ting, E. Esarey, P. Sprangle, and J. Krall, *Phys. Rev. E* 55, 5924 (1997); B. Hafizi, A. K. Ganguly, A. Ting, C. I. Moore, and P. Sprangle, *Phys. Rev. E* 60, 4779 (1999); F. V. Hartemann *et al.*, *Phys. Rev. E* 58, 5001 (1999); Y. I. Salamin and C.H. Keitel, *Appl. Phys.*

Lett. **77**, 1082 (2000); Y. I. Salamin and F. H. M. Faisal, Phys. Rev. A **61**, 043801 (2000); Y. I. Salamin, F. H. M. Faisal and C. H. Keitel, Phys. Rev. A **62**, 53809 (2000); H. Hora, Nature **333**, 337 (1988).

47. Y.I. Salamin, et al, *Phys. Rev. Lett* *88*, No 095005, (2002), PP. 1-4.
48. Y.I. Salamin, C.H. Keitel, *laser physics*, in press.

Appendix B

C++ Code

```
/* ***** done by: ashraf titi *****
thesis code: for case of two beams slitley different wavelength
lambda1=2=lambda1*1.1
title: " The vacuum beat-wave electron
laser accelerator and associated radiative effects "
*/
#include <conio.h>
#include <stdio.h>
#include <stdlib.h>
#include <math.h>
#include <iostream.h>
#include <fstream.h>
#include <conio.h>
#include <iomanip.h>
long double minimum(long double,long double,long double,long double,long double,long double);
long double f1(long double,long double,long double,long double,long double,long double,long double);
long double f2(long double,long double,long double,long double,long double,long double,long double);
long double f3(long double,long double,long double,long double,long double,long double,long double);
long double f4(long double,long double,long double,long double,long double,long double,long double);
long double f5(long double,long double,long double,long double,long double,long double,long double);
long double f6(long double,long double,long double,long double,long double,long double,long double);
long double Egain(long double,long double,long double,long double,long double,long double);
long double eta(long double , long double);
long double beta0(long double);
long double Gammainv(long double,long double,long double);
long double E1(long double,long double,long double);
long double E2(long double,long double,long double);

// computes the amplitude E in the feild equations.

/** fields for the two tightly focused laser beams **
long double EX(long double,long double,long double,long double);
// computes the x component of electric feild.
long double EY(long double,long double,long double,long double);
// computes the y component of electric feild.
long double EZ(long double,long double,long double,long double);
// computes the z component of electric feild.
long double BMAGX(long double,long double,long double,long double);
// computes the x component of magnetic feild.
long double BMAGY(long double,long double,long double,long double);
// computes the y component of magnetic feild.
long double BMAGZ(long double,long double,long double,long double);

/** fields for the first focused laser beam *****

long double EX1(long double,long double,long double,long double);
```

```

// computes the x component of electric feild.
long double EY1(long double,long double,long double,long double);
// computes the y component of electric feild.
long double EZ1(long double,long double,long double,long double);
long double BMAGX1(long double,long double,long double,long double);
// computes the x component of magnetic feild.
long double BMAGY1(long double,long double,long double,long double);
// computes the y component of magnetic feild.
long double BMAGZ1(long double,long double,long double,long double);

//**** fields for the second focused laser beam ****

long double EX2(long double,long double,long double,long double);
// computes the x component of electric feild.
long double EY2(long double,long double,long double,long double);
// computes the y component of electric feild.
long double EZ2(long double,long double,long double,long double);
// computes the z component of electric feild.
long double BMAGX2(long double,long double,long double,long double);
// computes the x component of magnetic feild.
long double BMAGY2(long double,long double,long double,long double);
// computes the y component of magnetic feild.
long double BMAGZ2(long double,long double,long double,long double);

//*****
long double Wz1(long double);// computes W(z).
long double S1(long double,long double,long double,long double, long double );
// computes the quantities Sn
long double C1(long double,long double,long double,long double, long double );
// computes the quantities Cn
long double Wz2(long double);// computes W(z).
long double S2(long double,long double,long double,long double, long double );
// computes the quantities Sn
long double C2(long double,long double,long double,long double, long double );
// computes the quantities Cn
//*****
const long double ech=4.8*pow(10.0,-10.0); // charge of electron in esu units
const long double m=9.1*pow(10.0,-28.0); // mass of electron gram.
const long double pi=3.14159265358979;
const long double c=3.0*pow(10.0,10.0); // speed of light
const long double alpha =1.1;
const long double P=1000.0;
const long double W0=7.0 *pow(10.0,-4.0);
const long double psi0= 0.0*pi/180.0;
const long double gamma0=6.5;
const long double theta=10.0*pi/180.0; // angle of electron injection
const long double thetai=0.0; //angle between the two laser beams
const long double D=(ech/(m*c));
const long double lamda1=1.0*pow(10.0,-4.0); // wavelength of laser
const long double lamda2=lamda1/alpha;

```

```

const long double k1=2.0*pi/lamda1;
const long double zr1=k1*(W0*W0)/2.0;
const long double eps1=W0/zr1;
const long double q1=(lamda1/W0)*(sqrtl(P/(0.0216*(1.0+powl(eps1,2.0)/4.0+powl(eps1,4.0)/8.0) )));
const long double omega1=2.0*pi*c/lamda1;
const long double E01=q1*m*c*omega1/ech;
const long double k2=2.0*pi/lamda2;
const long double zr2=k2*(W0*W0)/2.0;
const long double eps2=W0/zr2;
const long double q2=(lamda2/W0)*(sqrtl(P/(0.0216*(1.0+powl(eps2,2.0)/4.0+powl(eps2,4.0)/8.0) )));
const long double omega2=2.0*pi*c/lamda2;          // angular frequency of
laseRx.784995826*powl(10.0,15.0);
const long double E02=q2*m*c*omega2/ech;
const long double s=0.0*zr1;

```

```

void main()

```

```

{

```

```

//Constants// This is where all the constants and initial conditions are declared.

```

```

//const long double hmax = 0.00000000000000000001;
const long double hmax = 0.0000000000000001;
const long double TOL= 1000;
const long double hmin = 0.000000000000000000000001;
const long double bxIni =(beta0(gamma0))*sinl(theta);
const long double byIni = 0.0;
const long double bzIni = (beta0(gamma0))*cosl(theta);
const long double yIni= 0.0;
const long double zIni= -0.3;
const long double tIni= 0.0;
const long double xIni= -(s-zIni)*tanl(theta);

```

```

//Variables// This is where all the variables in the problem are defined.

```

```

long double h = hmax;
long double fbx = 0.0;
long double fby = 0.0;
long double fbz = 0.0;
long double fx =0.0;
long double fy = 0.0;
long double fz =0.0;
long double t = tIni;
long double x = xIni;
long double y = yIni;
long double z = zIni;
long double bx= bxIni;
long double by= byIni;
long double bz= bzIni;
long double bya = by;
long double bxa = bx;
long double bza = bz;
long double xa = x;

```

```

long double ya = y;
long double za = z;
long double k1bx,k1by,k1bz,k1x,k1y,k1z;
long double k2bx,k2by,k2bz,k2x,k2y,k2z;
long double k3bx,k3by,k3bz,k3x,k3y,k3z;
long double k4bx,k4by,k4bz,k4x,k4y,k4z;
long double k5bx,k5by,k5bz,k5x,k5y,k5z;
long double k6bx,k6by,k6bz,k6x,k6y,k6z;
long double Rbx,Rby,Rbz,Rx,Ry,Rz,R;
long double delta = 0.0;
long double ycheck = 0.0;
// This is the beginning of the loop that will continue calculating the variables
// until the predefined tolerance is met.
ofstream outfile_test("GainVsGamma0p1.dat",ios::app);
//outfile_test<<" "<<za<<" "<<Egain(bxIni,byIni,bzIni,bxIni,byIni,bzIni)<<endl;
//cout<<" "<<za<<" "<<Egain(bxIni,byIni,bzIni,bxIni,byIni,bzIni)<<endl;
int j=0;
long double max =Egain(bx,by,bz,bxIni,byIni,bzIni);
for (;)
{
    if (z>=0.9)
        break;
    //
    // The method to determine when the calculation can stop.
    // The formulas to calculate the K values that are used to approximate
    // the variables.
    xa = x;
    ya = y;
    za = z;
    bxa = bx;
    bya = by;
    bza = bz;

    fx =f1(t,xa,bxa,ya,bya,za,bza);
    fbx =f2(t,xa,bxa,ya,bya,za,bza);
    fy =f3(t,xa,bxa,ya,bya,za,bza);
    fby =f4(t,xa,bxa,ya,bya,za,bza);
    fz =f5(t,xa,bxa,ya,bya,za,bza);
    fbz =f6(t,xa,bxa,ya,bya,za,bza);

    k1x = h*fx;
    k1bx = h*fbx;
    k1y = h*fy;
    k1by = h*fby;
    k1z = h*fz;
    k1bz = h*fbz;

    bxa = bx + 0.25*k1bx;
    bya = by + 0.25*k1by;

```

bza = bz + 0.25*k1bz;
xa = x + 0.25*k1x;
ya = y + 0.25*k1y;
za = z + 0.25*k1z;

fx =f1(t+(1.0/4.0)*h,xa,bxa,ya,bya,za,bza);
fbx =f2(t+(1.0/4.0)*h,xa,bxa,ya,bya,za,bza);
fy =f3(t+(1.0/4.0)*h,xa,bxa,ya,bya,za,bza);
fby =f4(t+(1.0/4.0)*h,xa,bxa,ya,bya,za,bza);
fz =f5(t+(1.0/4.0)*h,xa,bxa,ya,bya,za,bza);
fbz =f6(t+(1.0/4.0)*h,xa,bxa,ya,bya,za,bza);

k2x = h*fx;
k2bx = h*fbx;
k2y = h*fy;
k2by = h*fby;
k2z = h*fz;
k2bz = h*fbz;

bxa = bx + 0.09375*k1bx + 0.28125*k2bx;
bya = by + 0.09375*k1by + 0.28125*k2by;
bza = bz + 0.09375*k1bz + 0.28125*k2bz;
xa = x + 0.09375*k1x + 0.28125*k2x;
ya = y + 0.09375*k1y + 0.28125*k2y;
za = z + 0.09375*k1z + 0.28125*k2z;

fx =f1(t+(3.0/8.0)*h,xa,bxa,ya,bya,za,bza);
fbx =f2(t+(3.0/8.0)*h,xa,bxa,ya,bya,za,bza);
fy =f3(t+(3.0/8.0)*h,xa,bxa,ya,bya,za,bza);
fby =f4(t+(3.0/8.0)*h,xa,bxa,ya,bya,za,bza);
fz =f5(t+(3.0/8.0)*h,xa,bxa,ya,bya,za,bza);
fbz =f6(t+(3.0/8.0)*h,xa,bxa,ya,bya,za,bza);

k3x = h*fx;
k3bx = h*fbx;
k3y = h*fy;
k3by = h*fby;
k3z = h*fz;
k3bz = h*fbz;

bxa = bx + 0.879380974056*k1bx - 3.2771961766*k2bx + 3.32089212563*k3bx;
bya = by + 0.879380974056*k1by - 3.2771961766*k2by + 3.32089212563*k3by;
bza = bz + 0.879380974056*k1bz - 3.2771961766*k2bz + 3.32089212563*k3bz;
xa = x + 0.879380974056*k1x - 3.2771961766*k2x + 3.32089212563*k3x;
ya = y + 0.879380974056*k1y - 3.2771961766*k2y + 3.32089212563*k3y;
za = z + 0.879380974056*k1z - 3.2771961766*k2z + 3.32089212563*k3z;

fx =f1(t+(12.0/13.0)*h,xa,bxa,ya,bya,za,bza);
fbx =f2(t+(12.0/13.0)*h,xa,bxa,ya,bya,za,bza);
fy =f3(t+(12.0/13.0)*h,xa,bxa,ya,bya,za,bza);

fb_y = f₄(t+(12.0/13.0)*h, x_a, b_x_a, y_a, b_y_a, z_a, b_z_a);
f_z = f₅(t+(12.0/13.0)*h, x_a, b_x_a, y_a, b_y_a, z_a, b_z_a);
fb_z = f₆(t+(12.0/13.0)*h, x_a, b_x_a, y_a, b_y_a, z_a, b_z_a);

k_{4x} = h*f_x;
k_{4bx} = h*fb_x;
k_{4y} = h*f_y;
k_{4by} = h*fb_y;
k_{4z} = h*f_z;
k_{4bz} = h*fb_z;

b_x_a = b_x + 2.03240740741*k_{1bx} - 8.0*k_{2bx} + 7.17348927875*k_{3bx} - 0.20589668616*k_{4bx};
b_y_a = b_y + 2.03240740741*k_{1by} - 8.0*k_{2by} + 7.17348927875*k_{3by} - 0.20589668616*k_{4by};
b_z_a = b_z + 2.03240740741*k_{1bz} - 8.0*k_{2bz} + 7.17348927875*k_{3bz} - 0.20589668616*k_{4bz};
x_a = x + 2.03240740741*k_{1x} - 8.0*k_{2x} + 7.17348927875*k_{3x} - 0.20589668616*k_{4x};
y_a = y + 2.03240740741*k_{1y} - 8.0*k_{2y} + 7.17348927875*k_{3y} - 0.20589668616*k_{4y};
z_a = z + 2.03240740741*k_{1z} - 8.0*k_{2z} + 7.17348927875*k_{3z} - 0.20589668616*k_{4z};

f_x = f₁(t+h, x_a, b_x_a, y_a, b_y_a, z_a, b_z_a);
fb_x = f₂(t+h, x_a, b_x_a, y_a, b_y_a, z_a, b_z_a);
f_y = f₃(t+h, x_a, b_x_a, y_a, b_y_a, z_a, b_z_a);
fb_y = f₄(t+h, x_a, b_x_a, y_a, b_y_a, z_a, b_z_a);
f_z = f₅(t+h, x_a, b_x_a, y_a, b_y_a, z_a, b_z_a);
fb_z = f₆(t+h, x_a, b_x_a, y_a, b_y_a, z_a, b_z_a);

k_{5x} = h*f_x;
k_{5bx} = h*fb_x;
k_{5y} = h*f_y;
k_{5by} = h*fb_y;
k_{5z} = h*f_z;
k_{5bz} = h*fb_z;

b_x_a = b_x - 0.296296296296*k_{1bx} + 2.0*k_{2bx} - 1.38167641326*k_{3bx} + 0.452972709552*k_{4bx} - 0.275*k_{5bx};
b_y_a = b_y - 0.296296296296*k_{1by} + 2.0*k_{2by} - 1.38167641326*k_{3by} + 0.452972709552*k_{4by} - 0.275*k_{5by};
b_z_a = b_z - 0.296296296296*k_{1bz} + 2.0*k_{2bz} - 1.38167641326*k_{3bz} + 0.452972709552*k_{4bz} - 0.275*k_{5bz};
x_a = x - 0.296296296296*k_{1x} + 2.0*k_{2x} - 1.38167641326*k_{3x} + 0.452972709552*k_{4x} - 0.275*k_{5x};
y_a = y - 0.296296296296*k_{1y} + 2.0*k_{2y} - 1.38167641326*k_{3y} + 0.452972709552*k_{4y} - 0.275*k_{5y};
z_a = z - 0.296296296296*k_{1z} + 2.0*k_{2z} - 1.38167641326*k_{3z} + 0.452972709552*k_{4z} - 0.275*k_{5z};

f_x = f₁(t+(1.0/2.0)*h, x_a, b_x_a, y_a, b_y_a, z_a, b_z_a);
fb_x = f₂(t+(1.0/2.0)*h, x_a, b_x_a, y_a, b_y_a, z_a, b_z_a);
f_y = f₃(t+(1.0/2.0)*h, x_a, b_x_a, y_a, b_y_a, z_a, b_z_a);
fb_y = f₄(t+(1.0/2.0)*h, x_a, b_x_a, y_a, b_y_a, z_a, b_z_a);
f_z = f₅(t+(1.0/2.0)*h, x_a, b_x_a, y_a, b_y_a, z_a, b_z_a);

```

fbz =f6(t+(1.0/2.0)*h,xa,bxa,ya,bya,za,bza);

k6x = h*fx;
k6bx = h*fbx;
k6y = h*fy;
k6by = h*fby;
k6z = h*fz;
k6bz = h*fbz;

//
// To Calculate the bvalues of error for v, by, x, y and check if the
// tolerance condition was met by each error value.
//

Rbx =(1.0/h)* fabs(0.002777777777778*k1bx - 0.0299415204678*k3bx - 0.0291998936736*k4bx +
0.02*k5bx + 0.0363636363636*k6bx);

Rby =(1.0/h)* fabs(0.002777777777778*k1by - 0.0299415204678*k3by - 0.0291998936736*k4by
+0.02*k5by + 0.0363636363636*k6by);

Rbz =(1.0/h)* fabs(0.002777777777778*k1bz - 0.0299415204678*k3bz - 0.0291998936736*k4bz
+0.02*k5bz + 0.0363636363636*k6bz);

Rx =(1.0/h)* fabs(0.002777777777778*k1x - 0.0299415204678*k3x - 0.0291998936736*k4x +
0.02*k5x + 0.0363636363636*k6x);

Ry =(1.0/h)* fabs(0.002777777777778*k1y - 0.0299415204678*k3y - 0.0291998936736*k4y +
0.02*k5y + 0.0363636363636*k6y);

Rz = (1.0/h)*fabs(0.002777777777778*k1z - 0.0299415204678*k3z - 0.0291998936736*k4z +
0.02*k5z + 0.0363636363636*k6z);

if ((Rbx <= TOL) && (Rby <= TOL) && (Rbz <= TOL) && (Rx <= TOL) && (Ry <= TOL)&& (Rz
<= TOL))
{
// Approximation was acceptable and so calculate approximation for v,by,
// x and y. Increase the value of t and increment the counter i.
// output the calculated results.
//
t = t + h;
bx = bx + 0.115740740741*k1bx + 0.548927875244*k3bx + 0.535331384016*k4bx - 0.2*k5bx;
by = by + 0.115740740741*k1by + 0.548927875244*k3by + 0.535331384016*k4by - 0.2*k5by;
bz = bz + 0.115740740741*k1bz + 0.548927875244*k3bz + 0.535331384016*k4bz - 0.2*k5bz;
x = x + 0.115740740741*k1x + 0.548927875244*k3x + 0.535331384016*k4x - 0.2*k5x;
y = y + 0.115740740741*k1y + 0.548927875244*k3y + 0.535331384016*k4y - 0.2*k5y;
z = z + 0.115740740741*k1z + 0.548927875244*k3z + 0.535331384016*k4z - 0.2*k5z;
}

```



```

}/**
long double f2(long double T,long double X,long double BX,long double Y,long double BY,long double Z,
long double BZ)
{ return D*(sqrtl(1.0-(BX*BX+BY*BY+BZ*BZ)))*
BX*BX*EX(T,X,Y,Z)+BX*BY*EY(T,X,Y,Z)+BX*BZ*EZ(T,X,Y,Z) -EX(T,X,Y,Z) -
BY*BMAGZ(T,X,Y,Z)+BZ*BMAGY(T,X,Y,Z) );
}/**
long double f3(long double T,long double X,long double BX,long double Y,long double BY,long double Z,
long double BZ)
{ return c*BY;
}/**
long double f4(long double T,long double X,long double BX,long double Y,long double BY,long double Z,
long double BZ)
{return D*(sqrtl(1.0-(BX*BX+BY*BY+BZ*BZ)))*
BY*BX*EX(T,X,Y,Z)+BY*BY*EY(T,X,Y,Z)+BY*BZ*EZ(T,X,Y,Z) -EY(T,X,Y,Z)
+BX*BMAGZ(T,X,Y,Z) );
}/**
long double f5(long double T,long double X,long double BX,long double Y,long double BY,long double Z,
long double BZ)
{return c*BZ;
}
}/**
long double f6(long double T,long double X,long double BX,long double Y,long double BY,long double Z,
long double BZ)
{
return D*(sqrtl(1.0-(BX*BX+BY*BY+BZ*BZ)))*
BZ*BX*EX(T,X,Y,Z)+BZ*BY*EY(T,X,Y,Z)+BZ*BZ*EZ(T,X,Y,Z) -EZ(T,X,Y,Z) -
BX*BMAGY(T,X,Y,Z) );
}
}/**
*****
*****
***** Fields for the two tightly focused
beams.*****
long double EX(long double T,long double X,long double Y,long double Z)
{ return EX1(T,X,Y,Z)+EX2(T,X,Y,Z)*cos(thetai)-EY2(T,X,Y,Z)*sin(thetai);
}
}/**
long double EY(long double T,long double X,long double Y,long double Z)
{
return EY1(T,X,Y,Z)+EY2(T,X,Y,Z)*cos(thetai)+EX2(T,X,Y,Z)*sin(thetai);
}
}/**

```

```

long double EZ(long double T,long double X,long double Y,long double Z)
{
    return EZ1(T,X,Y,Z)+EZ2(T,X,Y,Z);
}
//*****

long double BMAGX(long double T,long double X,long double Y,long double Z)
{
    return -BMAGY2(T,X,Y,Z)*sin(theta);
}

//*****

long double BMAGY(long double T,long double X,long double Y,long double Z)
{
    return BMAGY1(T,X,Y,Z)+BMAGY2(T,X,Y,Z)*cos(theta);
}

//*****

long double BMAGZ(long double T,long double X,long double Y,long double Z)
{
    return BMAGZ1(T,X,Y,Z)+BMAGZ2(T,X,Y,Z);}

//***** Feilds for first beat wave
*****
//*****

long double EX1(long double T,long double X,long double Y,long double Z)
{

    long double x1=X; //
    long double y1=Y; // conversion formalas from X,Y,Z to x1,y1,z1
    long double z1=Z; //
    long double r=sqrtl(x1*x1+y1*y1);
    long double zeta=x1/W0;
    long double ro=r/W0;
    return E1(x1,y1,z1)*( S1(0.0,T,x1,y1,z1)+1.0*powl(eps1,2.0)*(1.0*powl(zeta,2.0)*S1(2.0,T,x1,y1,z1) -
1.0*powl(ro,4.0)*S1(3.0,T,x1,y1,z1)/4.0 )+ 1.0*powl(eps1,4.0)* ( S1(2.0,T,x1,y1,z1)/8.0-
1.0*powl(ro,2.0)*S1(3.0,T,x1,y1,z1)/4.0
-1.0*powl(ro,2.0)*(1.0*powl(ro,2.0)-16.0*powl(zeta,2.0))*S1(4.0,T,x1,y1,z1)/16.0 -
1.0*powl(ro,4.0)*(1.0*powl(ro,2.0)+2.0*powl(zeta,2.0))*S1(5.0,T,x1,y1,z1)/8.0
+1.0*powl(ro,8.0)*S1(6.0,T,x1,y1,z1)/32.0 ) );

}

//*****

long double EY1(long double T,long double X,long double Y,long double Z)
{
    long double x1=X; //
    long double y1=Y; // conversion formalas from X,Y,Z to x1,y1,z1
    long double z1=Z; //

```

```

long double r=sqrtl(x1*x1+y1*y1);
long double zeta=x1/W0;
long double ro=r/W0;
long double v=y1/W0;
return E1(x1,y1,z1)*zeta*v*( 1.0*powl(eps1,2.0)*S1(2.0,T,x1,y1,z1)+1.0*powl(eps1,4.0)*
1.0*powl(ro,2.0)*S1(4.0,T,x1,y1,z1) -1.0*powl(ro,4.0)*S1(5.0,T,x1,y1,z1)/4.0 );
}

//*****
long double EZ1(long double T,long double X,long double Y,long double Z)
{
long double x1=X; //
long double y1=Y; // conversion formalas from X,Y,Z to x1,y1,z1
long double z1=Z; //
long double r=sqrtl(x1*x1+y1*y1);
long double zeta=x1/W0;
long double ro=r/W0;
return E1(x1,y1,z1)*zeta*( eps1*C1(1.0,T,x1,y1,z1) + 1.0*powl(eps1,3.0)*(-1.0*C1(2.0,T,x1,y1,z1)/2.0
+ 1.0*powl(ro,2.0)*C1(3.0,T,x1,y1,z1) - 1.0*powl(ro,4.0)*C1(4.0,T,x1,y1,z1)/4.0 )
+ 1.0*powl(eps1,5.0)*(- 3.0*C1(3.0,T,x1,y1,z1)/8.0 - 3.0*powl(ro,2.0)*C1(4.0,T,x1,y1,z1)/8.0 +
17.0*powl(ro,4.0)*C1(5.0,T,x1,y1,z1)/16.0 -3.0*powl(ro,6.0)*C1(6.0,T,x1,y1,z1)/8.0
+1.0*powl(ro,8.0)*C1(7.0,T,x1,y1,z1)/32.0 ) );
}

//*****
long double BMAGX1(long double T,long double X,long double Y,long double Z)
{
long double x1=X; //
long double y1=Y; // conversion formalas from X,Y,Z to x1,y1,z1
long double z1=Z; //
return 0;
}

//*****
long double BMAGY1(long double T,long double X,long double Y,long double Z)
{
long double x1=X; //
long double y1=Y; // conversion formalas from X,Y,Z to x1,y1,z1
long double z1=Z; //
long double r=sqrtl(x1*x1+y1*y1);
long double zeta=x1/W0;
long double ro=r/W0;
return E1(x1,y1,z1)*( S1(0.0,T,x1,y1,z1)+1.0*powl(eps1,2.0)*(1.0*powl(ro,2.0)*S1(2.0,T,x1,y1,z1)/2.0-
1.0*powl(ro,4.0)*S1(3.0,T,x1,y1,z1)/4.0 )+ 1.0*powl(eps1,4.0)*(- 1.0*S1(2.0,T,x1,y1,z1)/8.0 +
1.0*powl(ro,2.0)*S1(3.0,T,x1,y1,z1)/4.0
+5.0*powl(ro,4.0)*S1(4.0,T,x1,y1,z1)/16.0 -1.0*powl(ro,6.0)*S1(5.0,T,x1,y1,z1)/4.0
+1.0*powl(ro,8.0)*S1(6.0,T,x1,y1,z1)/32.0 ) );
}

```

```
}
```

```
//*****
```

```
long double BMAGZ1(long double T,long double X,long double Y,long double Z)
```

```
{
```

```
long double x1=X; //
```

```
long double y1=Y; // conversion formalas from X,Y,Z to x1,y1,z1
```

```
long double z1=Z; //
```

```
long double r=sqrtl(x1*x1+y1*y1);
```

```
long double zeta=x1/W0;
```

```
long double ro=r/W0;
```

```
long double v=y1/W0;
```

```
return E1(x1,y1,z1)*v*( eps1*C1(1.0,T,x1,y1,z1) + 1.0*powl(eps1,3.0)*( C1(2.0,T,x1,y1,z1)/2.0 +  
1.0*powl(ro,2.0)*C1(3.0,T,x1,y1,z1)/2.0 - 1.0*powl(ro,4.0)*C1(4.0,T,x1,y1,z1)/4.0 )  
+ 1.0*powl(eps1,5.0)*( 3.0*C1(3.0,T,x1,y1,z1)/8.0 +3.0*powl(ro,2.0)*C1(4.0,T,x1,y1,z1)/8.0 +  
3.0*powl(ro,4)*C1(5.0,T,x1,y1,z1)/16.0 - 1.0*powl(ro,6.0)*C1(6.0,T,x1,y1,z1)/4.0  
+1.0*powl(ro,8.0)*C1(7.0,T,x1,y1,z1)/32.0 ) ); }
```

```
// ***** Feilds for the second
```

```
beam*****
```

```
long double EX2(long double T,long double X,long double Y,long double Z)
```

```
{
```

```
long double x2=X*cos(thetai)+Y*sin(thetai); //
```

```
long double y2=Y*cos(thetai)-X*sin(thetai); // conversion formalas from X,Y,Z to x2,y2,z2
```

```
long double z2=Z; //
```

```
long double r=sqrtl(x2*x2+y2*y2);
```

```
long double zeta=x2/W0;
```

```
long double ro=r/W0;
```

```
return E2(x2,y2,z2)*( S2(0.0,T,x2,y2,z2)+1.0*powl(eps2,2.0)*(1.0*powl(zeta,2.0)*S2(2.0,T,x2,y2,z2) -  
1.0*powl(ro,4.0)*S2(3.0,T,x2,y2,z2)/4.0 )+ 1.0*powl(eps2,4.0)* ( S2(2.0,T,x2,y2,z2)/8.0-  
1.0*powl(ro,2.0)*S2(3.0,T,x2,y2,z2)/4.0  
- 1.0*powl(ro,2.0)*(1.0*powl(ro,2.0)-16.0*powl(zeta,2.0))*S2(4.0,T,x2,y2,z2)/16.0 -  
1.0*powl(ro,4.0) *(1.0*powl(ro,2.0)+2.0*powl(zeta,2.0))*S2(5.0,T,x2,y2,z2)/8.0  
+1.0*powl(ro,8.0)*S2(6.0,T,x2,y2,z2)/32.0 ) );  
}
```

```
//*****
```

```
long double EY2(long double T,long double X,long double Y,long double Z)
```

```
{
```

```
long double x2=X*cos(thetai)+Y*sin(thetai); //
```

```
long double y2=Y*cos(thetai)-X*sin(thetai); // conversion formalas from X,Y,Z to x2,y2,z2
```

```
long double z2=Z; //
```

```
long double r=sqrtl(x2*x2+y2*y2);
```

```
long double zeta=x2/W0;
```

```
long double ro=r/W0;
```

```
long double v=y2/W0;
```

```
return E2(x2,y2,z2)*zeta*v*( 1.0*powl(eps2,2.0)*S2(2.0,T,x2,y2,z2)+1.0*powl(eps2,4.0)*(  
1.0*powl(ro,2.0)*S2(4.0,T,x2,y2,z2) - 1.0*powl(ro,4.0)*S2(5.0,T,x2,y2,z2)/4.0 ));  
}
```

```

//*****
long double EZ2(long double T,long double X,long double Y,long double Z)
{
    long double x2=X*cos(thetai)+Y*sin(thetai); //
    long double y2=Y*cos(thetai)-X*sin(thetai); // conversion formalas from X,Y,Z to x2,y2,z2
    long double z2=Z; //
    long double r=sqrtl(x2*x2+y2*y2);
    long double zeta=x2/W0;
    long double ro=r/W0;
    return E2(x2,y2,z2)*zeta*( eps2*C2(1.0,T,x2,y2,z2) + 1.0*powl(eps2,3.0)*( -1.0*C2(2.0,T,x2,y2,z2)/2.0
+ 1.0*powl(ro,2.0)*C2(3.0,T,x2,y2,z2) - 1.0*powl(ro,4.0)*C2(4.0,T,x2,y2,z2)/4.0 )
        +1.0*powl(eps2,5.0)*( -3.0*C2(3.0,T,x2,y2,z2)/8.0 - 3.0*powl(ro,2.0)*C2(4.0,T,x2,y2,z2)/8.0 +
17.0*powl(ro,4.0)*C2(5.0,T,x2,y2,z2)/16.0 -3.0*powl(ro,6.0)*C2(6.0,T,x2,y2,z2)/8.0
+1.0*powl(ro,8.0)*C2(7.0,T,x2,y2,z2)/32.0 ) );
}

```

```

//*****
//*****
long double BMAGX2(long double T,long double X,long double Y,long double Z)
{
    long double x2=X*cos(thetai)+Y*sin(thetai); //
    long double y2=Y*cos(thetai)-X*sin(thetai); // conversion formalas from X,Y,Z to x2,y2,z2
    long double z2=Z; //
    return 0;
}

```

```

//*****
long double BMAGY2(long double T,long double X,long double Y,long double Z)
{
    long double x2=X*cos(thetai)+Y*sin(thetai); //
    long double y2=Y*cos(thetai)-X*sin(thetai); // conversion formalas from X,Y,Z to x2,y2,z2
    long double z2=Z; //
    long double r=sqrtl(x2*x2+y2*y2);
    long double zeta=x2/W0;
    long double ro=r/W0;
    return E2(x2,y2,z2)*( S2(0.0,T,x2,y2,z2)+1.0*powl(eps2,2.0)*(1.0*powl(ro,2.0)*S2(2.0,T,x2,y2,z2)/2.0-
1.0*powl(ro,4.0)*S2(3.0,T,x2,y2,z2)/4.0 )+ 1.0*powl(eps2,4.0)* ( -1.0*S2(2.0,T,x2,y2,z2)/8.0 +
1.0*powl(ro,2.0)*S2(3.0,T,x2,y2,z2)/4.0
        +5.0*powl(ro,4.0)*S2(4.0,T,x2,y2,z2)/16.0 -1.0*powl(ro,6.0)*S2(5.0,T,x2,y2,z2)/4.0
+1.0*powl(ro,8.0)*S2(6.0,T,x2,y2,z2)/32.0 ) );
}

```

```

//*****
long double BMAGZ2(long double T,long double X,long double Y,long double Z)
{
    long double x2=X*cos(thetai)+Y*sin(thetai); //
    long double y2=Y*cos(thetai)-X*sin(thetai); // conversion formalas from X,Y,Z to x2,y2,z2
    long double z2=Z; //
    long double r=sqrtl(x2*x2+y2*y2);
    long double zeta=x2/W0;
    long double ro=r/W0;
}

```

```

long double v=y2/W0;

return E2(x2,y2,z2)*v*( eps2*C2(1.0,T,x2,y2,z2) + 1.0*powl(eps2,3.0)*( C2(2.0,T,x2,y2,z2)/2.0 +
1.0*powl(ro,2.0)*C2(3.0,T,x2,y2,z2)/2.0 - 1.0*powl(ro,4.0)*C2(4.0,T,x2,y2,z2)/4.0 )
+1.0*powl(eps2,5.0)*( 3.0*C2(3.0,T,x2,y2,z2)/8.0 +3.0*powl(ro,2.0)*C2(4.0,T,x2,y2,z2)/8.0 +
3.0*powl(ro,4)*C2(5.0,T,x2,y2,z2)/16.0 -1.0*powl(ro,6.0)*C2(6.0,T,x2,y2,z2)/4.0
+1.0*powl(ro,8.0)*C2(7.0,T,x2,y2,z2)/32.0 ) );
}
//***** finish fields
*****
//***** fields amplitude
*****

```

```

long double E1(long double X,long double Y,long double Z)
{ long double r=sqrtl(X*X+Y*Y);
return E01*(W0/Wz1(Z))*expl(-1.0*(r*r)/(Wz1(Z)*Wz1(Z)));
}

```

```

//*****

```

```

long double Wz1(long double Z)
{return W0*sqrtl(1.0+ powl((Z/zr1),2.0));
}

```

```

long double S1(long double N,long double T,long double X,long double Y, long double Z )
{
long double psi,psip,psir,psig,r,Rs;
r=sqrtl(X*X+Y*Y);
Rs=Z+((zr1*zr1)/Z);
psir=k1*r*r/(2.0*Rs);
psip=omega1*T-(k1*Z);
psig=atanl(Z/zr1);
psi=psi0+psip-psir+psig;
return (1.0*powl(W0/Wz1(Z),N))*sinl(psi+N*psig);
}

```

```

long double C1(long double N,long double T,long double X,long double Y, long double Z )
{
long double psi,psip,psir,psig,r,Rc;
r=sqrtl(X*X+Y*Y);
Rc=Z+((zr1*zr1)/Z);
psir=k1*r*r/(2.0*Rc);
psip=omega1*T-k1*Z;
psig=atanl(Z/zr1);
psi=psi0+psip-psir+psig;
return (1.0*powl(W0/Wz1(Z),N))*cosl(psi+N*psig);
}
//***** fields amplitude
*****

```

```

long double E2(long double X,long double Y,long double Z)
{
long double r=sqrtl(X*X+Y*Y);
return E02*(W0/Wz2(Z))*expl(-1.0*(r*r)/(Wz2(Z)*Wz2(Z)));
}

//*****

long double Wz2(long double Z)
{
return W0*sqrtl(1.0+ powl((Z/zr2),2.0));
}

long double S2(long double N,long double T,long double X,long double Y, long double Z )
{
long double psi,psip,psir,psig,r,Rs;
r=sqrtl(X*X+Y*Y);
Rs=Z+((zr2*zr2)/Z);
psir=k2*r*r/(2.0*Rs);
psip=omega2*T-(k2*Z);
psig=atanl(Z/zr2);
psi=psi0+psip-psir+psig;
return (1.0*powl(W0/Wz2(Z),N))*sinl(psi+N*psig);
}

long double C2(long double N,long double T,long double X,long double Y, long double Z )
{
long double psi,psip,psir,psig,r,Rc;
r=sqrtl(X*X+Y*Y);
Rc=Z+((zr2*zr2)/Z);
psir=k2*r*r/(2.0*Rc);
psip=omega2*T-k2*Z;
psig=atanl(Z/zr2);
psi=psi0+psip-psir+psig;

return (1.0*powl(W0/Wz2(Z),N))*cosl(psi+N*psig);
}

long double Egain(long double BXa,long double BYa,long double BZa,long double BX0,long double
BY0,long double BZ0 )
{
return (1000.0/1.6)*m*c*c*( 1.0/(sqrtl(1.0-(BXa*BXa+BYa*BYa+BZa*BZa)))- (1.0/(sqrtl(1.0-
(BX0*BX0+BY0*BY0+BZ0*BZ0)))) ) );
}
long double beta0(long double gamma)
{
return sqrtl(1.0-(1.0/(gamma*gamma)));}

```

Filename: c++ code
Directory: C:\Documents and Settings \Ashraf\Desktop\thesis-print
Template: C:\Documents and Settings \Ashraf\Application
Data\Microsoft\Templates\Normal.dot
Title: /* ***** done by: ashraf titi *****
Subject:
Author: Ashraf Titi
Keywords:
Comments:
Creation Date: ?
Change Number: 3
Last Saved On: ?
Last Saved By: Ashraf Titi
Total Editing Time: 33 Minutes
Last Printed On: ?
As of Last Complete Printing
Number of Pages: 15
Number of Words: 4,500 (approx.)
Number of Characters: 25,654 (approx.)